

PREDICTING CALIFORNIA WILDFIRE SPREAD WITH TIME-SERIES AND SPATIAL-TEMPORAL MODELS

BENJAMÍ PARELLADA I CALDERER

Thesis supervisor

PADHRAIC SMYTH (University of California, Irvine)

Tutor: JAVIER BÉJAR ALONSO (Department of Computer Science)

Degree

Master's Degree in Artificial Intelligence

Master's thesis

School of Engineering

Universitat Rovira i Virgili (URV)

Faculty of Mathematics

Universitat de Barcelona (UB)

Barcelona School of Informatics (FIB)

Universitat Politècnica de Catalunya (UPC) - BarcelonaTech

ABSTRACT

Wildfires have become increasingly frequent and severe worldwide, posing significant threats to ecosystems, human life, and property. Precise prediction of wildfire spread is crucial for effective mitigation and management strategies. In this thesis, we utilize data from the VIIRS and GOES satellite instruments to develop a novel dataset to understand the physical dynamics of wildfires. By sampling along active fire lines, we capture detailed information that has not been previously analyzed in the literature. We investigate the modeling of wildfire dynamics in California by applying both time series methods and spatio-temporal modeling techniques to this data.

Initially, we apply univariate time series models to predict Burned Fire Area using only historical data of the target feature. Traditional statistical models, especially the Autoregressive Integrated Moving Average (ARIMA) model, consistently outperform neural network architectures like RNNs, LSTMs, and more advanced models such as DeepAR. ARIMA's superior performance is attributed to its robustness in handling the inherent noise and intermittent activity in wildfire time series data, as well as the limited size of the datasets, which hampers the training of deep learning models.

Next, we enhance the time series predictive capabilities by incorporating additional covariates. Ensemble methods, particularly Extreme Gradient Boosting (XGBoost), outperform both traditional linear models and complex neural networks in predicting the fire growth in our new data. Environmental variables such as Vapor Pressure Deficit are more influential in predicting fire spread than operational factors like suppression personnel. Shapley Additive Explanations analysis indicates that immediate past behavior and specific weather conditions are key drivers of wildfire dynamics, while the impact of firefighting efforts is less clear, likely due to data limitations.

Further, we investigate spatio-temporal modeling approaches using both Cellular Automata (CA) and neural network models like ConvLSTM. While these models show promise in simulated environments, they struggle to generalize to real-world wildfire events. The CA model offers interpretability and aligns somewhat with known parameters in simulation, but requires refinement to handle the complexities of actual wildfires. Neural network models achieve higher performance metrics in simulations but suffer from a lack of transparency and generalizability when applied to real data.

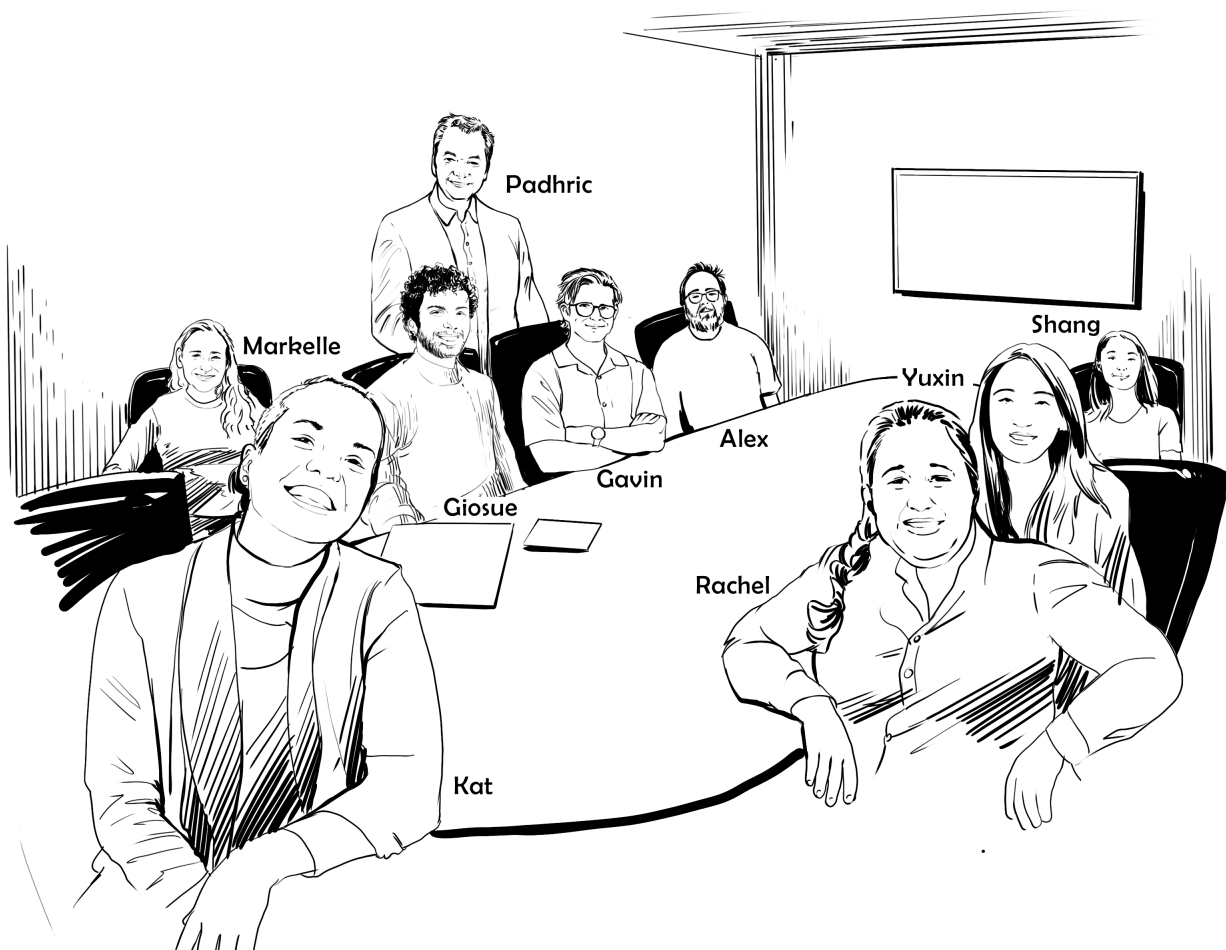
Our research underscores the challenges in modeling wildfire spread due to the complex interactions of environmental and operational factors and the limitations of existing datasets. The findings suggest that while advanced machine learning models hold potential, traditional statistical methods currently provide more reliable predictions in certain contexts. Enhancing data quality and quantity, incorporating more diverse topographical and climatic locations, and developing models tailored to the unique characteristics of wildfire data are essential steps for future research.

By comparing the predictive performance of different modeling approaches and providing insights into the factors driving wildfire spread, this thesis contributes to the advancement of wildfire behavior modeling. The methodologies and findings presented have the potential to support real-time wildfire management and ecological impact assessments, ultimately aiding in the mitigation of wildfire risks.

ACKNOWLEDGMENTS

I would like to express my deepest gratitude to Prof. Padhraic Smyth for giving me the invaluable opportunity to collaborate at UCI. Working with you and the group has been an unforgettable experience, filled with both learning and personal growth in a remarkably short time.

I'm grateful to everyone in the DataLab group for your support and for making my stay so memorable. A special thanks to Kat for warmly welcoming me from the moment I landed in California, for showing me around, and for helping me find my footing. I am also profoundly thankful to Giosue for his unwavering collaboration and guidance throughout every phase of this project. As well as the fellow group members—Markelle, Gavin, Alex, Rachel, Yuxin, and Shang—thank you for the inspiring research discussions and for offering me a glimpse into the challenges and rewards of pursuing a PhD.



I would also like to extend my sincere thanks to Professors James Randerson and Efi Foufoula-Georgiou who gave their expertise from a climate perspective sharing their insightful contributions, and for helping me understand the broader significance of this research. I am deeply grateful to Yang and Tina for their invaluable assistance

with data procuring, which played a crucial role in the success of this project. And to Rebecca and Rachel for their consistent support and the enriching weekly discussions that greatly aided my progress.

I extend my heartfelt appreciation to Armin, Davide, Dima, Iris, Kat, Kyungming, Nilab, and everyone else in room 4059. The countless hours we spent together not only shaped my experience in Irvine, but also made me feel truly at home. Without your company, I would have missed out on much of what makes this journey unforgettable.



I am also deeply grateful to Javier Béjar for his invaluable guidance and oversight of this thesis. To my family, for their unwavering and eternal support—this journey would have been impossible without you.

A special thank you to Roger Bock, whose encouragement made sure I didn't spend even more time in the office than I already did!

Finally, I wish to thank the Balsells family, whose generosity made this entire experience possible. Without their financial support, I would not have been able to embark on this transformative journey.

Benjamí Parellada

CONTENTS

Abstract	ii
Acknowledgements	iii
List of Figures	xi
List of Tables	xii
1 Introduction	2
1.1 Context and Justification	4
1.1.1 California's Wildfire Crisis	5
1.1.2 Economic and Environmental Impact	5
1.1.3 Public Health and Social Implications	6
1.1.4 Global Perspective	6
1.1.5 The Imperative for Understanding and Prediction	7
1.2 Scope	8
1.3 Objectives	9
1.4 Research Questions	10
1.5 Outline of the Thesis	10
2 Data	13
2.1 Data Sources	13
2.1.1 Fire Detection Data	13
2.1.2 Weather Data	15
2.1.3 Topographic Data	16
2.1.4 Human Intervention	17
2.1.5 Data Integration for Wildfire Modeling	18
2.2 Related Work	19
2.3 Data Processing	20
2.3.1 DataCube	20
2.3.2 Fire Events Data Suite (FEDS)	23
2.3.3 GOES Fire Event Reconstruction (GOFER)	25
2.3.4 Conversion to Time-Series Data	26
2.4 Statistics	26
2.4.1 Overview of Datasets	27
2.4.2 Target Variable: Fire Spread	29
2.4.3 Covariates: Fire	31

2.4.4	Covariates: Weather	33
2.4.5	Covariates: Topology	36
2.4.6	Covariates: Fuel	37
2.4.7	Covariates: Human Intervention	39
2.4.8	Dimensionality Reduction	41
3	Univariate Time Series	43
3.1	Background	43
3.1.1	Stationarity	44
3.1.2	Autocorrelation Analysis	45
3.1.3	STL Decomposition	47
3.2	Methodology	48
3.2.1	Models	48
3.2.2	Data Split	54
3.2.3	Evaluation	56
3.3	Results	59
3.3.1	Local Models	59
3.3.2	Global Models	60
3.3.3	Model Evaluation	61
3.3.4	Qualitative Analysis	61
3.4	Discussion	62
3.4.1	Future Work	63
4	Multivariate Time Series	65
4.1	Background	65
4.2	Methodology	66
4.2.1	Data Preprocessing	66
4.2.2	Data Splitting and Evaluation	67
4.2.3	Feature Selection	67
4.2.4	Model Evaluation	67
4.2.5	Explainability with SHAP Values	68
4.2.6	Models	68
4.3	Results	72
4.3.1	Explainability	74
4.3.2	Final Evaluation Metrics	79
4.3.3	Lead Time Analysis	80
4.4	Discussion	80
4.4.1	Future Work	82
5	Spatial-Temporal Modeling	84
5.1	Related Work	85
5.2	Methodology	86

5.2.1	Cellular Automata	86
5.2.2	Image-to-Image Problem Definition	92
5.2.3	Evaluation Metrics	94
5.2.4	Training Procedure	95
5.3	Results	97
5.4	Discussion	100
5.4.1	Future Work	102
6	Discussion	104
7	References	108

LIST OF FIGURES

1.1	Example of a sequoia from California’s Sequoia National Park with fire damage; they are resistant to fire and can survive even with these conditions.	2
1.2	Satellite images from with red highlighting active fire seen in infrared.	6
1.3	Plume of smoke from Canadian wildfires reaching Europe, as depicted by NASA’s GEOS-FP model showing black carbon density over the Atlantic Ocean.	7
2.1	Comparison of the North California fires on August 30, 2021, using Terra/MODIS (left) and Suomi NPP/VIIRS (right) layers, overlaid on corrected reflectance from NOAA-20/VIIRS. The VIIRS sensor detects significantly more thermal anomalies than MODIS, highlighting its higher sensitivity to smaller fires. Images were extracted using NASA Worldview.	14
2.2	Fire hot spots and a large plume of smoke are seen in this GOES-16 fire temperature RGB imagery with GeoColor enhancement of the Camp Fire in northern California on November 8, 2018. Source: NOAA/CIRA	16
2.3	Visualization of a slice of the DataCube for the Creek Fire at time step 500. The leftmost panel displays the fire progression overlaid on terrain elevation. Surrounding panels illustrate various environmental and human-related covariates.	23
2.4	Schematic diagram of fire tracking: (a) At time step t , two fire objects are present. Colored and grey dots represent newly detected and previously detected VIIRS active fire pixels, respectively. Brown segments along the fire perimeter indicate active fire fronts. (b) At time $t + 1$, new fire pixels (in red) are clustered into C1, C2, and C3. C1 forms a new fire object (Fire 3), C2 contributes to the growth of Fire 1, and C3 causes Fire 2 to merge with Fire 1 when they grow close enough. Fire perimeters and active fire fronts are updated for each fire object at every time step. Source [73].	24
2.5	Schematic diagram of converting the fire into time-series. The line in blue represents the active fire line, where the environmental variables are sampled to obtain the fire dynamics.	26
2.6	Number of fires per year in the FEDS and GOFER datasets. FEDS data spans from 2014 to 2022, while GOFER data is available from 2019 to 2022.	27
2.7	Average fire duration per year in the FEDS and GOFER datasets. This metric indicates the typical lifespan of fires captured in each dataset over time.	27

2.8	Total fire area burned per year in the FEDS and GOFER datasets. This figure reflects the cumulative impact of wildfires annually as captured by each dataset.	28
2.9	Number of observations per year in the FEDS and GOFER datasets. The higher number of observations in GOFER reflects its hourly temporal resolution compared to the twice-daily updates in FEDS.	28
2.10	Average <i>dfarea</i> by hour in the GOFER dataset. The plot shows increased fire spread during the afternoon hours, with reduced activity during nighttime.	30
2.11	An example of false fire detection by VIIRS. VIIRS reflectance bands corrected for 2019-01-03, showing detected hotspots (left). Corresponding Google Earth image of the area, revealing solar panel fields (right). The VIIRS detection mistakenly identifies the solar panels as active fires due to high reflectance and thermal characteristics.	31
2.12	Relationship between the change in fire area ($y^{(t+1)}$) and the active fire line length at time t on a logarithmic scale. The plot indicates that larger active fire lines are associated with greater increases in burned area at the next time step.	32
2.13	Correlation matrices for fire variables: (left) FEDS dataset; (right) GOFER dataset. The color intensity indicates the strength of the Pearson correlation coefficients between variables, with darker colors representing stronger correlations.	33
2.14	Correlation matrices of weather variables for the FEDS (left) and GOFER (right) datasets. The color intensity indicates the strength of the correlation between variables, with darker colors representing stronger correlations.	33
2.15	Relationship between change in fire area ($y^{(t+1)}$) and Vapor Pressure Deficit (VPD). Higher VPD values are associated with greater fire spread.	35
2.16	Relationship between change in fire area ($y^{(t+1)}$) and (left) wind speed, (right) mean temperature. Both variables show a positive association with fire spread.	35
2.17	Relationship between change in fire area ($y^{(t+1)}$) and relative humidity. Higher relative humidity is associated with reduced fire spread.	36
2.18	Correlation matrices of topological variables for the FEDS (left) and GOFER (right) datasets. Color intensity indicates the strength of the Pearson correlation coefficients, with darker colors representing stronger correlations.	37
2.19	Relationship between the change in fire area ($y^{(t+1)}$) and elevation at time t . Elevation changes above 2.5 meters are associated with reduced fire spread.	37
2.20	Fire Spread Across Different Fuel Classes and Land Covers. Left: Scott and Burgan Fire Behavior Fuel Model, Right: Anderson Land Cover Classification System	38
2.21	Effect of Fuel Load on Fire Spread	38
2.22	Correlation matrices of human intervention variables for the FEDS (left) and GOFER (right) datasets. Darker colors represent stronger correlations (Pearson coefficients).	39

2.23	Normalized difference in fire spread compared to total personnel from the previous time step.	40
2.24	PCA biplot for the FEDS dataset. Data was normalized using a standard scaler. Point density is plotted instead of individual points for clarity.	41
3.1	Accumulated Burned Fire Area over Time for Different Resolutions: (Left) 12-hour resolution (FEDS), (Right) 1-hour resolution (GOFER)	45
3.2	Difference in Burned Area for Sample Fires from FEDS: (Left) Raw Differences, (Right) Log-transformed Differences $\log(Y_t + 1)$	45
3.3	Autocorrelation Function of Differenced Burned Area: (Left) August Complex, (Right) Creek	46
3.4	Autocorrelation Function of Differenced Burned Area in FEDS: (Left) August Complex, (Right) Creek	47
3.5	STL Decomposition of Burned Fire Area: (Left) FEDS Dataset with 12-hour Resolution, (Right) GOFER Dataset with 1-hour Resolution	48
3.6	Comparison of Randomized CV vs. Out-of-Sample (OOS) Evaluation. The blue and orange dots represent the training and test sets, respectively. In the usual k-fold CV setup, the testing instances are chosen randomly across the series. In OOS evaluation, the test set is always reserved from the end of the series.	54
3.7	Schematic of the Expanding Window (left) setup where the training set keeps expanding and Rolling Window (right) where the training window is fixed and moves. The blue and orange boxes represent the training and test sets, respectively.	55
3.8	Number of unique fires per year in each data split. This results in 188 unique fires (5,279 observations) for training, 48 fires (1,450 observations) for validation, and 50 fires (1,765 observations) for testing.	56
3.9	Example of two fires (FEDS on the left, GOFER on the right) being predicted by the ARIMA vs. True Values.	62
4.1	SHAP waterfall plot illustrating the contributions of individual features to the model output for a specific instance. These are also the top most important variables according to XGBoost.	75
4.2	SHAP dependence plots for Previous Active Fire Line Length (left), and Total Personnel (right).	76
4.3	SHAP dependence plots for VPD (left), and the Previous Fire Growth (right).	76
4.4	Time series plot of true and predicted burned area, along with relevant features, for a selected fire in the FEDS dataset.	78
4.5	Time series plot of true and predicted burned area, along with relevant features, for a selected fire in the GOFER dataset.	79
5.1	Illustration of the Moore neighborhood for a central cell s_i . Each surrounding cell represents a neighbor in the set $\mathcal{N}(i)$	87

5.2	State diagram of the automata, illustrating transitions between <i>Unburned</i> (<i>U</i>), <i>Burning</i> (<i>B</i>), and <i>Extinguished</i> (<i>E</i>) states along with their respective probabilities. A priori, transitions marked in red have zero probability, while those in orange may have non-zero probability.	87
5.3	Representation of the Moore neighborhood for a cellular automata at time t and $t + 1$. The grid at t shows the initial states with potential influences on the central cell s_i indicated by arrows. The grid at $t + 1$ illustrates the state transitions where s_i and its neighbors change to $s_i^{(t+1)}$. White cells are <i>Unburned</i> , red cells are <i>Burning</i> , and gray cells are <i>Extinguished</i>	88
5.4	Example of a simulation at an advanced time step. From left to right: previous state, target state, VPD, and Fuel.	95
5.5	Evolution of Predicted Fire Spread. The left panel displays the predicted fire states for the first 400 time steps, while the right panel shows the corresponding target states for the subsequent 500 time steps. In the images, white indicates <i>Burned</i> areas, black represents <i>Unburned</i> regions, and red denotes <i>Burning</i> areas. For both panels we have Previous State, Prediction, and Target state. The predictions come from the CA.	100

LIST OF TABLES

2.1	Correlation coefficients between weather variables at the active fire line and ignition point for the FEDS and GOFER datasets. High correlation values indicate similar information content from both locations.	34
3.1	Performance Metrics for Local Models on the FEDS Dataset.	59
3.2	Performance Metrics for Local Models on the GOFER Dataset.	60
3.3	Performance Metrics for Global Models on the FEDS Dataset.	60
3.4	Performance Metrics for Global Models on the GOFER Dataset.	61
4.1	Performance Metrics on the Validation Set of FEDS.	73
4.2	Performance Metrics on the Validation Set of GOFER.	73
4.3	Comparison of Machine Learning Models on FEDS and GOFER Datasets.	80
5.1	Quantitative Evaluation Metrics for Wildfire Spread Models on Simulation.	98
5.2	Parameter Estimation for Cellular Automata Model.	99

CHAPTER 1

INTRODUCTION

Wildfires, also known as forest fires or bushfires, have historically been an integral component of many ecosystems worldwide. They play a vital role in maintaining ecological balance by clearing out dead or overgrown vegetation, returning nutrients to the soil, and promoting the growth of diverse plant species [1]. This natural cycle of destruction and renewal has shaped landscapes and biodiversity for millennia [2].

A key example of this ecological adaptation is *Serotiny*, a trait exhibited by certain plant species, where seed release is triggered by environmental factors such as fire, rather than occurring at seed maturation. The giant sequoia species (*Sequoiadendron giganteum*) in North America is one of the most iconic examples of a serotinous species. These trees rely on the intense heat from fires to open their cones and release seeds, allowing their reproduction to take place when fires expose mineral-rich soil and clear the canopy for light penetration [3]. However, this process requires that fires occur at an appropriate interval. Increasingly frequent, high-severity wildfires pose a major threat to this balance. When fires are too frequent or severe, they can destroy both the seedlings and mature groves, preventing recovery and reproduction [4]. For instance, it is estimated that up to 20% of the population of mature sequoias in California's Sierra



Figure 1.1: Example of a sequoia from California's Sequoia National Park with fire damage; they are resistant to fire and can survive even with these conditions.

Nevada died since 2015, while also noticing a significant drop in the emergence of new seedlings due to excessive heat [5]. These trends raise concerns about the long-term viability of these one-of-a-kind trees in their native range.

Furthermore, in recent decades, wildfires have increased significantly in frequency, intensity, and scale worldwide, particularly in regions like California, Australia, the Mediterranean, and Canada [6]. In California, large fires (\geq 400 hectares) have become more common since the 1980s, burning more severely and impacting ecosystems more heavily [7]; extreme fire weather days have recently more than doubled [8]. Southeastern Australia experienced a marked rise in wildfire severity during the devastating 2019–2020 season, linked to extreme fire weather conditions [9, 10]. The Mediterranean is expected to see continued increases in heat-induced wildfires during summer heatwaves [11], and Canada has documented severe wildfire seasons contributing to atmospheric pollution and ecosystem damage [12].

Several factors contribute to the surge in wildfire activity. Climate warming has increased fuel aridity, doubling the forest fire area in the western U.S. since the 1980s, largely due to anthropogenic climate change [13]. Drier landscapes resulting from prolonged droughts, higher temperatures, and altered precipitation patterns are more susceptible to ignition; declining summer precipitation and extended dry periods have heightened wildfire activity, with reduced rain days being particularly influential [14]. Historical fire suppression policies and deforestation have led to an accumulation of fuel loads, creating a feedback loop that increases the risk of larger, uncontrollable fires [15]. Land-use changes and human activities have caused unnatural buildups of vegetation, intensifying fire activity and severity in forests across the western U.S. [16].

Furthermore, the increasing severity and frequency of wildfires pose significant threats to ecosystems, human life, and property. Predicting the spread of wildfires has become imperative for effective mitigation and management strategies [6, 17]. Accurate predictions enable timely evacuation orders, optimal allocation of firefighting resources, and the development of preventative measures to minimize the impact on vulnerable communities and critical habitats [18]. Understanding fire dynamics and spread patterns is essential, especially in the context of climate change and evolving land-use practices that alter the behavior of wildfires [6, 17, 19].

In this thesis, we will study the fire dynamics and spread of wildfires using both time series models and spatial-temporal models. By leveraging data derived from processed satellite imagery, we aim to enhance predictive capabilities and provide deeper insights into the factors driving wildfire spread. This research seeks to contribute to improved wildfire behavior modeling and support real-time wildfire management and

ecological impact assessments.

1.1 CONTEXT AND JUSTIFICATION

Thus, wildfires have emerged as a pressing global concern, with their frequency and severity escalating due to a combination of climate change, human activities, and evolving land-use patterns [6, 13, 20]. Regions like California are highly impacted by this crisis, where the convergence of prolonged droughts, high temperatures, and complex terrain creates a flammable environment [21, 22]. The increasing incidence of wildfires leads to devastating consequences, including loss of life, destruction of property, environmental degradation, and significant economic burdens [23, 24].

A critical challenge in managing wildfires is their inherent unpredictability. The rapid ignition and spread of fires are thought to be influenced by factors such as weather conditions, vegetation types, and human intervention [6, 19]. Traditional wildfire prediction models, which often rely on historical data and static assumptions, are insufficient in capturing the complex and stochastic nature of fire behavior under current and future climatic scenarios [25].

Accurate and timely prediction of wildfire spread is paramount for effective disaster response and mitigation [26]. Enhanced predictive capabilities enable authorities to issue early warnings, optimize the allocation of firefighting resources, and implement strategic land and forest management practices. Moreover, precise modeling of wildfire behavior is essential for safeguarding public health, protecting ecosystems, and minimizing economic losses [27, 28, 29, 30].

Advancements in remote sensing, high-resolution satellite imagery, and real-time data analytics facilitates the development of sophisticated models that can simulate fire dynamics with greater accuracy [25] as well as obtain novel metrics to assess the damages [31, 32]. Incorporating machine learning algorithms and uncertainty quantification methods can further refine these models by accounting for the probabilistic nature of environmental variables [25].

This study focuses on addressing the gaps in current wildfire prediction methodologies by exploring innovative approaches that integrate advanced technologies and analytical techniques. By emphasizing the prediction aspect of wildfire management, we aim to contribute to the development of robust models that can better inform decision-making processes. Understanding and quantifying the uncertainties associated with wildfire behavior are crucial steps toward enhancing the resilience of communities and ecosystems in the face of this escalating threat.

1.1.1 CALIFORNIA'S WILDFIRE CRISIS

Recent events in California underscore the escalating severity of wildfires in the region. While the state has historically experienced seasonal wildfires, the unprecedented size and destructiveness of recent fires mark a significant departure from past patterns. According to the [California Department of Forestry and Fire Protection \(CAL FIRE\)](#), from 2010 to 2020, California saw a substantial increase in both the number of fires and the acreage burned [33]. In 2020 alone, the state faced its worst wildfire season on record, with over 8,600 fires consuming more than 4.3 million acres (1.7 million hectares) and resulting in 33 fatalities [33]. To put this into perspective, the European Union's worst fire year this century was in 2017, with 1.2 million hectares burned and 127 fatalities [34]. Considering that California is approximately 15% smaller than Spain, the magnitude of the wildfires in California highlights the severity of the crisis.

Several notable incidents illustrate the escalating crisis:

- **The Camp Fire (2018):** This devastating fire in Northern California became the deadliest and most destructive wildfire in the state's history. While only lasting 18 days in November, it resulted in 85 civilian fatalities and destroyed nearly 19,000 structures, primarily in the town of Paradise [23, 35]. The estimated economic impact exceeded \$16.5 billion, including over \$4 billion in insured property losses [36], causing bankruptcy to the company *Pacific Gas & Electric* (PG&E) which was found responsible for the fire.
- **The Mendocino Complex Fire (2018):** At the time, this was the largest recorded [Complex Fire](#) in California, burning over 459,000 acres (around 185,000 ha) [37]. The firefighting efforts cost approximately \$201 million, highlighting the immense resources required to combat such large-scale fires [38].
- **The August Complex Fire (2020):** This fire surpassed the Mendocino Complex to become the largest in California's history, scorching over 1 million acres (417,898 ha). It took three months for the suppression efforts to contain the fire [39].

1.1.2 ECONOMIC AND ENVIRONMENTAL IMPACT

As illustrated already, wildfires have far-reaching economic consequences that extend well beyond the immediate damage. Direct costs include firefighting expenses, property damage, and infrastructure loss. For example, California's wildfire protection and suppression expenditures have skyrocketed, with the state spending over \$3.3 billion on wildfire suppression in the 2022-2023 [40]. Indirect costs encompass lost income, decreased tourism, and long-term health care expenses due to smoke-related



(a) Camp Fire - November 8, 2018.



(b) Mendocino Fire - August 15, 2018.

Figure 1.2: Satellite images from with red highlighting active fire seen in infrared.

illnesses [41]. Which is estimated to cost the United States between \$71.1 billion and \$347.8 billion annually when considering both direct and indirect losses [41]. In California, the total economic impact of the 2018 wildfires was estimated to be around \$148.5 billion, accounting for property damage, health costs, and economic disruption [24].

Environmentally, the consequences are equally severe. Wildfires contribute to deforestation, soil erosion, and loss of biodiversity. They release significant amounts of carbon dioxide and other greenhouse gases, which exacerbate climate change—a contributing factor to the increased fire activity in the first place [42].

1.1.3 PUBLIC HEALTH AND SOCIAL IMPLICATIONS

Wildfires pose substantial risks to public health. Smoke from fires contains a complex mixture of gases and fine particles that can penetrate deep into the lungs. Exposure can lead to respiratory issues, cardiovascular problems, and exacerbation of chronic diseases like asthma and bronchitis [29]. During the 2020 wildfire season, air quality in parts of California reached hazardous levels, with the Air Quality Index (AQI) exceeding 300 in some areas—far above the “acceptable” threshold of 100 [43].

The health impacts are not limited to the immediate vicinity of the fires. Smoke can travel hundreds or even thousands of miles, affecting air quality across states and regions. For instance, smoke from the 2020 California fires reached the East Coast of the United States and even Europe, illustrating the far-reaching consequences of these events [44, 45]. More recently, the smoke from Canadian wildfires on August 2024 have been detected to arrive at the south Europe (Figure 1.3).

1.1.4 GLOBAL PERSPECTIVE

While we focus on California, the wildfire crisis is global. In recent years, Canada has contended with some of the most intense wildfire seasons on record. In 2023,

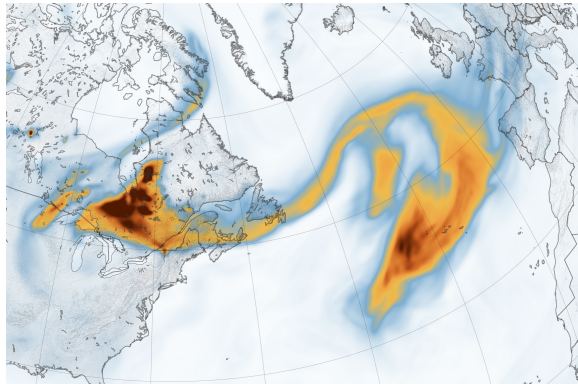


Figure 1.3: Plume of smoke from Canadian wildfires reaching Europe, as depicted by NASA’s GEOS-FP model showing black carbon density over the Atlantic Ocean.

vast areas of the country were ablaze in flames, with over 15 million hectares burned [46]. These fires led to mass evacuations and significant air quality issues, not only within Canada but also impacting neighboring countries. The economic and environmental repercussions in Canada have been substantial, with firefighting expenditures skyrocketing, and the loss of extensive forested regions disastrous [47].

Australia’s experience during the 2019-2020 “Black Summer” bushfires further exemplifies the worldwide impact of wildfires. The catastrophic fires consumed over 19 million hectares, destroyed more than 3,000 homes, claimed at least 33 human lives, and 1 billion animals [48]. The disaster inflicted an estimated economic cost of \$20 billion dollars, marking it as the most expensive natural catastrophe in the country’s history [48]. Furthermore, it is estimated that the cost of the smoke caused between 12 and 50 million Australian dollars in disruptions in Sydney.

In the Amazon rainforest, rampant deforestation and land clearing have escalated fire activity, threatening a critical global carbon sink and a hotspot of biodiversity [49]. Similarly, Siberia has witnessed extensive wildfires, with millions of acres burned, significantly contributing to greenhouse gas emissions [50]. Regions such as the Mediterranean and parts of Africa are also facing increasing wildfire threats due to rising temperatures and prolonged droughts [50].

1.1.5 THE IMPERATIVE FOR UNDERSTANDING AND PREDICTION

Given the escalating dangers, understanding and predicting wildfire spread have become essential. Wildfires are complex and dynamic events influenced by numerous interrelated factors such as weather conditions, topography, vegetation types, and human activities. The inherent unpredictability of these factors poses significant challenges to accurately forecasting wildfire behavior, yet doing so is critical for effective management and mitigation strategies.

To effectively tackle these challenges, accurate prediction models are indispensable tools that serve multiple critical functions:

- **Early Warning Systems:** Providing timely alerts to residents and authorities to initiate evacuations and mobilize resources [30]. Accurate predictions of fire spread paths and intensities can significantly reduce loss of life and property by enabling proactive measures.
- **Resource Allocation:** Optimizing the deployment of firefighting personnel and equipment to areas of greatest need [27]. Predictive models help prioritize regions at higher risk, ensuring that limited resources are used efficiently.
- **Land Management:** Informing policies on controlled burns, forest thinning, and other preventive measures [26]. Understanding potential fire behavior assists in designing landscapes that are more resilient to wildfires.
- **Climate Modeling:** Enhancing the accuracy of climate models by integrating the feedback effects of wildfires on atmospheric conditions [51]. Wildfires contribute to greenhouse gas emissions and aerosol concentrations, influencing climate patterns.

Traditional methods of predicting wildfire behavior often rely on simple models that do not account for the rapidly changing variables influencing wildfires. These models typically assume that past fire behavior will predict future events, which may not hold true in the context of shifting climate patterns, evolving vegetation dynamics, and increased human intervention [6, 52]. Therefore, there is an urgent need for more sophisticated approaches that can accommodate the complexity and variability of wildfire behavior.

1.2 SCOPE

This thesis focuses on predicting wildfire spread in California by utilizing time-series analytical methods and spatio-temporal modeling techniques applied to data derived from processed satellite imagery. California serves as an ideal case study due to its extensive history of wildfires, rich availability of datasets, and significant efforts dedicated to wildfire suppression and management. The state's diverse topography, climate variations, and vegetation types provide a comprehensive environment for understanding the complex dynamics of wildfires.

The research is confined to the region of California, allowing for a detailed examination of wildfire behavior within a specific geographical context. By concentrating on this area, the study leverages abundant information to develop and validate data-driven approaches that may be applicable to other regions facing similar challenges.

The scope includes collecting and processing high-resolution satellite imagery and relevant ancillary data pertinent to California wildfires, utilizing datasets from sources such as NASA’s MODIS and VIIRS instruments and the European Space Agency’s Sentinel missions.

The project focuses on interpreting model results to identify key factors driving wildfire spread, assessing the influence of environmental variables, human activities, and climate conditions. While economic impact assessments and optimization of firebreak placements are acknowledged as important, they are beyond the scope of this thesis. By defining these boundaries, the thesis maintains a focused approach, aiming to contribute to the field of wildfire behavior modeling and enhance prediction accuracy for real-time wildfire management in California. The methodologies and insights developed may also be transferable to other fire-prone regions, demonstrating the broader applicability of data-driven approaches to wildfire prediction and management.

1.3 OBJECTIVES

The primary objective of this research is to develop and evaluate predictive models for wildfire spread in California using satellite imagery data, aiming to enhance prediction accuracy and provide insights that can support mitigation strategies and downstream analyses. The study seeks to create a comprehensive *DataCube* that integrates multidimensional data to facilitate detailed analyses and support tasks such as estimating the economic impact of wildfires on infrastructure and communities.

A key goal is to apply and compare time-series methods for predicting temporal patterns of wildfire spread. This involves investigating whether incorporating covariates like weather variables, vegetation indices, and topographical features into the time-series models enhances the understanding of the physical processes governing fire dynamics in a temporal context.

To achieve this, it is essential to evaluate the predictive performance of various modeling approaches. We emphasize the need in handling complex, high-dimensional data and their effectiveness in both a tabular setting, and spatio-temporal settings. Additionally, there is an attempt to quantify the impact of suppression efforts on wildfire spread, recognizing the challenges due to data limitations and the pervasive nature of suppression activities in California. Identifying and analyzing key environmental, climatic, and anthropogenic factors influencing wildfire spread is another important objective. By providing insights into how these factors contribute to fire dynamics, the research aims to inform policymakers and stakeholders in developing targeted mitigation and adaptation strategies.

1.4 RESEARCH QUESTIONS

These objectives can be summarized in the following key questions:

- RQ1: How effectively can traditional time series models predict wildfire spread using univariate data derived from satellite imagery?
- RQ2: Can incorporating environmental covariates into multivariate time series models improve the accuracy of wildfire spread predictions compared to univariate models?
- RQ3: What is the impact of suppression efforts on the predictive modeling of wildfire spread, and how significant are these factors in the models?
- RQ4: Can spatio-temporal models effectively predict wildfire spread in simulated environments, and what are the limitations when applying these models to real-world data?

By addressing these questions, the thesis aims to advance the field of wildfire modeling through a data-driven approach that not only predicts fire spread but also enhances the interpretability of the models. The ultimate goal is to provide actionable insights that can inform effective wildfire management and mitigation strategies, contributing to the safety and resilience of communities in California and beyond.

1.5 OUTLINE OF THE THESIS

This thesis is structured to provide a comprehensive exploration of predicting wildfire spread in California through time-series analytical methods and spatial-temporal modeling techniques, utilizing processed satellite imagery data. The chapters are organized to build upon each other, offering a logical progression from introduction to conclusion.

Chapter 1 sets the stage by detailing the importance of studying wildfires, particularly in California. It highlights the escalating dangers posed by wildfires globally and justifies the focus on California due to its extensive data availability, diverse ecosystems, and significant suppression efforts. If you are here, you should have already read the chapter and should know what it is about.

Chapter 2 delves into the data aspect of the research. It begins by discussing the original satellite sources used, such as MODIS, VIIRS, and Sentinel satellites, and explains why these sources are suitable for the study. The chapter details the pre-processing steps required to transform raw satellite imagery into usable data. A significant focus is placed on the development of a comprehensive *DataCube*, which

integrates multidimensional data to support downstream tasks like predicting wildfire spread.

Chapter 3 presents the univariate time-series aspect of the study, providing a comprehensive overview of time-series analysis methodologies. It covers both classical statistical techniques and modern deep learning approaches used to predict univariate time-series data.

Chapter 4 builds on Chapter 3. It introduces multivariate time-series models by incorporating environmental covariates. It examines classical machine learning models such as Support Vector Machines (SVM) and demonstrates how integrating additional data factors improves prediction accuracy compared to univariate time-series models.

Chapter 5 focuses on spatial-temporal methodologies for predicting wildfire spread. It mirrors the structure of Chapter 3 and 4 but delves into models that account for both spatial and temporal dynamics. The chapter begins by discussing the creation of a physical simulator for wildfires using a cellular automata model with defined transition probabilities among states (burning, extinguished, unburned). This simulator serves as a tool to generate data for training and validating models.

Chapter 6, and final chapter, provides a comprehensive discussion of the work done, summarizing the key findings and their implications for wildfire prediction and management.

CHAPTER 2

DATA

In this chapter, we describe the satellite instruments and data sources utilized in the rest of the project to model and predict wildfire spread in California. We provide detailed information on each data source, including their spatial and temporal resolutions, capabilities, and relevance to wildfire monitoring. The data sources are grouped according to their function in wildfire modeling: fire detection, weather data, topographic data, and suppression data. Additionally, we discuss ancillary datasets that offer essential environmental variables and land surface characteristics for our analysis. Furthermore, a literature review on different alternatives and a statistical feature analysis of our methodology are presented.

2.1 DATA SOURCES

2.1.1 FIRE DETECTION DATA

Accurate and timely detection of wildfires is critical for monitoring and predicting fire spread. The primary satellite instruments used for fire detection are:

- **Moderate Resolution Imaging Spectroradiometer (MODIS)**
- **Visible Infrared Imaging Radiometer Suite (VIIRS)**
- **Geostationary Operational Environmental Satellites (GOES)**

Each instrument provides unique capabilities that contribute to a comprehensive understanding of wildfire behavior.

MODERATE RESOLUTION IMAGING SPECTRORADIOMETER (MODIS)

The MODIS is an instrument aboard NASA's Terra and Aqua satellites, launched in 1999 and 2002, respectively [53]. MODIS plays a crucial role in Earth observation,

offering data for land, ocean, and atmospheric monitoring.

Key characteristics relevant to fire detection include:

- **Spatial Resolution:** Offers multiple resolutions depending on the spectral band. For active fire detection, thermal infrared bands at 1 km resolution are used, while other bands are offered at resolutions 250 m and 500 m.
- **Temporal Resolution:** Provides near-global coverage every 1 to 2 days, with Terra crossing the equator in the morning (around 10:30 AM local time) and Aqua in the afternoon (around 1:30 PM local time).
- **Fire Detection Products:** The MODIS Active Fire and Thermal Anomalies product (MOD14/MYD14) detects active fires and provides information on fire location, radiative power, and confidence levels [54].

MODIS data have been instrumental in global fire monitoring due to their long-term data record and consistent observations.

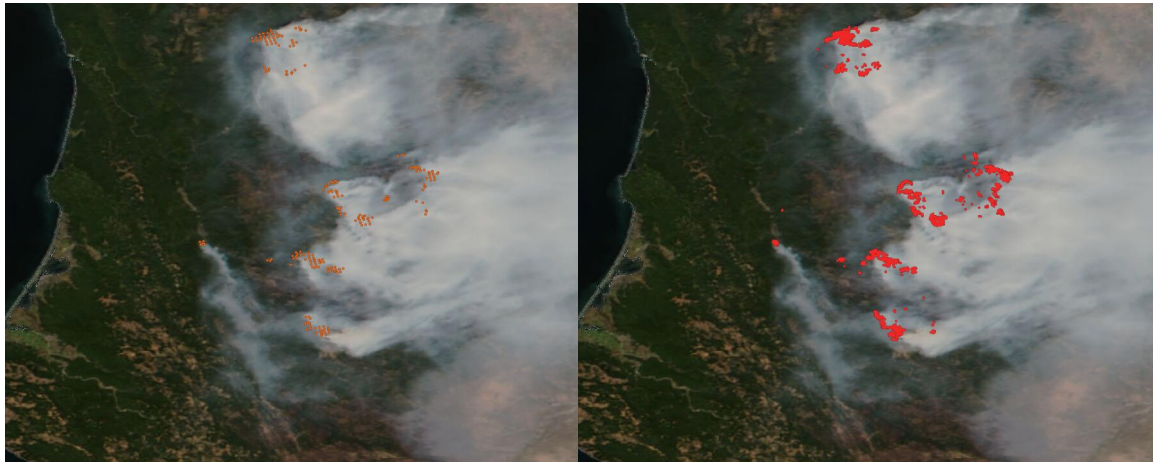


Figure 2.1: Comparison of the North California fires on August 30, 2021, using Terra/MODIS (left) and Suomi NPP/VIIRS (right) layers, overlaid on corrected reflectance from NOAA-20/VIIRS. The VIIRS sensor detects significantly more thermal anomalies than MODIS, highlighting its higher sensitivity to smaller fires. Images were extracted using NASA Worldview.

VISIBLE INFRARED IMAGING RADIOMETER SUITE (VIIRS)

The VIIRS is an instrument aboard the Suomi National Polar-orbiting Partnership (Suomi-NPP) satellite and NOAA-20 satellite [55]. VIIRS builds upon MODIS capabilities with improved spatial resolution and radiometric performance.

Key characteristics include:

- **Spatial Resolution:** Provides data at 375 m (Imaging Bands, I-bands) and

750 m (Moderate Bands, M-bands). The 375 m active fire detection significantly enhances the detection of smaller and cooler fires compared to MODIS.

- **Temporal Resolution:** Similar to MODIS, offers global coverage twice daily, with overpass times around 1:30 AM and 1:30 PM local time.
- **Fire Detection Products:** The VIIRS 375 m Active Fire product (VNP14IMG) provides high-resolution fire detection with improved mapping of fire perimeters and better sensitivity to smaller fires [56].

VIIRS data are crucial for capturing detailed fire dynamics due to their higher spatial resolution.

GEOSTATIONARY OPERATIONAL ENVIRONMENTAL SATELLITES (GOES)

The GOES series, operated by the National Oceanic and Atmospheric Administration (NOAA), where we focus on GOES-16 (GOES-East) and GOES-17 (GOES-West) [57]. These satellites provide continuous observation over the Western Hemisphere from geostationary orbit.

Key features relevant to wildfire monitoring:

- **Spatial Resolution:** The Advanced Baseline Imager provides infrared bands at a spatial resolution of 2 km at the sub-satellite point.
- **Temporal Resolution:** Offers imagery every 5 minutes over the continental United States and full-disk images every 10 to 15 minutes.
- **Fire Detection Products:** The GOES Fire/Hot Spot Characterization product detects active fires, providing fire location, radiative power, temperature, area, and quality indicators [58].

GOES data are vital for capturing rapid changes in fire behavior due to their high temporal resolution.

2.1.2 WEATHER DATA

Weather conditions significantly influence wildfire behavior. Atmospheric variables such as temperature, humidity, wind speed, and wind direction affect fire ignition, spread, and intensity. Only one primary source of weather data used:

ERA5-LAND REANALYSIS DATA

ERA5-Land is a global land-surface reanalysis dataset produced by the European Centre for Medium-Range Weather Forecasts (ECMWF), providing a detailed record of land meteorological variables [59].

Key characteristics include:

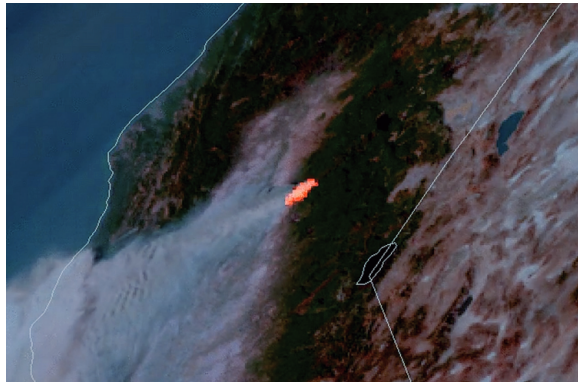


Figure 2.2: Fire hot spots and a large plume of smoke are seen in this GOES-16 fire temperature RGB imagery with GeoColor enhancement of the Camp Fire in northern California on November 8, 2018. Source: NOAA/CIRA

- **Spatial Resolution:** Provides data at a horizontal resolution of 9 km (0.1 degrees).
- **Temporal Resolution:** Hourly estimates of atmospheric variables.
- **Variables:** Includes temperature, wind speed and direction, humidity, precipitation, soil moisture, and more.
- **Applications:** Used for climate monitoring, weather forecasting, and as input for environmental models.

2.1.3 TOPOGRAPHIC DATA

Topography plays a crucial role in wildfire spread, affecting factors like fuel availability and fire propagation. The primary sources of topographic data are:

- **LANDFIRE Landscape Data**
- **National Land Cover Database (NLCD)**

LANDFIRE LANDSCAPE DATA

The LANDFIRE (Landscape Fire and Resource Management Planning Tools) program provides geospatial products to support wildland fire management and ecological assessments [60].

Key aspects include:

- **Content:** Offers spatial data layers on vegetation, fuel characteristics, elevation, slope, aspect, canopy cover, and more.
- **Spatial Resolution:** Data are provided at a 30 m resolution.

- **Applications:** Commonly used by fire behavior and effects models such as FARSITE and FlamMap [61, 62].

These datasets are essential for modeling fire behavior and assessing potential fire effects on the landscape.

NATIONAL LAND COVER DATABASE (NLCD)

The NLCD is a land cover database produced by the Multi-Resolution Land Characteristics (MRLC) Consortium, providing nationwide data on land cover and land cover change [63].

Key characteristics include:

- **Spatial Resolution:** 30 m resolution.
- **Content:** Provides land cover classification, impervious surfaces, and canopy cover.
- **Applications:** Used in environmental assessments, land management, and modeling of ecological processes, including wildfire behavior.

NLCD data complement LANDFIRE by providing detailed land cover information.

2.1.4 HUMAN INTERVENTION

Understanding human factors and infrastructure is important for modeling wildfire suppression efforts and potential impacts. The key datasets include:

- Microsoft Building Footprints
- U.S. Forest Service Data
- ICS-209 Incident Status Summary Reports

MICROSOFT BUILDING FOOTPRINTS

Microsoft has released a dataset of building footprints generated using computer vision algorithms on satellite imagery [64]. This dataset includes over 125 million building footprints across the United States.

Key characteristics:

- **Spatial Coverage:** Nationwide coverage, including California.
- **Format:** Polygon shapefiles representing building outlines.
- **Applications:** Useful for assessing potential wildfire impacts on human structures and planning evacuation or protection measures.

U.S. FOREST SERVICE DATA

The U.S. Forest Service provides various datasets relevant to wildfire management, including information on:

- **Fire Perimeters:** Historical fire perimeters indicating the areas affected by past wildfires.
- **Infrastructure:** Locations of roads, trails, and facilities within national forests.
- **Vegetation and Fuel Models:** Data on forest composition and fuel characteristics.

These datasets are essential for understanding the potential spread of wildfires and planning suppression efforts.

ICS-209 INCIDENT STATUS SUMMARY REPORTS

The ICS-209 forms are used to report incident status information for large wildfires and other significant incidents [65].

- **Content:** Provides detailed information on incident location, size, resources assigned, weather conditions, and other operational details.
- **Temporal Resolution:** Updated regularly during active incidents.
- **Applications:** Used for situational awareness, resource allocation, and historical analysis of suppression efforts.

ICS-209 data offer valuable insights into suppression activities and can be used to model human intervention in wildfire spread.

2.1.5 DATA INTEGRATION FOR WILDFIRE MODELING

By integrating fire detection, weather, topographic, and suppression data enhances the accuracy of wildfire modeling and prediction. The combined data provide:

- **Comprehensive Environmental Profiles:** Merging satellite data with land surface characteristics, atmospheric conditions, and human factors.
- **Improved Spatial and Temporal Resolution:** Leveraging the strengths of each data source to achieve finer resolutions.
- **Enhanced Predictive Capabilities:** Utilizing diverse datasets to inform sophisticated models that can better simulate fire dynamics and suppression efforts.

This integrated approach allows for a more robust analysis of wildfire behavior, contributing to more effective prediction and management strategies.

2.2 RELATED WORK

In this section, we review several notable datasets that have been emerging in this field of wildfire prediction and modeling, highlighting their features, applications, and limitations.

The Multimodal Dataset for Wildfire Risk Prediction in Cyprus combines diverse data modalities to predict wildfire risk [66]. Incorporating meteorological data, vegetation indices, topographical features, and indicators of human activity (as proxied by human trails and streets), the dataset offers high-resolution spatial data (MODIS) suitable for localized risk assessments. Its multimodal nature enables the exploration of how environmental and anthropogenic factors interact to influence wildfire occurrence, aiding in the development of comprehensive risk prediction models and informing policy decisions related to wildfire prevention and management.

Another regional dataset, FireCube, was developed to support the modeling and analysis of wildfires in Greece [67]. FireCube integrates satellite observations, meteorological data, and geographical information into a daily datacube format. This structured approach allows for efficient spatiotemporal analysis of wildfire patterns and environmental conditions. FireCube’s high temporal resolution and regional specificity make it particularly useful for detailed studies of fire dynamics and for developing localized predictive models in the Greek landscape.

In the context of the western United States, SMLFire1.0 is a stochastic machine learning model and dataset that employs stochastic modeling techniques to capture the inherent randomness and uncertainty in wildfire occurrences [68]. By integrating climate data, vegetation indices, historical fire records, and human factors, SMLFire1.0 supports probabilistic predictions of wildfire activity. This approach is valuable for risk assessment and strategic planning, as it accounts for the variability and unpredictability characteristic of wildfire behavior in this region.

Similarly, the Next Day Wildfire Spread dataset focuses on short-term wildfire spread prediction [69]. By combining MODIS active fire data with meteorological variables, vegetation indices, and topographical information, this dataset aims to predict the spatial extent of wildfires one day in advance. Its global coverage enhances its applicability across diverse environmental contexts, making it a valuable resource for operational forecasting and emergency response planning. The dataset’s emphasis on next-day predictions addresses the critical need for timely information in wildfire management.

In the Mediterranean region, the Mesogeos dataset serves as a comprehensive resource for data-driven wildfire modeling [70]. Mesogeos encompasses a wide array of

variables, including high-resolution meteorological data, satellite imagery, land cover maps, elevation models, and socioeconomic factors. This dataset supports various tasks such as wildfire ignition risk assessment, spread modeling, and impact analysis.

Finally, one of the more recent contributions is the WildfireSpreadTS dataset, which provides multi-modal time series data aimed at predicting wildfire spread [71]. It integrates meteorological variables, vegetation indices, and active fire maps derived from satellite observations to capture the temporal dynamics of wildfires. Designed to facilitate spatial-temporal modeling techniques, WildfireSpreadTS enables researchers to predict future fire spread based on historical patterns and environmental conditions.

Despite the significant contributions of these datasets, limitations persist. Many are region-specific, which can restrict their applicability to other geographic areas with different environmental conditions. Variations in spatial and temporal resolutions can affect the granularity and accuracy of models developed using these datasets. Moreover, the integration of diverse data types—such as meteorological variables, topographical information, vegetation characteristics, and human activity indicators—is not uniformly addressed across existing datasets, potentially hindering the development of comprehensive predictive models.

Our study seeks to address these limitations by introducing a novel dataset that integrates fire detection data, high-resolution weather variables, detailed topographic information, and human intervention metrics within a unified framework. By providing fine-grained spatial and temporal resolutions and ensuring accessibility to the research community, our dataset aims to enhance the accuracy of wildfire prediction models. This comprehensive approach facilitates the development of sophisticated models capable of simulating fire dynamics more effectively, ultimately contributing to improved wildfire management strategies and mitigation efforts.

2.3 DATA PROCESSING

In this section, we describe the processing steps involved in preparing the datasets used for wildfire modeling in our project. The datasets include a novel DataCube, the Fire Events Data Suite (FEDS), and the GOES Fire Event Reconstruction (GOFER). Each dataset serves a unique purpose and undergoes specific processing to extract relevant information for wildfire analysis.

2.3.1 DATACUBE

The DataCube is a collection of spatially and temporally aligned features that provide essential environmental and human-related variables for wildfire modeling. It integrates the data from the sources described in Section 2.1, such as satellite imagery,

meteorological data, topographic information, land cover databases, and human infrastructure datasets. Currently, it is a prototype, such that currently there is only one fire in it—the *Creek Fire*—to test and refine our approach before expanding it to include additional fires. The final goal of the DataCube will be to model wildfire spread and damages.

Once the DataCube is refined, the intent is to release it publicly. Thus, we ensure spatial alignment, temporal consistency, and consistent resolution across the different channels with minimal processing. The spatial extent of the Creek Fire was determined by creating a 5-kilometer buffer around the fire perimeter obtained from the *Monitoring Trends in Burn Severity* (MTBS) dataset [72]. MTBS provides detailed maps of burn severity and fire perimeters across the United States from 1984 to the present, derived from Landsat imagery. The purpose of this is to obtain a bit more context than the final perimeter burned, so any model learned is not bounded by the end of the actual fire and can predict further out.

Within the defined bounding box, we extracted relevant data layers and reprojected all datasets to a common coordinate reference system (WGS84). We resampled the data to a uniform spatial resolution of 30 meters, matching the highest resolution datasets from the *National Land Cover Database* (NLCD) and *LANDFIRE*. This resampling ensures spatial consistency, allowing accurate comparison and analysis of variables.

For instance, the NLCD and LANDFIRE datasets, originally at 30-meter resolution, were used directly without resampling. The *ERA5-Land* meteorological data, initially at a coarser resolution of 0.1 degrees (approximately 9 km), were interpolated to match the 30-meter grid. Similarly, the *GOES* active fire data, with a spatial resolution of approximately 2 km, were processed to integrate seamlessly with the 30-meter grid. Finally, for the *Microsoft Building Footprints and Road Networks*, the vector data is converted to raster format at 30 m resolution.

Temporal alignment is also essential, particularly for meteorological variables from ERA5-Land, which were aligned to match the time steps of interest, in this case, hourly. This alignment ensures that all variables correspond accurately across time for any given location, which is critical for dynamic wildfire modeling.

The DataCube includes the following covariates:

- **Topographic Variables:**
 - **Elevation** (km): Derived from LANDFIRE datasets.
 - **Slope** (degrees): Derived from LANDFIRE datasets.
 - **Aspect** (degrees): Derived from LANDFIRE datasets.

- **Land Cover and Fuels:**
 - **Land Cover** (categorical): Classes from NLCD.
 - **Fuel Class** (categorical): Scott and Burgan fuel models from LANDFIRE.
 - **Fuel Load** (tonnes/hectare): Fuel Characteristic Classification System (FCCS) fuel loads from LANDFIRE.
- **Meteorological Variables** (from ERA5-Land, resampled to 30 m):
 - **Mean Temperature** (°C)
 - **Dew Point Temperature** (°C)
 - **Relative Humidity** (%)
 - **Vapor Pressure Deficit** (Pa)
 - **Wind Components** (u and v, m/s)
 - **Wind Speed** (m/s)
 - **Surface Pressure** (Pa)
 - **Precipitation** (mm/h)
- **Human-Environment Variables:**
 - **Distance to Nearest Road** (km): Calculated from LANDFIRE road network data.
 - **Building Locations**: Binary mask indicating the presence of buildings, derived from Microsoft Building Footprints, rasterized to 30 m resolution.
 - **Wildfire Suppression Difficulty Index (SDI97)**: Categorized values indicating the difficulty of fire suppression efforts, obtained from the U.S. Forest Service.

The DataCube is stored as a collection of GeoTIFF files, organized into folders specific to the fire event. Each variable is represented as a raster layer with consistent spatial dimensions and resolutions. For meteorological variables, multi-band GeoTIFFs are used, where each band corresponds to a temporal snapshot (e.g., hourly data). In the case for the Creek Fire we have 1575 bands for each time-series.

By integrating these covariates into the DataCube, we establish an easy-to-use and structured foundation for modeling wildfire behavior. The focus on the Creek Fire allows us to test and refine our data processing methods and modeling approaches. This initial application is a crucial step before incorporating additional variables and expanding the dataset to include more fire events, ultimately enhancing the robustness and applicability of our wildfire modeling efforts.

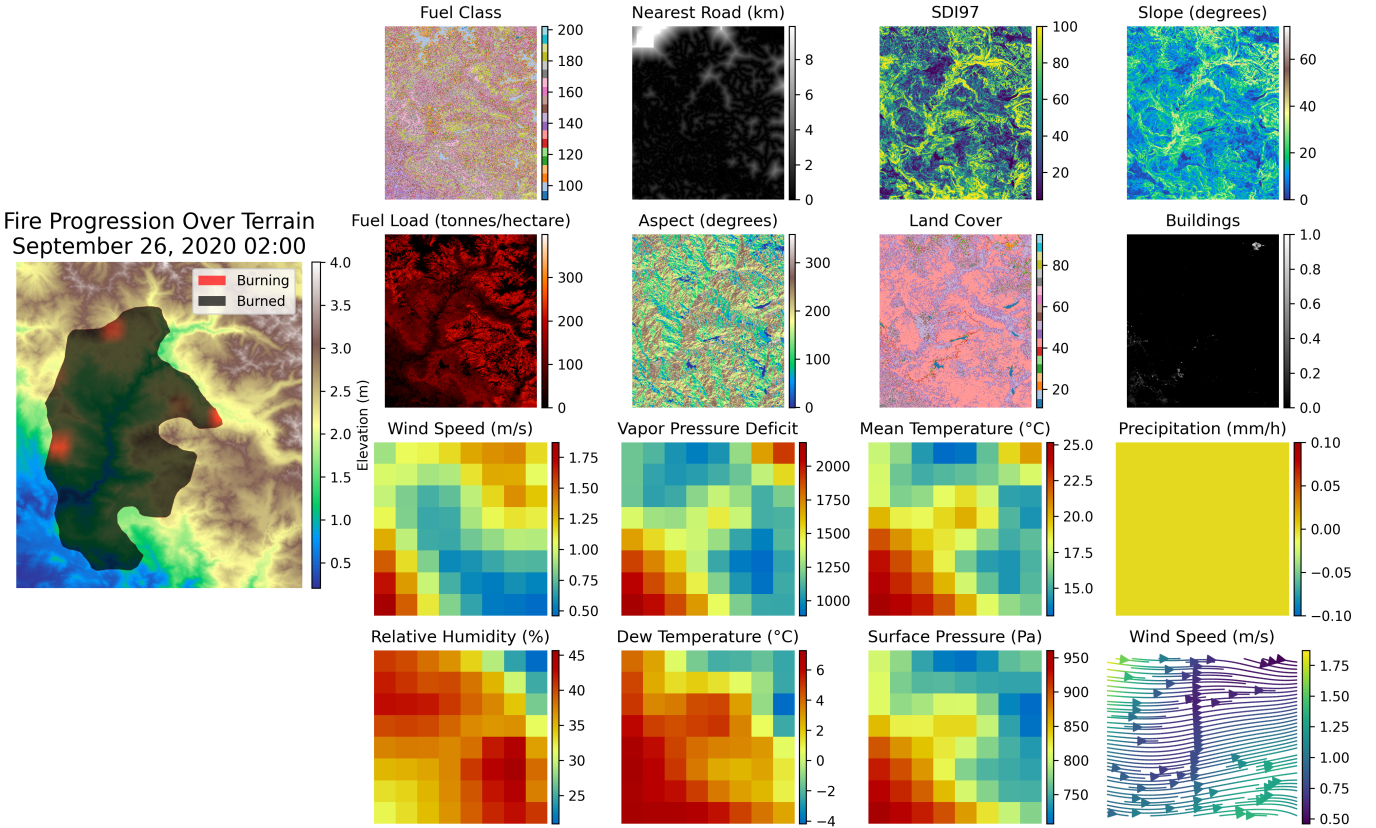


Figure 2.3: Visualization of a slice of the DataCube for the Creek Fire at time step 500. The leftmost panel displays the fire progression overlaid on terrain elevation. Surrounding panels illustrate various environmental and human-related covariates.

2.3.2 FIRE EVENTS DATA SUITE (FEDS)

The Fire Events Data Suite (FEDS) [73] is designed to dynamically track the growth of individual wildfires using data from the Visible Infrared Imaging Radiometer Suite (VIIRS) aboard the Suomi-NPP satellite. VIIRS provides high-resolution (375 meters) active fire detections, typically available twice daily.

In this section, we shall describe how we process the data into a tabular time-series data. The purpose of this is to understand the physical-dynamics of fires and understand how the different covariates impact this spread.

FEDS begins by extracting VIIRS active fire detections within the study area. Each detection includes attributes such as geographical location, fire radiative power (FRP), and confidence levels. We filter the data to retain only high-confidence detections classified as vegetation fires. This ensures that the dataset focuses on relevant wildfire activity while minimizing false positives.

To group active fire detections into individual fire events, FEDS employs spatial

clustering algorithms. Nearby fire pixels detected within the same time step are clustered together to form potential fire objects. The clustering process may utilize data structures like ball trees for efficient nearest-neighbor searches.

FEDS tracks these fire objects over time, updating their perimeters and attributes as new detections are received. When new clusters are in proximity to existing fire objects, they are merged, and their attributes are combined. This dynamic tracking allows for monitoring fires as they grow, split, or merge with other fires.

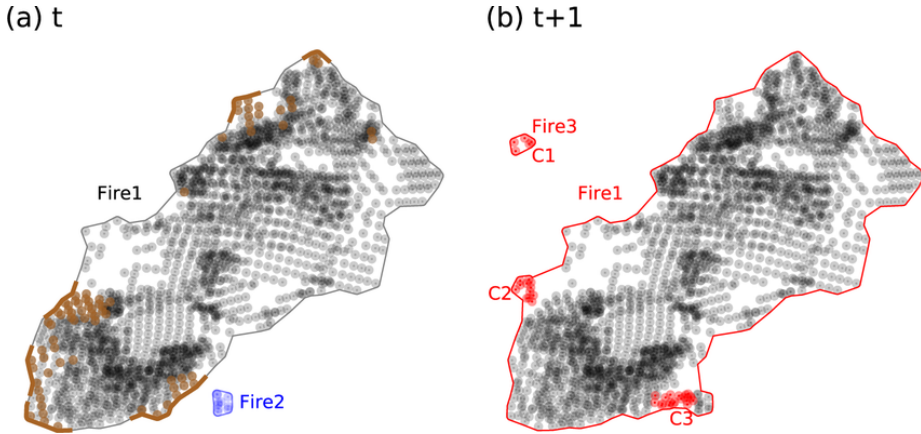


Figure 2.4: Schematic diagram of fire tracking: (a) At time step t , two fire objects are present. Colored and grey dots represent newly detected and previously detected VIIRS active fire pixels, respectively. Brown segments along the fire perimeter indicate active fire fronts. (b) At time $t + 1$, new fire pixels (in red) are clustered into C1, C2, and C3. C1 forms a new fire object (Fire 3), C2 contributes to the growth of Fire 1, and C3 causes Fire 2 to merge with Fire 1 when they grow close enough. Fire perimeters and active fire fronts are updated for each fire object at every time step. Source [73].

To delineate the spatial extent of each fire object, FEDS uses the **alpha shape algorithm**. The alpha shape is a generalization of the convex hull that can capture the concavities and complex geometries of fire perimeters. An optimal alpha parameter (α) is selected based on the characteristics of the wildfires in the study area (e.g., $\alpha = 1$ km for California fires).

The algorithm processes all fire pixels associated with a fire object to generate a concave hull representing the fire perimeter at each time step. To account for the size of the VIIRS pixels and possible gaps between detections, a buffer equal to half the pixel width (approximately 187.5 meters) is applied to the perimeter.

The **active fire line** represents the segments of the fire perimeter that are currently burning. FEDS identifies the active fire line by selecting portions of the perimeter within a certain distance (e.g., 500 meters) of the newly detected active fire pixels. This information is critical for understanding fire behavior and planning suppression

efforts.

2.3.3 GOES FIRE EVENT RECONSTRUCTION (GOFER)

The GOES Fire Event Reconstruction (GOFER) [74] utilizes data from the Advanced Baseline Imager on the Geostationary Operational Environmental Satellites (GOES-16 and GOES-17) to reconstruct wildfire progression with high temporal resolution (every 10 to 15 minutes). Although the spatial resolution is coarser (approximately 2 km), the frequent observations provide valuable insights into rapid changes in fire behavior.

GOES provides active fire detections with associated fire mask codes indicating detection confidence levels. GOFER remaps these codes to continuous confidence values ranging from 0 to 1, facilitating more nuanced processing. For example, a fire mask code representing high confidence might be assigned a value of 0.95.

To improve spatial coverage and accuracy, GOFER combines data from GOES-East and GOES-West satellites. The maximum confidence values from both satellites are considered for each pixel.

Parallax effects, resulting from the satellites' viewing angles and the Earth's terrain, can cause spatial displacement of fire detections. GOFER corrects for parallax using high-resolution digital elevation models (e.g., USGS 3D Elevation Program), adjusting the geolocation of fire detections to their true ground positions.

GOFER applies a dynamic smoothing kernel to the confidence values to reduce noise and create coherent fire perimeters. The kernel size is based on the spatial resolution of the data. After smoothing, an optimized confidence threshold (e.g., 0.95) is applied to filter out low-confidence detections, isolating areas most likely representing active fire fronts.

The thresholded confidence maps are converted from raster to vector format to generate fire perimeters at each time step. Edge smoothing algorithms are applied to eliminate unnatural edges resulting from the pixel-based raster data. Simplification techniques are used to reduce geometric complexity while preserving the accuracy of the fire perimeter, setting a maximum allowable error (e.g., 100 meters).

GOFER identifies the active fire line by intersecting the fire perimeter with high-confidence active fire detections. The fire spread rate is calculated by measuring the expansion of the fire perimeter over time, using methods such as the maximum axis of expansion or area-weighted expansion. This provides insights into the dynamics of fire growth and helps in modeling fire behavior.

2.3.4 CONVERSION TO TIME-SERIES DATA

After obtaining the different FEDS and GOFER fire objects, we convert the data into time-series format to facilitate dynamic modeling of wildfire spread. This transformation captures the temporal evolution of fires, enabling us to analyze changes in fire behavior and environmental conditions over time.

For the FEDS dataset, we focus on fires with multiple time steps to ensure meaningful temporal dynamics. At each time step, we extract variables around the ignition point using a 5-kilometer buffer along the active fire line. Continuous variables (e.g., temperature, wind speed) are averaged within these areas, while categorical variables like land cover and fuel class are assigned based on the most frequent category. Meteorological variables are averaged over a 12-hour period—from the current hour up to 11 hours prior—to account for recent weather influences on fire behavior.

For the GOFER dataset, which offers higher temporal resolution, we extract variables around the active fire line at each time step without additional temporal averaging. This allows us to capture rapid changes in fire dynamics and environmental conditions.

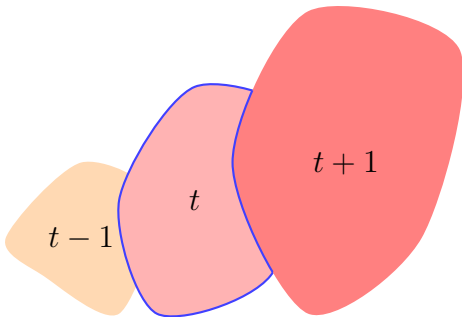


Figure 2.5: Schematic diagram of converting the fire into time-series. The line in blue represents the active fire line, where the environmental variables are sampled to obtain the fire dynamics.

By structuring the data as time series, we enable the application of temporal modeling techniques that ignore the spatial dependency and extract the physical process that makes wildfires spread. This approach enhances our ability to predict wildfire spread more accurately and supports effective wildfire management strategies by capturing the complex interplay between fire behavior and environmental factors.

2.4 STATISTICS

To gain a comprehensive understanding of our tabular time-series datasets, we analyze the key statistics of the Fire Events Data Suite (FEDS) and the GOES Fire

Event Reconstruction (GOFER) datasets, which depending on the satellite will use different fire detection ground truth. This examination provides insights into the datasets' coverage, temporal resolution, and the scale of fire events they capture.

2.4.1 OVERVIEW OF DATASETS

The FEDS dataset comprises 277 unique fires, totaling 8,494 observations. In contrast, the GOFER dataset includes 28 unique fires with a higher number of observations at 19,718. The discrepancy in the number of observations arises from the differing temporal resolutions: GOFER provides hourly data, whereas FEDS offers updates twice daily.

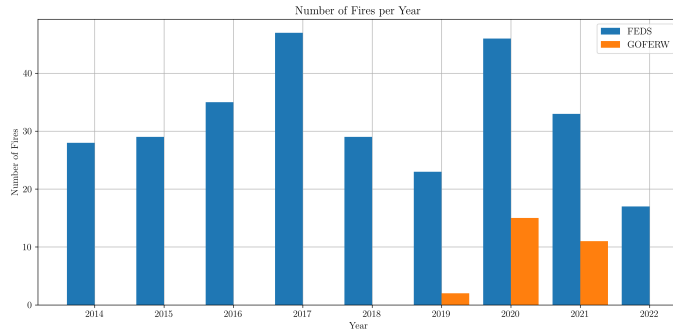


Figure 2.6: Number of fires per year in the FEDS and GOFER datasets. FEDS data spans from 2014 to 2022, while GOFER data is available from 2019 to 2022.

Figure 2.6 illustrates the number of fires recorded each year in both datasets. The FEDS dataset covers a broader time frame from 2014 to 2022, providing a longer historical perspective on wildfire activity. In contrast, the GOFER dataset contains data from 2019 to 2022. The limited temporal coverage of GOFER is due to the current constraints in the data extraction process, which is not fully automated for earlier years, making it challenging to include more fires from previous years.

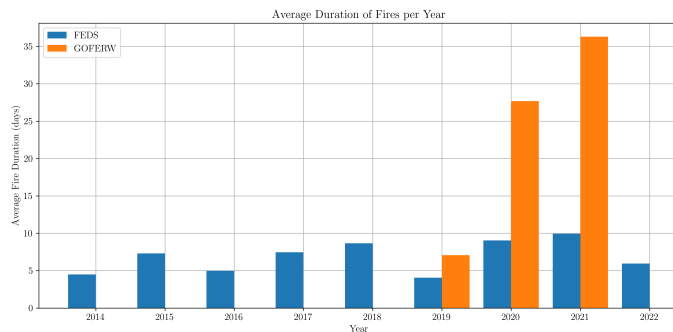


Figure 2.7: Average fire duration per year in the FEDS and GOFER datasets. This metric indicates the typical lifespan of fires captured in each dataset over time.

[Figure 2.7](#) presents the average duration of fires per year in both datasets. Notably, in 2020 and 2021, the average fire duration in the GOFER dataset is significantly longer than in the FEDS dataset. This difference arises because GOFER focuses on large fires, which tend to burn for extended periods.

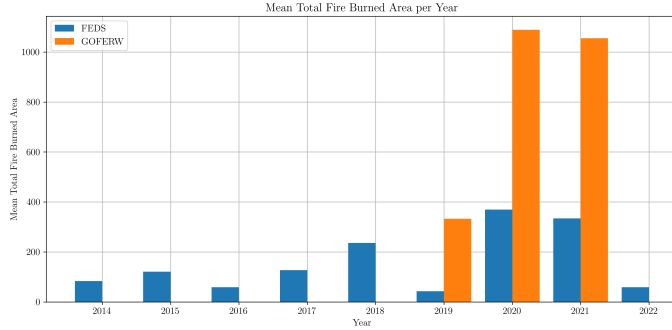


Figure 2.8: Total fire area burned per year in the FEDS and GOFER datasets. This figure reflects the cumulative impact of wildfires annually as captured by each dataset.

[Figure 2.8](#) shows the total area burned by wildfires each year according to the FEDS and GOFER datasets. This metric is essential for assessing the overall severity and environmental impact of wildfires over time. It also helps in evaluating the comprehensiveness of each dataset in capturing significant fire events. Again, since GOFER only has a few very big fires, the average is way bigger than in FEDS.

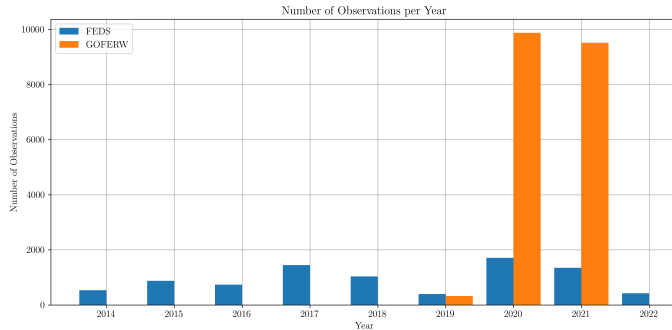


Figure 2.9: Number of observations per year in the FEDS and GOFER datasets. The higher number of observations in GOFER reflects its hourly temporal resolution compared to the twice-daily updates in FEDS.

[Figure 2.9](#) depicts the number of observations recorded each year in both datasets. Despite having fewer unique fires, GOFER has a substantially higher number of observations due to its higher temporal resolution. The hourly data from GOFER allows for more granular tracking of fire progression, which is advantageous for modeling rapid changes in fire behavior.

2.4.2 TARGET VARIABLE: FIRE SPREAD

In this study, our primary objective is to predict the increase in burned area from one time step to the next, effectively modeling fire spread over time. We achieve this by analyzing the polygons representing burned areas obtained from the FEDS and GOFER datasets at each time step. The difference in burned area between consecutive time steps serves as the target variable for our predictive models.

Mathematically, if $A^{(t)}$ denotes the burned area polygon at time step t , and $A^{(t+1)}$ represents the burned area at the next time step $t + 1$, then our target variable is defined as:

$$y^{(t+1)} = A^{(t+1)} - A^{(t)}$$

Our goal is to predict $y^{(t+1)}$ using a set of covariates $\mathbf{X}^{(t)}$ available at time step t .

An important observation in both the FEDS and GOFER datasets is that a significant number of time steps have a *dfarea* (difference in fire area) of zero. This indicates periods where there is no detected increase in the burned area between consecutive time steps. In the GOFER dataset, the median *dfarea* is 0 km², and the 75th percentile is also 0 km², highlighting that more than 75% of the observations show no increase in burned area at the hourly resolution. In the FEDS dataset, although the median *dfarea* is higher at 0.53 km², there is still a substantial proportion of time steps with no area growth, especially during nighttime periods.

This prevalence of zero values can be attributed to several factors:

- **Temporal Resolution:** At higher temporal resolutions (e.g., hourly in GOFER), the incremental changes in burned area can be minimal or below the detection threshold of the satellite sensors, resulting in recorded zero growth.
- **Fire Behavior:** Fires may naturally have periods of low activity due to factors like reduced fuel availability, increased humidity, or firefighting efforts.
- **Detection Limitations:** Satellite-based fire detection is influenced by atmospheric conditions, sensor capabilities, and algorithm thresholds, which may fail to detect small increments in burned area.

As illustrated in [Figure 2.10](#), there is a noticeable increase in fire spread during the afternoon hours, peaking in the late afternoon, and a decline during the night. Moreover, analyzing the *dfarea* by time of day in the FEDS dataset reveals that fire spread tends to be greater during the daytime compared to nighttime. The mean *dfarea* during the day is approximately 7.73 km², while at night it decreases to about 3.55 km². This pattern aligns with expected fire behavior, as higher temperatures and lower humidity during the day promote fire spread, whereas cooler and more

humid conditions at night suppress it.

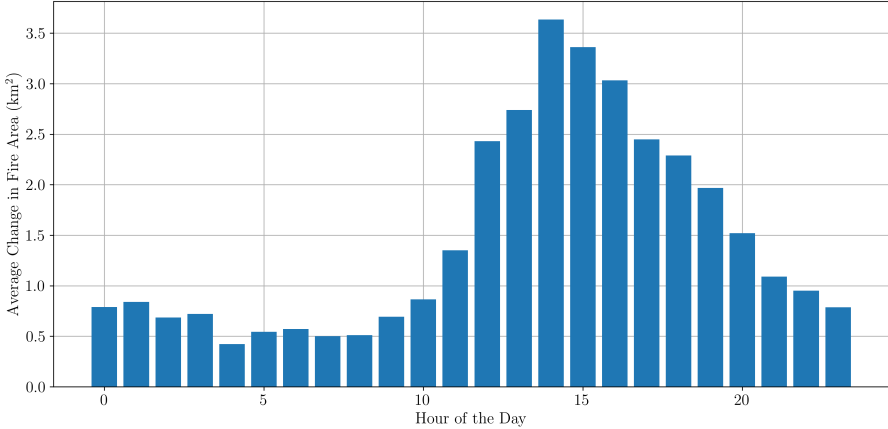


Figure 2.10: Average $dfarea$ by hour in the GOFER dataset. The plot shows increased fire spread during the afternoon hours, with reduced activity during nighttime.

CHALLENGES IN FIRE DETECTION

Accurately detecting and monitoring wildfires using satellite data is inherently challenging due to various factors that can affect the reliability of fire detection products. Some of the main issues include:

- **Cloud Cover:** Clouds can obscure the satellite's view of the Earth's surface, hindering the detection of active fires.
- **Controlled Burns:** Agricultural or prescribed fires may be detected as wildfires, leading to false positives.
- **Smoke and Atmospheric Conditions:** Smoke plumes and atmospheric aerosols can interfere with the sensors' ability to detect thermal anomalies.
- **Other Heat Sources:** Industrial activities, volcanic activity, and solar reflection from surfaces like solar panels can be misinterpreted as fire hotspots.

It is important to note that all fire detection products we use, such as those from MODIS, VIIRS, and GOES satellites, are not perfect. They rely on algorithms that detect thermal anomalies or hotspots on the land surface [75]. These algorithms use predefined thresholds and contextual tests to determine whether a pixel represents an active fire. However, they may not always accurately distinguish between actual fires and other sources of heat or reflection. As can be visualized in Figure 2.11 which illustrates an example where VIIRS detected a hotspot in an area that, upon closer examination using high-resolution imagery, is actually a solar panel field. The reflectance and thermal properties of the solar panels can trigger false fire detections.



Figure 2.11: An example of false fire detection by VIIRS. VIIRS reflectance bands corrected for 2019-01-03, showing detected hotspots (left). Corresponding Google Earth image of the area, revealing solar panel fields (right). The VIIRS detection mistakenly identifies the solar panels as active fires due to high reflectance and thermal characteristics.

While there are some limitations, we will take the satellite detections in all datasets (FEDS, GOFER, DataCube) as the ground truth. After removing the detections that are solar panel fields, of course.

All covariates are data extracted at time step t , or a previous time step. Therefore, we can use any of these variables to predict $y^{(t+1)}$, the change in burned area at the next time step. Throughout this thesis, references to the target feature, increase/change in area, or fire spread prediction all pertain to forecasting $y^{(t+1)}$.

2.4.3 COVARIATES: FIRE

We examine the impact of the *Active Fire Line Length* on the change in fire spread by plotting their relationship on a logarithmic scale (see [Figure 2.12](#)). The plot shows that as the active fire line length increases, the subsequent fire spread also tends to increase. This observation makes sense because the active fire line represents the outermost perimeter of the burning area. A larger active fire line suggests a greater potential for the fire to expand and consume more vegetation compared to a smaller active fire line.

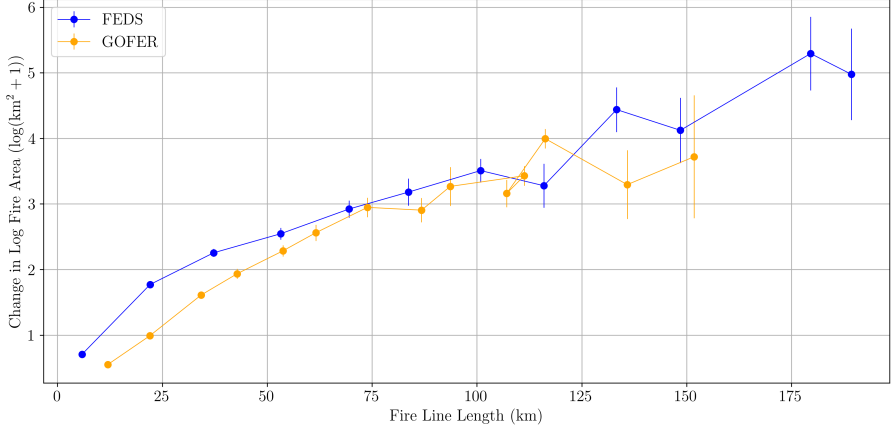


Figure 2.12: Relationship between the change in fire area ($y^{(t+1)}$) and the active fire line length at time t on a logarithmic scale. The plot indicates that larger active fire lines are associated with greater increases in burned area at the next time step.

Figure 2.13 presents the correlation matrices for the fire variables in the FEDS and GOFER datasets. We will continue our analysis focusing on those figures. The accumulated burned area ($A^{(t)}$) at time t and the fire perimeter (the current perimeter of the fire polygon) are highly correlated, as one would expect. Both variables measure aspects of the fire’s size, and as the burned area increases, the perimeter typically expands correspondingly.

In wildfires, the Fire Radiative Power (FRP) is usually considered quite important. Measured in megawatts (MW), it provides information on the radiant heat output of detected fires. It has been demonstrated in small-scale experimental fires that the amount of radiant heat energy released per unit time (FRP) is related to the rate at which fuel is being consumed. This relationship arises because the combustion of carbon-based fuel to CO₂ releases a specific amount of heat energy [76].

However, in our analysis, *meanFRP* does not exhibit a strong correlation with other variables, showing only a modest correlation (0.13) with the target feature $y^{(t+1)}$. This suggests that while FRP is theoretically linked to fire intensity and fuel consumption rates, it may not be a strong predictor of the change in burned area in our datasets, possibly due to measurement uncertainties or the influence of other factors.

The variable representing the number of new pixels indicates the count of new VIIRS fire detections observed at time t . This variable can provide insight into the fire’s activity level, as a higher number of new detections may correspond to increased fire spread or intensity.

Overall, these fire variables exhibit varying degrees of correlation with one another, which is not surprising given that they are derived using the same satellite instru-

ments and processing methodologies.

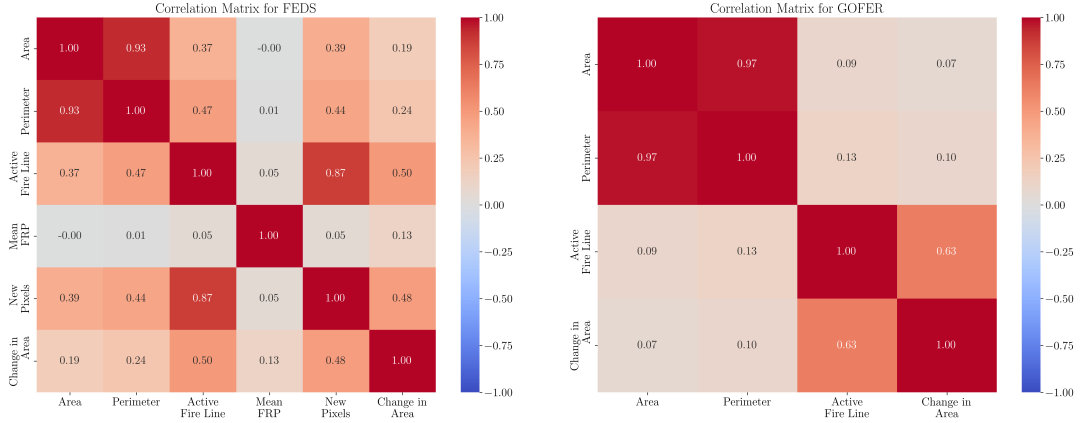


Figure 2.13: Correlation matrices for fire variables: (left) FEDS dataset; (right) GOFER dataset. The color intensity indicates the strength of the Pearson correlation coefficients between variables, with darker colors representing stronger correlations.

2.4.4 COVARIATES: WEATHER

We sample weather data from two locations: the active fire line and the ignition point. Upon examining the correlations between different weather variables and the change in burned area, we observe that for both the FEDS and GOFER datasets, variables such as Vapor Pressure Deficit (VPD), mean temperature, and wind speed are most positively correlated with fire spread. Conversely, relative humidity and dew point temperature show negative correlations. In the FEDS dataset, dew point temperature appears less relevant.

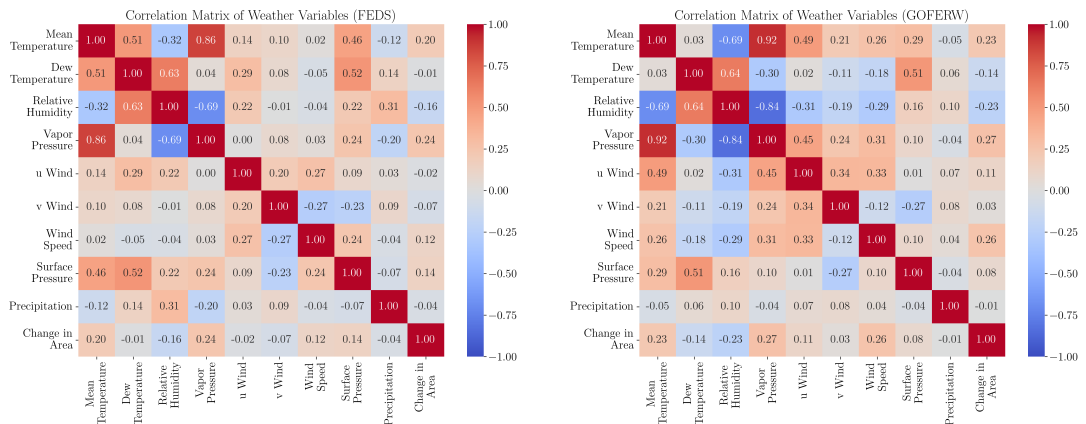


Figure 2.14: Correlation matrices of weather variables for the FEDS (left) and GOFER (right) datasets. The color intensity indicates the strength of the correlation between variables, with darker colors representing stronger correlations.

Overall, weather variables extracted at the ignition point do not provide significant

additional information compared to those extracted at the active fire line. This is evident from the high correlations between corresponding variables at both locations, as shown in [Table 2.1](#). This redundancy is expected since the spatial resolution of the meteorological data is relatively coarse, resulting in similar values over nearby areas.

Table 2.1: Correlation coefficients between weather variables at the active fire line and ignition point for the FEDS and GOFER datasets. High correlation values indicate similar information content from both locations.

Variable	FEDS Correlation	GOFER Correlation
Mean Temperature	0.978	0.970
Dew Point Temperature	0.980	0.955
Relative Humidity	0.973	0.967
Vapor Pressure Deficit	0.975	0.972
U-component Wind	0.956	0.878
V-component Wind	0.973	0.926
Wind Speed	0.955	0.882
Surface Pressure	0.957	0.858
Precipitation	0.980	0.817

Vapor Pressure Deficit (VPD) is considered an important factor in wildfire dynamics [[77](#), [78](#)]. VPD measures the difference between the amount of moisture in the air and the amount it can hold when saturated; it reflects the atmosphere's drying power. Generally, as VPD increases, the risk of fire spread also increases due to the enhanced drying of vegetation.

VPD is calculated from temperature and relative humidity using the formula:

$$\text{VPD} = e_{\text{sat}}(T) \times \left(1 - \frac{\text{RH}}{100}\right),$$

where $e_{\text{sat}}(T)$ is the saturation vapor pressure at temperature T , and RH is the relative humidity in percent.

Observing [Figure 2.15](#), we notice an increase in fire spread with higher VPD values. The decrease at the highest VPD values is likely due to a smaller number of observations under extreme conditions, which may not represent the overall trend.

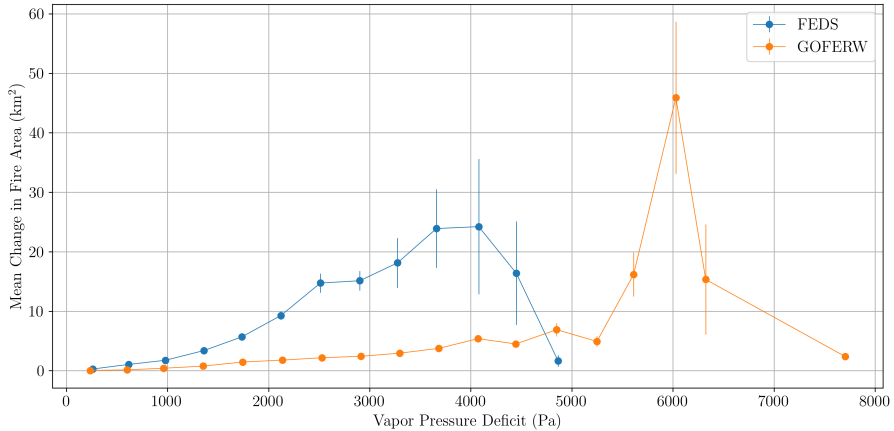


Figure 2.15: Relationship between change in fire area ($y^{(t+1)}$) and Vapor Pressure Deficit (VPD). Higher VPD values are associated with greater fire spread.

Similarly, wind speed shows a positive correlation with fire spread (Figure 2.16, left). Strong winds can facilitate the rapid spread of fires by carrying embers and increasing oxygen supply to the fire front. Mean temperature also exhibits a positive relationship with fire spread (Figure 2.16, right), as higher temperatures can dry out fuels and lower the ignition threshold.

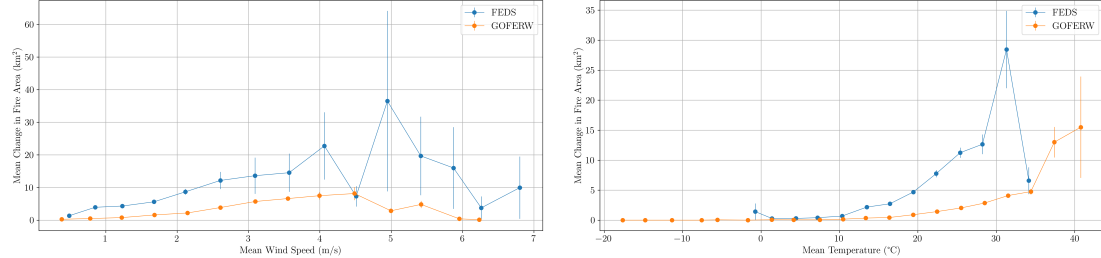


Figure 2.16: Relationship between change in fire area ($y^{(t+1)}$) and (left) wind speed, (right) mean temperature. Both variables show a positive association with fire spread.

Conversely, relative humidity shows a negative correlation with fire spread (Figure 2.17). Higher relative humidity indicates more moisture in the air, which can dampen fuels and reduce the likelihood of fire spread.

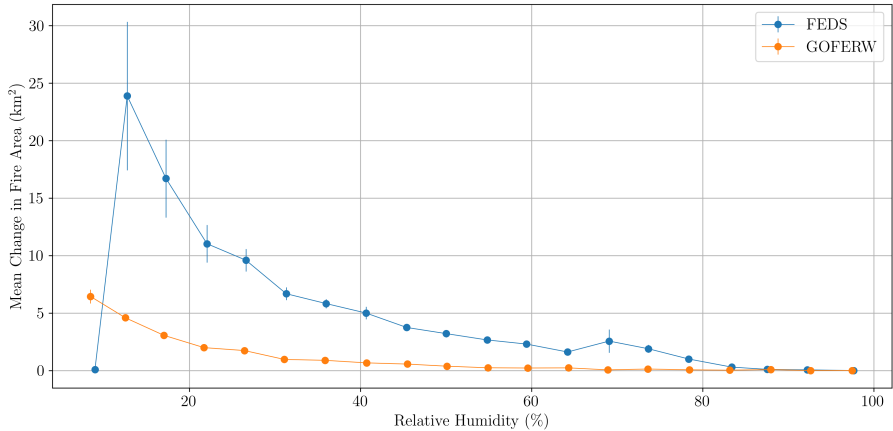


Figure 2.17: Relationship between change in fire area ($y^{(t+1)}$) and relative humidity. Higher relative humidity is associated with reduced fire spread.

2.4.5 COVARIATES: TOPOLOGY

Topological variables capture the terrain characteristics that influence wildfire spread. Among these, elevation stands out as the most significant factor. Higher elevations can act as natural barriers, limiting the fire's ability to jump over terrain obstacles. Observing Figure 2.19 seems to indicate that changes in elevation significantly affect the change in burned area, as illustrated. Specifically, when elevation differentials exceed 2.5 meters, fires struggle to expand, resulting in smaller spreads.

Other topological variables, such as slope and topographic variance, show weaker correlations with the target feature (Figure 2.18), suggesting that their impact on fire spread is more nuanced and may depend on specific temporal contexts. This variability indicates that while terrain features are important, their influence on fire dynamics is less straightforward compared to elevation.

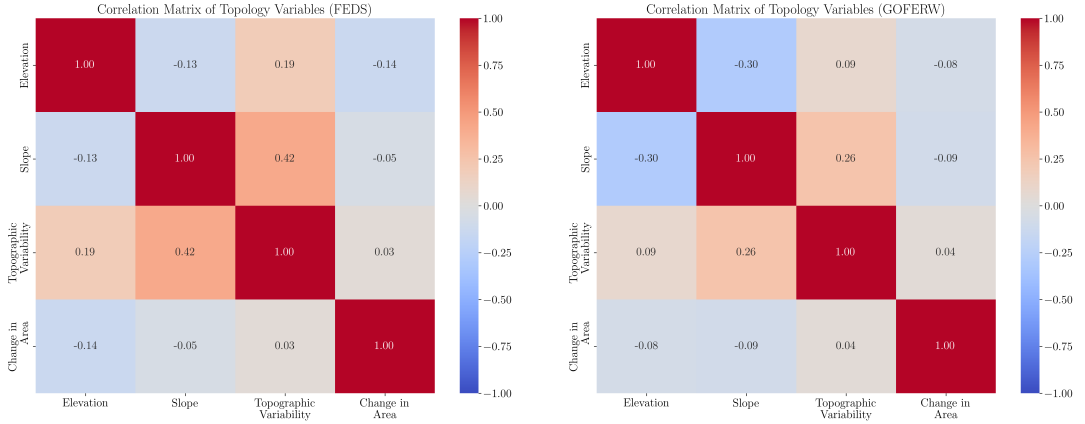


Figure 2.18: Correlation matrices of topological variables for the FEDS (left) and GOFER (right) datasets. Color intensity indicates the strength of the Pearson correlation coefficients, with darker colors representing stronger correlations.

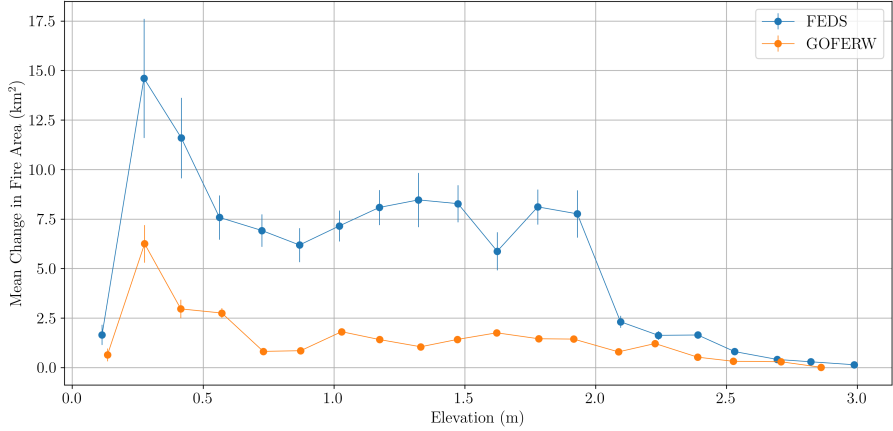


Figure 2.19: Relationship between the change in fire area ($y^{(t+1)}$) and elevation at time t . Elevation changes above 2.5 meters are associated with reduced fire spread.

2.4.6 COVARIATES: FUEL

Fuel refers to the type of combustible materials in the environment, primarily represented by two variables: fuel load and fuel class. For fuel load, we reference [79], and for fuel class, we utilize two distinct models: the Scott and Burgan Fire Behavior Fuel Model [80] and the Anderson Land Cover Classification System [81].

The 40 Scott and Burgan Fire Behavior Fuel Model provides a more detailed breakdown of fuel loads, incorporating dynamic components like herbaceous materials that shift between live and dead states, which affect fire behavior. It expands on Anderson's model, offering more detailed representations for grass, shrub, timber fuels. This distinction allows for better simulation of fuel dynamics in different environmental conditions.

For fuel class (Figure 2.20), observations show a relationship between specific classes and fire behavior. Non-burnable (NB) areas generally exhibit lower fire spread compared to grasslands, especially high-load grass categories like GR7 and GR8, which display rapid and extensive fire spread. GR2 and TU5, representing low-load grass and high-load timber shrub, also show noticeable increases in fire spread.

We can also witness some of these effects in Anderson's land cover model. Water bodies exhibit the lowest fire spread, while evergreen and mixed forests show higher spread. Shrublands and grasslands, especially cultivated crops, also exhibit varied effects, likely due to their scarcity in the dataset.

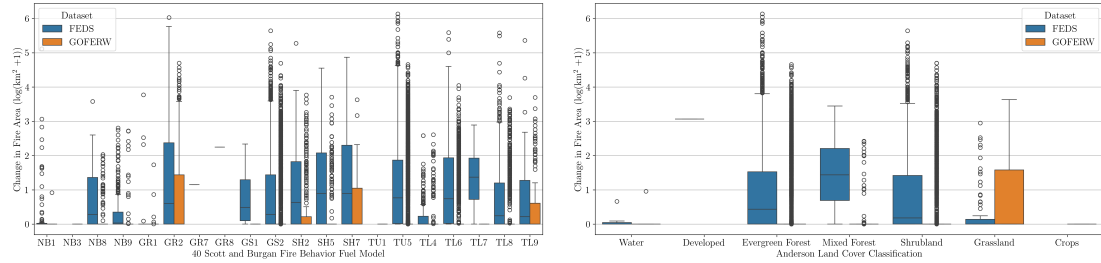


Figure 2.20: Fire Spread Across Different Fuel Classes and Land Covers. Left: Scott and Burgan Fire Behavior Fuel Model, Right: Anderson Land Cover Classification System

As for the fuel load, there appears to be no significant correlation between it and fire spread, as indicated by the low correlation coefficient (-0.07). Moreover, in Figure 2.21, we can see that there is no clear increase in the fire spread depending on the fuels that are nearby. This could be due that we are analyzing some of the more severe fires and the effect is not as pronounced as other factors are more relevant.

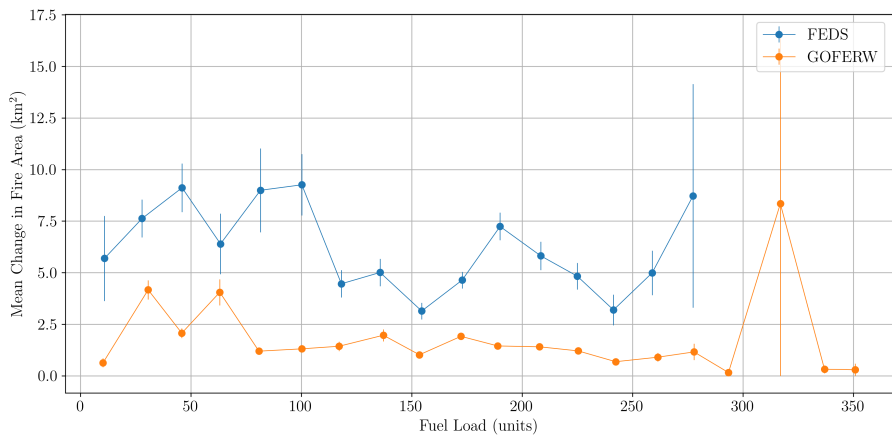
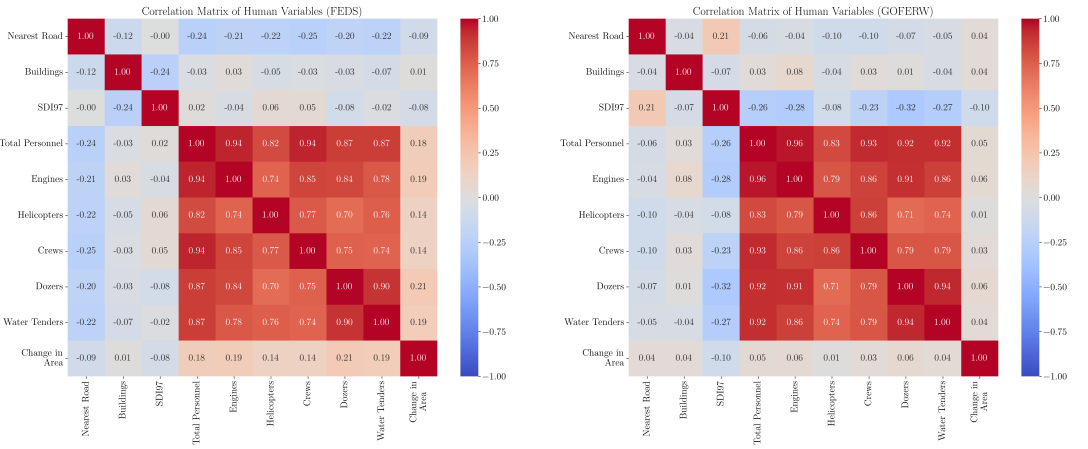


Figure 2.21: Effect of Fuel Load on Fire Spread

2.4.7 COVARIATES: HUMAN INTERVENTION

Several covariates reflect human intervention, such as nearby buildings, distance to the nearest road, and the Wildfire Suppression Difficulty Index at the 97th percentile (SDI97). Additionally, suppression efforts data from ICS209 reports include variables like total personnel, engines, helicopters, crews, dozers, and water tenders. Roads, in particular, also act as fire breaks.

The key question is whether these interventions affect wildfire spread. Intuitively, we expect that more personnel and equipment should lead to reduced fire spread. However, as shown in [Figure 2.22](#), there is a small positive correlation between suppression efforts and fire spread. This is likely because as fires become more intense, more resources are deployed to control them.



[Figure 2.22](#): Correlation matrices of human intervention variables for the FEDS (left) and GOFER (right) datasets. Darker colors represent stronger correlations (Pearson coefficients).

Furthermore, suppression variables are highly correlated, thus, we will use total personnel as a proxy for suppression efforts. Linear combinations of these, such as a PCA, and other dimensionality reduction algorithms have been tested to aggregate the suppression into one feature, but the benefits outweighed the ease to understand as just using total personnel. Searching for other correlations, we found that personnel is moderately correlated with accumulated fire area. Which makes sense since as the more a fire spreads out, the more places suppression units can be.

While there are many plots like the ones we have done before to try and understand our data better, they are quite misleading. These are not really cause and effect and could confuse the reader. Thus, these are omitted. Instead, to try and evaluate the effectiveness of suppression efforts, we compared the change in fire spread, $\log(y^{(t)} + 1) - \log(y^{(t-1)} + 1)$, to total personnel at time ($t - 1$) in [Figure 2.23](#). If the result is negative, it suggests that suppression efforts helped reduce the fire spread compared

to the previous time step. If positive, it indicates the fire continued to grow despite the efforts.

In the hourly data, suppression efforts do not appear to reduce fire spread, and in some cases, fire growth even increases despite significant intervention, suggesting a lack of control. However, in the 24-hour FEDS data, there is a clearer trend where more personnel seem to have a greater suppression effect, though this effect is not always consistent.

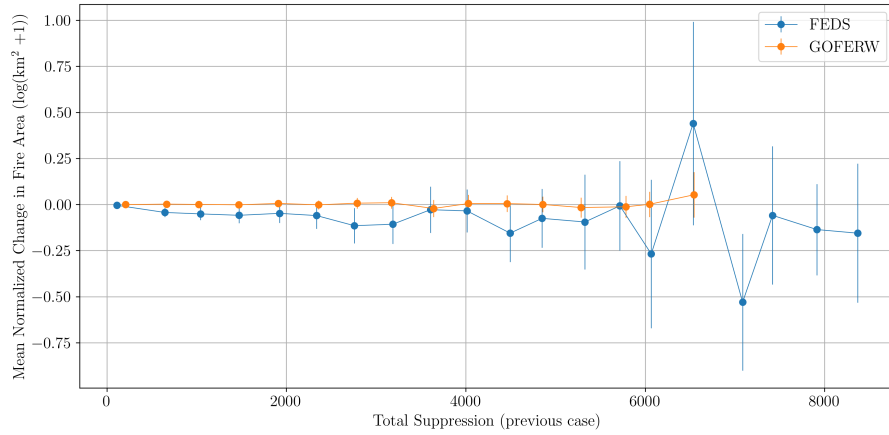


Figure 2.23: Normalized difference in fire spread compared to total personnel from the previous time step.

Overall, the impact of suppression efforts on fire spread is difficult to assess conclusively. The modeling section will explore whether there are underlying non-linear effects that may provide further insight.

2.4.8 DIMENSIONALITY REDUCTION

We applied dimensionality reduction techniques to gain further insight into the data, but the results were not particularly revealing. A biplot of the PCA, including the loadings, shows that fire spread (dfarea) is correlated with nearby buildings, wind speed, and vapor pressure deficit (VPD). However, these findings largely confirm what we have already observed in previous analyses, offering little additional information. With 2 principal components we explain 35% of the variance, and we need 8 to arrive at 85%.

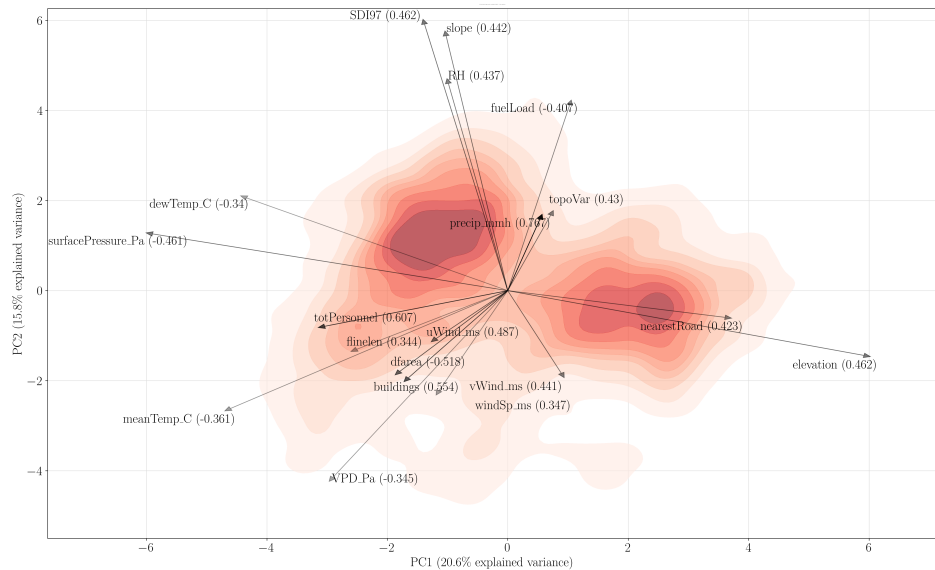


Figure 2.24: PCA biplot for the FEDS dataset. Data was normalized using a standard scaler. Point density is plotted instead of individual points for clarity.

CHAPTER 3

UNIVARIATE TIME SERIES

In this chapter, we explore the analysis of univariate time series, with a focus on predicting the Burned Fire Area using only the target feature’s signal. Specifically, the objective is to forecast the Burned Fire Area based on the previous time step or the difference between consecutive time steps.

Wildfires present unique challenges compared to typical time series encountered in classical literature. Unlike many time series that exhibit prolonged periods of fluctuation, wildfires are characterized by distinct beginnings and endings, often lasting no more than a few days. This finite timeframe introduces specific dynamics that must be accounted for in modeling.

Additionally, our datasets encompasses multiple wildfire events rather than a single continuous series. Traditional time series models typically rely on long, fluctuating sequences to predict future values, whereas our goal is to develop a model capable of predicting the evolution of any new wildfire event based on its initial progression.

3.1 BACKGROUND

A univariate time series consists of sequential observations of a single variable recorded at regular intervals. The primary aim of time series analysis is to uncover the underlying mechanisms that generate the observed data and to forecast future values accurately.

Time series data exhibit several key characteristics, including trends, seasonality, cycles, and irregular fluctuations. Understanding and modeling these components are essential for effective analysis and forecasting.

The **trend component** (T_t) represents the long-term increase or decrease in the data. **Seasonality** (S_t) refers to regular, periodic patterns that repeat over fixed

intervals, while the **random component** (R_t) captures random variations or noise inherent in the data.

Mathematically, a time series can be modeled by combining these components in either an additive or multiplicative manner:

$$Y_t = T_t + S_t + R_t \quad (\text{Additive Model}),$$

$$Y_t = T_t \times S_t \times R_t \quad (\text{Multiplicative Model}).$$

Determining the appropriate model structure depends on the nature of the underlying components.

3.1.1 STATIONARITY

Many time series models, such as the Autoregressive Integrated Moving Average (ARIMA) model, assume that the series is stationary. A stationary time series has constant statistical properties—mean, variance, and autocorrelation—over time. Non-stationarity can result from trends, seasonal effects, or structural changes within the data.

To achieve stationarity, differencing can be applied to remove trends and stabilize the mean:

$$\Delta Y_t = Y_t - Y_{t-1}.$$

For seasonal data with period s , seasonal differencing is employed:

$$\Delta_s Y_t = Y_t - Y_{t-s}.$$

This process may be repeated until stationarity is attained, which justifies predicting the increment of the fire area rather than the raw values. This transformation simplifies the modeling problem by mitigating non-stationary behavior.

Our goal is to predict the Burned Fire Area at a given time step based on the previous one (Figure 3.1). However, to achieve a more stationary series, we can take the difference between consecutive time steps, focusing on the change in burned area (Figure 3.2). This approach not only simplifies the problem but also standardizes the behavior across different fires, allowing us to model the spread of the fire independently of its size.

To handle the prevalence of zeros and substantial jumps in the target variable, we apply a logarithmic transformation:

$$\log(Y_t + 1).$$

This transformation addresses the skewness in the data and converts a potential multiplicative trend into an additive one, facilitating more straightforward modeling.

To assess the stationarity of the time series, we applied both the KPSS [82] and the ADF [83] tests for the Creek fire on the FEDS dataset on the logarithmic differences.

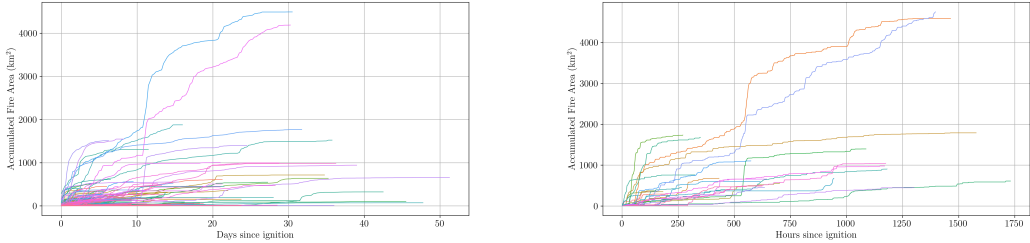


Figure 3.1: Accumulated Burned Fire Area over Time for Different Resolutions: (Left) 12-hour resolution (FEDS), (Right) 1-hour resolution (GOFER)

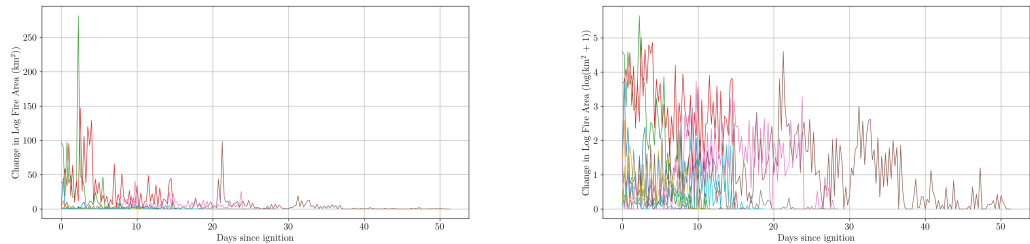


Figure 3.2: Difference in Burned Area for Sample Fires from FEDS: (Left) Raw Differences, (Right) Log-transformed Differences $\log(Y_t + 1)$

The KPSS test evaluates the null hypothesis that the series is stationary around a mean or trend, and our results (test statistic = 2.534, p-value = 0.01) indicated non-stationarity, as the test statistic exceeded all critical values. Conversely, the ADF test examines whether the series has a unit root (i.e., non-stationary), and the results (test statistic = -4.333, p-value = 0.0004) provided strong evidence against the null hypothesis, suggesting stationarity.

The disagreement with both tests suggest that the series is difference stationary, and adding higher order differencing could achieve stationarity. Nevertheless, while these findings are informative, we face limitations in applying these tests across multiple time series, as doing so could lead to inflated Type I errors, making the p-values statistically significant by chance. Additionally, increasing the number of differences would delay time-critical wildfire predictions, and although many models require stationarity, they are generally robust enough to handle non-stationary data to some extent.

3.1.2 AUTOCORRELATION ANALYSIS

Examining the autocorrelation function (ACF) of the differenced burned area increments Y_t reveals significant autocorrelations at various lags, particularly in the

GOFER dataset. The autocorrelation at lag k is defined as:

$$r_k = \frac{\sum_{t=k+1}^T (Y_t - \bar{Y})(Y_{t-k} - \bar{Y})}{\sum_{t=1}^T (Y_t - \bar{Y})^2},$$

where \bar{Y} is the mean of the series.

Positive autocorrelations at small lags indicate that consecutive observations are closely related, a common characteristic in trending time series. This phenomenon is evident in our data ([Figure 3.3](#)), where wildfire activity tends to decline after periods of expansion, reflecting the finite duration of each event.

Seasonal effects may also be present. Although individual wildfires do not span entire years, there is evidence of daily seasonality. Specifically, the ACF plots for the GOFER dataset show a slight increase at lag 24, corresponding to a 24-hour cycle ([Figure 3.3](#)). This pattern aligns with daily temperature fluctuations, which influence wildfire behavior.

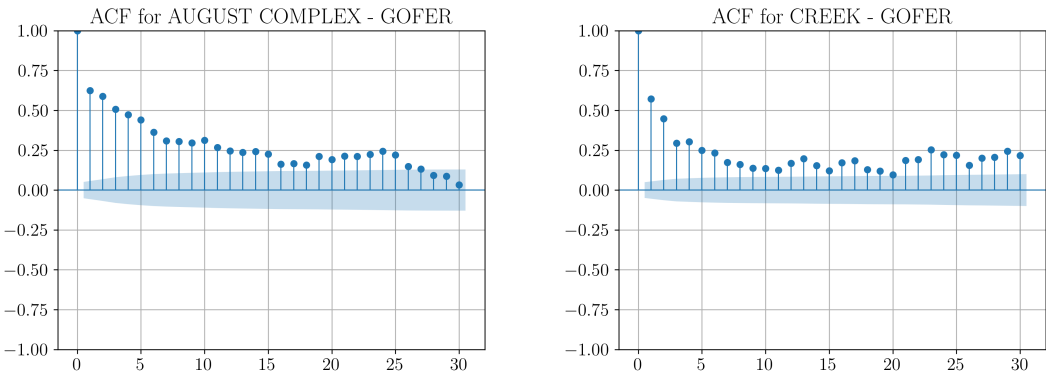


[Figure 3.3: Autocorrelation Function of Differenced Burned Area: \(Left\) August Complex, \(Right\) Creek](#)

In contrast, the FEDS dataset exhibits reduced autocorrelation due to the aggregation of data into 12-hour intervals ([Figure 3.4](#)), compared to the 1-hour intervals in GOFER. While some autocorrelations remain significant, particularly at lower lags, the overall pattern is less pronounced. This reduction is expected, as aggregation tends to smooth out short-term dependencies. Nevertheless, many fires in the FEDS dataset show negligible autocorrelation even at the first lag.

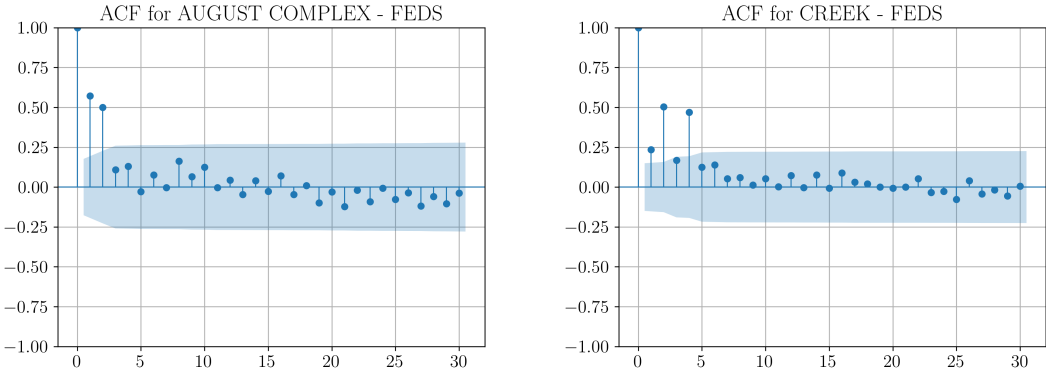


Figure 3.4: Autocorrelation Function of Differenced Burned Area in FEDS: (Left) August Complex, (Right) Creek

The presence of statistically significant autocorrelations in both datasets confirms that the series contain meaningful signal beyond random noise. This insight underscores the potential for developing robust predictive models based on the temporal dynamics of the burned area.

3.1.3 STL DECOMPOSITION

To further analyze the underlying components of the burned fire area time series, we employ the Seasonal-Trend Decomposition Procedure based on Loess (STL) [84]. STL is a robust and versatile method for decomposing a time series into its trend, seasonal, and residual components, allowing for the extraction of meaningful patterns from complex data.

For the FEDS dataset, we set the seasonal period to 2, corresponding to 12-hour intervals, effectively capturing a 24-hour daily cycle. Additionally, we specify a seasonal window of 11, which facilitates the extraction of the day-night periodicity from the data. This configuration successfully isolates the daily seasonal effects, providing a clear separation between trend and seasonality.

In contrast, the GOFER dataset presents a more intricate scenario due to the absence of the smoothed 12-hour intervals observed in FEDS. Here, we set the seasonal period to 24 hours to account for the daily seasonality directly. However, this approach introduces increased noise in the residual component, primarily because the finer granularity of GOFER data lacks the inherent smoothing present in the FEDS dataset. As a result, the residuals exhibit more variability, reflecting the challenges in isolating seasonality without the benefit of aggregated smoothing.

Furthermore, the residuals in the GOFER decomposition reveal discernible patterns. These patterns emerge as the STL algorithm attempts to extract seasonality in the

absence of a prominent trend, particularly during periods when the wildfire has been extinguished. This phenomenon indicates that some structured variability remains in the residuals, potentially due to abrupt changes in fire activity or other underlying factors not fully captured by the seasonal component.

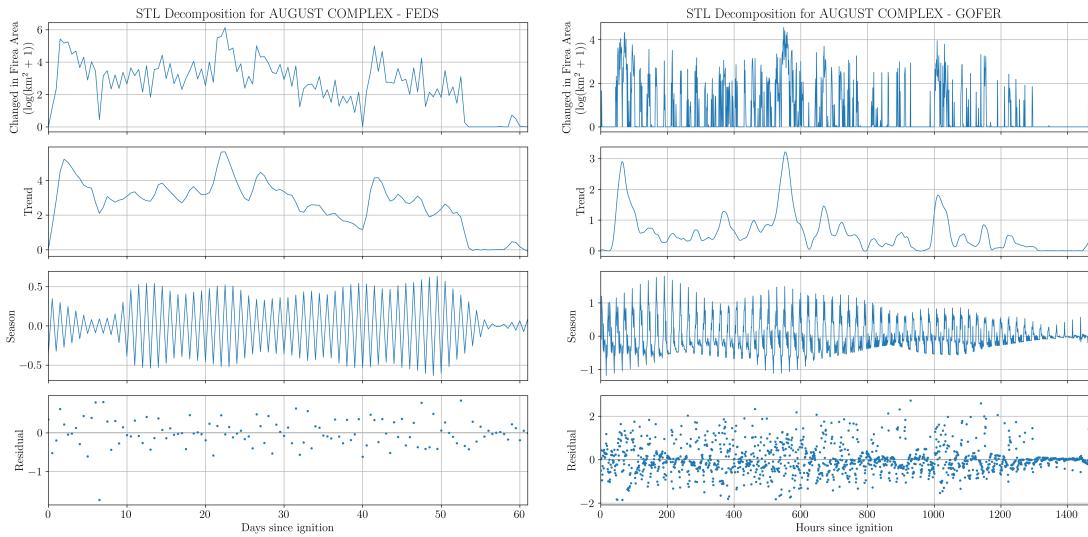


Figure 3.5: STL Decomposition of Burned Fire Area: (Left) FEDS Dataset with 12-hour Resolution, (Right) GOFER Dataset with 1-hour Resolution

3.2 METHODOLOGY

In this section, we describe the models tested, the evaluation metrics used, and the data splitting strategy implemented to ensure reliable and unbiased assessment of model performance. We evaluate a range of models, from simple baselines to advanced neural network architectures, to forecast the Burned Fire Area.

3.2.1 MODELS

We categorize the models into three groups: baseline models, traditional time series models, and neural network models. Additionally, we have the following two distinctions:

- **Global Models**, (e.g., RNNs and other machine learning techniques) are trained across multiple fires to capture patterns that generalize beyond individual time series. These models use training data from past fires to learn diverse temporal dynamics.
- **Local Models**, (e.g., ARIMA) are applied independently to each fire’s time series, using the full series for parameter estimation. In the validation phase, models are fitted up to the current time step to forecast the remainder. The

accuracy of these forecasts is then assessed by aggregating results across the rest of the series, respecting each fire's temporal dependencies.

BASELINE MODELS

NAIVE METHOD

The naive forecasting method is the simplest approaches in time series analysis and serves as a benchmark for comparing the performance of more sophisticated models. It assumes that the forecast for the next time period is equal to the last observed value, expressed mathematically as:

$$\hat{y}_{t+1} = y_t,$$

where \hat{y}_{t+1} is the forecasted value at time $t + 1$, and y_t is the observed value at time t . Despite its simplicity, the naive method can be surprisingly effective for data without trends or seasonal patterns, such as random walks [85]. It sets a minimal standard that other forecasting methods should surpass.

TRADITIONAL TIME SERIES MODELS

These models are considered *local models* as they do not maintain a state across time and are not trained in the traditional sense. Instead, they estimate parameters directly from the time series data.

AUTOREGRESSIVE INTEGRATED MOVING AVERAGE (ARIMA)

The Autoregressive Integrated Moving Average (ARIMA) model [86] is a versatile and widely used forecasting technique that combines autoregressive (AR), integrated (I), and moving average (MA) components. An ARIMA(p, d, q) model is formulated as:

$$\phi(B)(1 - B)^d y_t = \theta(B)\epsilon_t,$$

where $\phi(B)$ is the autoregressive operator of order p , $\theta(B)$ is the moving average operator of order q , d is the degree of differencing required to achieve stationarity, B is the backshift operator defined by $By_t = y_{t-1}$, and ϵ_t is an error term with zero mean and constant variance.

The AR component models the relationship between the current value and its past values. The MA component models the relationship between the current value and past forecast errors. The integration component (I) involves differencing the time series data d times to achieve stationarity. Parameters p , d , and q are typically identified using techniques such as the Autocorrelation Function or an information criteria (e.g. Akaike Information Criterion (AIC) [87]).

EXPONENTIAL SMOOTHING (ETS)

Exponential smoothing methods forecast future values by assigning exponentially decreasing weights to past observations. The ETS framework [88] generalizes exponential smoothing into a state space model that incorporates Error (E), Trend (T), and Seasonality (S) components.

The general form of the ETS model includes the following equations:

State Equations:

$$\begin{aligned}\ell_t &= \ell_{t-1} + b_{t-1} + \alpha\epsilon_t, \\ b_t &= b_{t-1} + \beta\epsilon_t, \\ s_t &= s_{t-m} + \gamma\epsilon_t.\end{aligned}$$

Observation Equation:

$$y_t = \ell_{t-1} + b_{t-1} + s_{t-m} + \epsilon_t.$$

Here, ℓ_t is the level component at time t , representing the baseline value of the series. The trend component b_t captures the slope or growth rate. The seasonal component s_t accounts for periodic fluctuations, with m being the seasonal period (e.g., 12 for monthly data with annual seasonality). The smoothing parameters α , β , and γ control the weighting of past observations and are estimated from the data. The error term ϵ_t is assumed to be white noise.

The ETS model can automatically select the appropriate forms (additive or multiplicative) for each component based on information criteria like the corrected Akaike Information Criterion (AICc). This flexibility allows the model to adapt to various patterns in the data, including trends and seasonal effects.

COMPLEX EXPONENTIAL SMOOTHING (CES)

The Complex Exponential Smoothing (CES) model [89] extends traditional exponential smoothing by modeling both trend and seasonal patterns using a complex-valued smoothing parameter. This approach allows the model to capture cyclical behaviors without requiring data differencing.

The CES model is expressed as:

$$y_t = [a + bt] \cos(\omega t) + [c + dt] \sin(\omega t) + \epsilon_t,$$

where a and b represent the level and trend coefficients for the cosine component, c and d are the level and trend coefficients for the sine component, ω is the frequency of the cyclical component, and ϵ_t is the error term assumed to be white noise.

THETA METHOD

The Theta method [90] enhances the accuracy of simple forecasting methods by adjusting the local curvatures of a time series. It decomposes the original series into several “theta lines,” each modified by a coefficient θ that adjusts the second differences of the data.

For the common case using two theta lines with coefficients $\theta = 0$ and $\theta = 2$, the method produces forecasts by averaging the extrapolated theta lines:

$$\hat{y}_t = \frac{1}{2} \left(y_t^{(0)} + y_t^{(2)} \right),$$

where $y_t^{(0)}$ represents a linear extrapolation capturing the long-term trend, and $y_t^{(2)}$ adjusts for curvature, emphasizing short-term movements and fluctuations.

By averaging these two components, the Theta method balances both long-term and short-term information, resulting in improved forecasting performance. It gained prominence after winning the M3 Forecasting Competition, demonstrating its effectiveness across a wide range of time series data.

NEURAL NETWORK MODELS

We evaluate several neural network architectures designed for time series forecasting, including Recurrent Neural Networks (RNNs), Transformer-based models, and other specialized architectures. For all neural models, we perform extensive hyperparameter tuning and report only the best configurations based on validation performance.

RECURRENT NEURAL NETWORKS (RNNs)

Recurrent Neural Networks are designed to model sequential data by maintaining a hidden state that captures information from previous time steps. The hidden state h_t at time t is computed as:

$$h_t = \sigma(W_h h_{t-1} + W_x x_t + b),$$

where x_t is the input at time t , W_h and W_x are weight matrices, b is a bias vector, and σ is an activation function such as tanh or ReLU.

However, traditional RNNs suffer from vanishing or exploding gradients when dealing with long sequences [91]. To address this, we utilize Long Short-Term Memory (LSTM) networks.

LONG SHORT-TERM MEMORY (LSTM)

LSTM networks [92] are a type of RNN that can capture long-term dependencies by incorporating gating mechanisms to control the flow of information. An LSTM cell contains three gates: the input gate i_t , forget gate f_t , and output gate o_t , along with

a cell state c_t :

$$\begin{aligned} f_t &= \sigma(W_f x_t + U_f h_{t-1} + b_f), \\ i_t &= \sigma(W_i x_t + U_i h_{t-1} + b_i), \\ \tilde{c}_t &= \tanh(W_c x_t + U_c h_{t-1} + b_c), \\ c_t &= f_t \odot c_{t-1} + i_t \odot \tilde{c}_t, \\ o_t &= \sigma(W_o x_t + U_o h_{t-1} + b_o), \\ h_t &= o_t \odot \tanh(c_t), \end{aligned}$$

where \odot denotes element-wise multiplication. The gates regulate the information flow, allowing the network to maintain long-term dependencies by deciding what information to keep or forget.

DEEPAR

DeepAR [93] is a probabilistic forecasting model that utilizes an autoregressive recurrent neural network trained on a large number of related time series. It models the conditional distribution of future values given past observations and covariates:

$$P(y_{t+1:t+H} | y_{1:t}, x_{1:t+H}^{(f)}, x^{(s)}),$$

where $y_{1:t}$ is the history of the target variable, $x_{1:t+H}^{(f)}$ are future covariates available at prediction time, and $x^{(s)}$ are static features.

The RNN updates its hidden state h_t using:

$$h_t = \text{RNN}(h_{t-1}, [y_{t-1}, x_t^{(f)}, x^{(s)}]),$$

and outputs parameters θ_t of a chosen probability distribution through:

$$\theta_t = \text{Linear}(h_t).$$

Predictions are generated by sampling from the distribution $P(y_t | \theta_t)$.

N-BEATS

N-BEATS [94] is a deep neural architecture forecasting time series using residual links and fully connected layers. It decomposes the series into trend and seasonal components:

$$\hat{y}_{t+1:t+H} = \sum_{i=1}^K \mathbf{G}_i \mathbf{f}_i(\mathbf{x}_t),$$

where K is the number of blocks, \mathbf{G}_i are basis functions, and \mathbf{f}_i are neural networks. The model successively models different components by iteratively removing the backcast from the input.

TIMEMIXER

TimeMixer [95] is an MLP-based architecture designed to model multiscale temporal variations in time series data by capturing both fine-scale and coarse-scale patterns. It decomposes the input time series into multiple scales using techniques like wavelet transforms or multi-resolution analysis. Each scale is processed separately through MLP layers to extract features corresponding to that temporal resolution. The outputs from these scales are aggregated to generate the final forecast, allowing the model to leverage both short-term and long-term patterns without relying on recurrent or convolutional architectures.

TEMPORAL FUSION TRANSFORMER (TFT)

The Temporal Fusion Transformer (TFT) [96] combines recurrent networks and attention mechanisms to handle complex temporal dynamics and heterogeneous data. It integrates static covariates, known future inputs, and historical inputs to produce accurate and interpretable forecasts. It outputs probabilistic forecasts by modeling the distribution of the target variable using Quantile Regression and is trained using the Quantile Loss function.

INFORMER

Informer [97] addresses the computational challenges of using Transformers for long-sequence forecasting by introducing techniques to reduce the quadratic time and memory complexity of standard Transformers. It employs a special Self-Attention, which selects a subset of dominant queries based on sparsity in the attention mechanism, reducing complexity from $O(L^2)$ to $O(L \log L)$.

TIMESNET

TimesNet [98] models multiple intra-period and inter-period temporal variations by transforming 1D time series into 2D tensors based on periods identified using the Fast Fourier Transform, thus capturing both periodicity and trend. The architecture includes Temporal 2D Variation Blocks that apply convolutional operations over the 2D representation of the time series, capturing temporal patterns at different scales and across periods. Additionally, an embedding layer maps the input sequence into a latent space suitable for 2D convolution operations. By leveraging 2D convolutions, TimesNet effectively models complex temporal dynamics without the need for recurrent or attention mechanisms.

PROPHET

Prophet [99] is a forecasting tool developed by Facebook that decomposes time series data into trend, seasonality, and holiday effects using an additive model:

$$y(t) = g(t) + s(t) + h(t) + \epsilon_t,$$

where $g(t)$ models the trend component using piecewise linear or logistic growth curves, $s(t)$ captures seasonality using Fourier series, $h(t)$ accounts for the effects of holidays or special events, and ϵ_t is the error term.

Prophet is robust to missing data, outliers, and shifts in the trend, making it suitable for real-world data with irregularities. The model parameters are estimated using maximum likelihood estimation. We apply Prophet to the Burned Fire Area data, allowing it to automatically detect and model trends and seasonal patterns.

TRAINING DETAILS FOR NEURAL MODELS

For all neural network models, we conduct hyperparameter tuning using grid search and random search strategies. Key hyperparameters include learning rates (from 1×10^{-4} to 1×10^{-2}), batch sizes (16, 32, 64), input sequence lengths (e.g., 2, 8, 16, 24 time steps), and hidden layer sizes. The number of epochs is determined using early stopping based on validation loss to prevent overfitting.

Models are trained using the Adam optimizer [100] with appropriate weight decay regularization. For probabilistic forecasting models like DeepAR and TFT, we use the Negative Log-Likelihood (NLL) or Quantile Loss functions as appropriate.

3.2.2 DATA SPLIT

In statistics and machine learning, selecting an appropriate data splitting strategy is essential for reliable model evaluation and mitigating overfitting. Hence, to establish robust baseline models and compare univariate with multivariate approaches, we require a data partitioning method that accounts for these temporal dependencies and the unique characteristics of each dataset. This task becomes particularly complex for time series data, where temporal dependencies must be respected. For example, we cannot directly use the classical k-fold CV scheme Figure 3.6, as it breaks the temporal dependency.

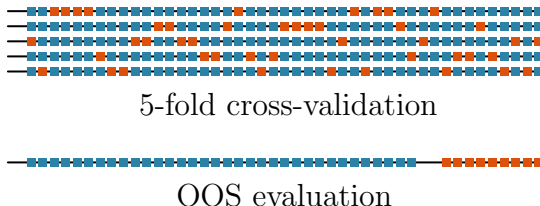


Figure 3.6: Comparison of Randomized CV vs. Out-of-Sample (OOS) Evaluation. The blue and orange dots represent the training and test sets, respectively. In the usual k-fold CV setup, the testing instances are chosen randomly across the series. In OOS evaluation, the test set is always reserved from the end of the series.

A better approach is to apply a time series cross-validation (tsCV) method with

an expanding window approach within each fire [101]. Starting with an initial window (e.g., the first 10 observations), the window expands incrementally, generating one-step-ahead forecasts at each step. This technique allows for a comprehensive performance evaluation while maintaining the temporal integrity of each time series. Additionally, this method enables continuous monitoring of a model’s performance over time, allowing for the detection and adaptation to concept drifts.

Moreover, tsCV closely mirrors real-world scenarios, where each new observation is incorporated into the model to improve forecasting accuracy. When new data becomes available, we can either update or recalibrate the model [102]. Recalibration refers to retraining the model weights or employing incremental learning, while updating involves using the trained model to predict with new data. Stateless machine learning models typically do not require retraining, whereas traditional time series models are expected to be refitted with new data. For stateful machine learning models, such as RNNs, updating requires stepping through all previous time steps. There are two different types of evaluation methods [Figure 3.7](#); we will use the expanding window approach.

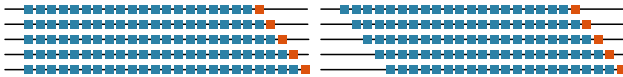


Figure 3.7: Schematic of the Expanding Window (left) setup where the training set keeps expanding and Rolling Window (right) where the training window is fixed and moves. The blue and orange boxes represent the training and test sets, respectively.

Nevertheless, this is referring to singular time-series. We have two wildfire datasets: FEDS, with over 250 fires, and GOFER, containing 28 fires. Each fire represents a distinct time series of varying lengths, creating a two-level structure. At the inner level, each fire’s time series has a temporal component that we must preserve, while at the outer level, the datasets comprise multiple distinct wildfires.

For **FEDS**, we propose a split at the fire level into training, validation, and testing sets ([Figure 3.8](#)). Specifically, fires from 2014 to 2020 are allocated for training and validation, while fires from 2021 and 2022 are reserved for testing. Notably, 2020 and 2021 were years of exceptionally high fire intensity in California, making this split appropriate for evaluating models on recent and severe fire events. This approach emulates real-world forecasting scenarios by evaluating models on newer fires.

Within the 2014–2020 period, we further divide the fires into training and validation sets using quantile-based binning of the final burned areas. This method partitions the fires into quantile bins based on their final sizes (total area burned), resulting in bins that are more evenly populated. By ensuring that each bin is represented in both the training and validation sets, we achieve a more equitable sample overall,

capturing the diverse range of fire sizes and behaviors.

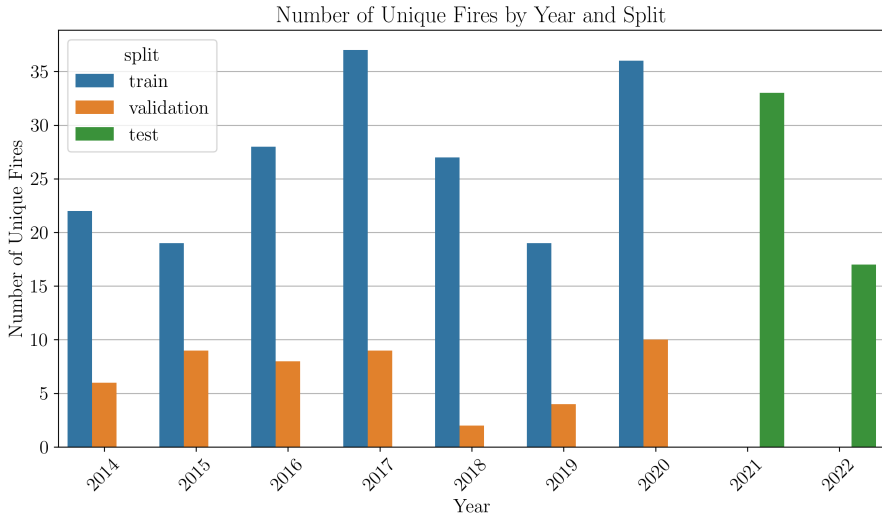


Figure 3.8: Number of unique fires per year in each data split. This results in 188 unique fires (5,279 observations) for training, 48 fires (1,450 observations) for validation, and 50 fires (1,765 observations) for testing.

By splitting at the fire level and employing quantile-based binning, we maintain the temporal integrity of each time series and ensure that both the training and validation sets cover a broad spectrum of fire behaviors. This approach allows us to evaluate models on entirely unseen fires, closely mimicking real-world forecasting scenarios.

For **GOFER**, which only contains 28 fires, a conventional split into training, validation, and test sets is less feasible due to the limited number of distinct fires. Thus, we will perform k-fold CV on the fires and evaluate each using a tsCV manner.

3.2.3 EVALUATION

In evaluating the forecasting models for wildfire behavior, it is crucial to address specific characteristics inherent in our datasets. Our two wildfire datasets, FEDS and GOFER, present unique challenges due to their structure and the nature of the data they contain. This subsection outlines the key evaluation considerations and the selection of appropriate error measures tailored to our use case.

- **Presence of Zeros:** Both FEDS and GOFER datasets exhibit a significant number of zeros. These zeros correspond to periods where there is no observable change in fire spread. The prevalence of zeros introduces complexities in the evaluation process, as certain error measures become undefined or biased when actual values are zero. For instance, measures like Mean Absolute Percentage Error (MAPE) and Symmetric Mean Absolute Percentage Error (sMAPE) encounter division by zero issues or extreme values when actual observations are

zero or near zero.

- **Importance of Non-Zero Values:** Accurately predicting non-zero changes is essential, as these events signify critical shifts in fire behavior. Failure to accurately forecast these changes can result in inadequate precautions and delayed responses, thereby diminishing the effectiveness of wildfire management strategies. Consequently, the selected error measures must prioritize the accurate prediction of non-zero values, ensuring that periods of inactivity do not overshadow the detection of meaningful fire behavior alterations.
- **Differences in Scale Across Fires:** The wildfires in the FEDS and GOFER datasets exhibit substantial variability in size and intensity, resulting in significant discrepancies in the scales of their respective time series. Scale-dependent error measures, such as RMSE and MAE, can be disproportionately influenced by larger fires, potentially masking the model's performance on smaller fires. To mitigate this issue, we applied a logarithmic transformation to the differences, which helps to reduce extreme variations in scale and makes the error measures more balanced across different fire sizes. Despite this transformation, the inherent differences in scale still necessitate the use of scale-free measures to accurately evaluate model performance across various time steps, series, and datasets.

SELECTION OF ERROR MEASURES

To effectively evaluate our forecasting models, we employ a combination of error measures that balance sensitivity to significant changes while maintaining robustness against the challenges posed by zero values. The following categories of error measures have been considered:

Scale-dependent measures, such as Mean Absolute Error (MAE) and Root Mean Squared Error (RMSE), assess forecast accuracy on the same scale as the data. These measures are advantageous when comparing models within datasets where series share similar scales. MAE is preferred for its simplicity and interpretability, representing the average of the absolute errors. RMSE, while more sensitive to larger errors due to the squaring of residuals, provides insight into the variance of forecast errors.

Given the presence of multiple series with varying scales in our datasets, **scale-independent measures** are essential for cross-series comparisons. Measures like Mean Absolute Scaled Error (MASE) normalize errors based on a benchmark method, typically the one-step naive forecast. This scaling ensures comparability across series with different scales and mitigates the influence of outliers. However, MASE requires

that the benchmark method performs consistently across all series, which may not hold in datasets with structural variability.

While percentage-based measures such as MAPE and sMAPE offer intuitive interpretations by expressing errors as percentages of actual values, they are problematic in our context due to the high frequency of zeros. These measures can produce undefined or excessively large values when actual observations are zero or near zero, making them unsuitable for our datasets.

Scaled error measures like Weighted Absolute Percentage Error (WAPE) and Root Mean Squared Scaled Error (RMSSE) address some limitations of percentage errors by aggregating errors over forecast horizons or across series. WAPE, for instance, sums absolute errors and actual values across the forecast horizon, reducing the impact of individual zeros. RMSSE extends this by incorporating squared errors, balancing sensitivity to significant deviations with robustness against zero values.

Thus, the following error measures are used to evaluate performance of our models:

- **Mean Absolute Error (MAE):** MAE provides a straightforward interpretation of average forecast error. When models are optimized for this, it approximates the median.

$$\text{MAE} = \frac{1}{n} \sum_{t=1}^n |y_t - \hat{y}_t|$$

where y_t is the actual value at time t , \hat{y}_t is the forecasted value at time t , and n is the number of observations.

- **Root Mean Squared Error (RMSE):** RMSE complements MAE by emphasizing larger errors, which is beneficial for detecting significant mispredictions in fire behavior changes.

$$\text{RMSE} = \sqrt{\frac{1}{n} \sum_{t=1}^n (y_t - \hat{y}_t)^2}$$

- **Root Mean Squared Logarithmic Error (RMSLE):** The logarithmic transformation reduces the impact of large errors and stabilizes variance, making the data approximately normal by scaling down the errors using a monotonic transformation. This measure produces unbiased forecasts, balancing over-predictions and under-predictions [103].

$$\text{RMSLE} = \sqrt{\frac{1}{n} \sum_{t=1}^n (\ln(y_t + 1) - \ln(\hat{y}_t + 1))^2}$$

This measure is particularly useful when dealing with data that may have exponential growth or when we want to penalize underestimations more than overestimations.

- **Weighted Absolute Percentage Error (WAPE):** WAPE aggregates absolute errors over the forecast horizon, scaling by the sum of actual values, which reduces the impact of individual zeros.

$$\text{WAPE} = \frac{\sum_{t=1}^n |y_t - \hat{y}_t|}{\sum_{t=1}^n |y_t|}$$

However, due to using absolute errors, WAPE can still favor models that predict constant zeros in intermittent series. This can be mitigated by incorporating squared errors in the numerator, as in the Weighted Root Mean Squared Percentage Error (WRMSPE).

$$\text{WRMSPE} = \sqrt{\frac{\sum_{t=1}^n (y_t - \hat{y}_t)^2}{\sum_{t=1}^n y_t^2}}$$

This modification penalizes larger errors more heavily, reducing the likelihood of models that predict constant zeros being favored.

3.3 RESULTS

In this section, we evaluate the performance of various models applied to the FEDS and GOFER datasets. We begin by analyzing local models, followed by global models, and conclude with a qualitative assessment of the selected models.

3.3.1 LOCAL MODELS

For the FEDS dataset ([Table 3.1](#)), the ARIMA model performs best in terms of MAE and WAPE. In contrast, the CES model achieves better results for RMSE, RMSLE, and WRMSPE. However, the differences in these metrics between ARIMA and CES are minimal. Given this marginal disparity, we opt to proceed with the ARIMA model for further analysis due to its overall consistency.

As for the GOFER dataset ([Table 3.2](#)), the naive model yields the best results for MAE and RMSE. However, ARIMA outperforms other models in terms of RMSLE and WAPE, while the ETS model does better in WRMSPE. Despite the naive model's strong performance, we prefer to use a more sophisticated model for deeper insights. Therefore, we select the ARIMA model for the GOFER dataset as well.

Table 3.1: Performance Metrics for Local Models on the FEDS Dataset.

	MAE	RMSE	RMSLE	WAPE	WRMSPE
Naive	4.4571	18.0008	1.1636	0.8746	0.8453
ARIMA	3.6903	15.9495	0.6168	0.7726	0.7367
Theta	3.9209	18.0737	0.6219	0.8209	0.8348
ETS	4.0006	18.5739	0.6216	0.8376	0.8579
CES	3.7022	15.3808	0.6064	0.7751	0.7104

Table 3.2: Performance Metrics for Local Models on the GOFER Dataset.

	MAE	RMSE	RMSLE	WAPE	WRMSPE
Naive	1.1909	3.5279	0.6846	1.2177	1.0183
ARIMA	1.3485	4.5269	0.6326	0.9482	0.8250
ETS	1.3678	4.3338	0.6328	0.9617	0.7891
Theta	1.3635	4.3295	0.6337	0.9601	0.7897
CES	1.3644	4.5141	0.6296	0.9562	0.8194

3.3.2 GLOBAL MODELS

For the FEDS dataset (Table 3.3), the DeepAR model achieves the best performance across all metrics except WAPE and WRMSPE. Notably, the simple RNN outperforms the LSTM network. This suggests that the added complexity of the LSTM does not provide a significant advantage in this context, and the simpler RNN is more effective for time series regression tasks in this dataset. Other methods, such as the TimeMixer and N-Beats models, underperform despite requiring substantial setup time. This underperformance may be attributed to overfitting, causing poor generalization to out-of-sample data.

As for the GOFER dataset (Table 3.4), while the results differ slightly, the DeepAR model again demonstrates strong performance, achieving the lowest error metrics in everything except RMSLE. Nevertheless, the ARIMA model still performs better, and in some cases, the naive model also surpasses the deep learning approaches. This outcome suggests that, given the 1-hour intervals in the GOFER dataset, the system exhibits Markovian properties, relying primarily on the immediate previous time step rather than long-term historical dependencies. In contrast, the FEDS dataset, with its 12-hour aggregation, may have greater dependency on previous observations.

Table 3.3: Performance Metrics for Global Models on the FEDS Dataset.

	MAE	RMSE	RMSLE	WAPE	WRMSPE
RNN	4.3345	12.1648	0.7909	0.8543	0.8864
LSTM	8.0608	25.9888	0.9299	0.8889	0.9472
DeepAR	4.1040	12.6008	0.7528	0.8089	0.9182
NBEATS	7.7504	25.2524	0.9317	0.8546	0.9204
TimeMixer	10.0075	26.7795	1.1015	1.1035	0.9760
Informer	5.4783	15.3160	0.9237	1.0797	1.1160
TFT	4.3341	12.7094	0.8078	0.8542	0.9261
TimesNet	7.2289	24.4603	0.9575	0.7971	0.8915
Prophet	5.2221	22.0492	0.7756	1.0292	1.6067

Table 3.4: Performance Metrics for Global Models on the GOFER Dataset.

	MAE	RMSE	RMSLE	WAPE	WRMSPE
RNN	1.6431	4.6215	0.6941	0.9684	0.8114
LSTM	1.8629	4.9561	0.7248	0.9784	0.7894
DeepAR	1.4605	4.6414	0.7376	0.9357	0.7875
NBEATS	2.0573	4.5303	0.8129	0.9835	0.7984
TimeMixer	1.5591	4.7862	0.7196	1.0723	0.8631
Informer	1.7129	4.5215	0.8312	0.9584	0.8114
TFT	1.4737	4.9561	0.7548	0.9384	0.8694
TimesNet	1.8401	4.3454	0.7358	1.0003	1.055
Prophet	1.7523	4.5204	0.7632	0.9999	1.034

3.3.3 MODEL EVALUATION

Based on the overall performance, the ARIMA model consistently achieves better or comparable results across both datasets. Therefore, we select the ARIMA model for further analysis on both the FEDS and GOFER datasets. We will not evaluate the ARIMA model on the test set at this stage, as we plan to continue working with this dataset in the next chapter and wish to avoid overusing the datasets.

3.3.4 QUALITATIVE ANALYSIS

To provide a visual comparison, we plot the true values of the target feature (fire growth) alongside the predictions from the naive and ARIMA models for both datasets (Figure 3.9).

We can observe that the naive model closely follows the true values but lags slightly behind due to its simplistic approach of using the previous value as the prediction. The ARIMA model, while similar to the naive model in some aspects, exhibits a delay in capturing the initial fire growth after the local training period. It takes a few time steps before it starts predicting values that align with the observed data. Additionally, the ARIMA model produces smoother predictions and does not fully capture the peaks observed in the true fire growth values, indicating a limitation in modeling sudden changes.

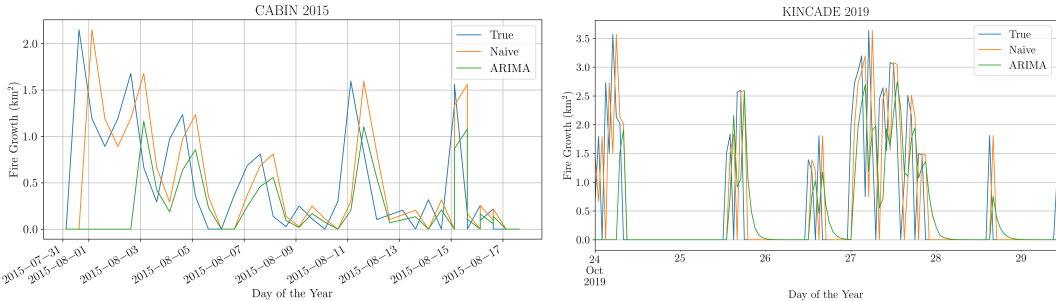


Figure 3.9: Example of two fires (FEDS on the left, GOFER on the right) being predicted by the ARIMA vs. True Values.

3.4 DISCUSSION

In this chapter, we conducted the first analysis using the FEDS and GOFER time series datasets to predict wildfire spread, specifically focusing on the active fire line. Predicting the evolution of the active fire line is a novel approach that has not been extensively explored in the literature, making our results first-of-its-kind. Due to the lack of prior studies and benchmarks on similar data, it was challenging to directly compare our findings, which is why we implemented a comprehensive evaluation using various models and metrics.

Our methodology involved applying both traditional time series models and neural network architectures to univariate time series data. We examined models ranging from simple baselines like the naive method to more complex approaches such as ARIMA, ETS, and several neural network models including RNNs, LSTMs, DeepAR, N-BEATS, and Transformers. We employed a careful data partitioning method that preserved the temporal integrity of the series and ensured that models were evaluated on entirely unseen fires, mimicking real-world forecasting scenarios.

The results indicated that traditional models, particularly ARIMA, outperformed the neural network models across both the FEDS and GOFER datasets. The ARIMA model achieved lower error metrics and demonstrated better generalization to unseen data. This performance disparity may be attributed to several factors:

- **Data Characteristics:** Wildfire time series data are inherently noisy and contain many zeros due to periods of inactivity. Traditional models like ARIMA are adept at handling such data, especially when appropriate differencing and transformations are applied.
- **Model Complexity:** Neural networks, especially deep architectures, require large amounts of data to train effectively. Our datasets, while rich in temporal information, may not provide sufficient volume for complex neural networks to capture meaningful patterns without overfitting.

- Training and Tuning: While the ARIMA model was carefully tuned using established statistical techniques and information criteria, it is possible that the neural network models were not optimally trained. Hyperparameter tuning for neural networks is a non-trivial task that requires extensive experimentation, which may not have been exhaustive enough.

Additionally, the neural network models might not have been fully adapted to the specific characteristics of wildfire time series data. For instance, recurrent models like LSTMs are designed to capture long-term dependencies, but wildfires often exhibit abrupt changes and short-term dependencies that may not be effectively captured by these models without specialized architectures or external information (next chapter).

3.4.1 FUTURE WORK

To enhance the applicability and effectiveness of wildfire forecasting models, future research should focus on several key areas:

- Enhanced Training: There is potential to improve the performance of neural network models through more rigorous hyperparameter tuning and training procedures. While we did do some hyperparameter search, it might have been too narrow to find parameters that really work.
- Fine-Tuning of GOFER and FEDS algorithms: Further refining the methodology of extracting the active fire line from GOES and VIIRS, as well as improved fire tracking, could potentially enhance data quality and model performance.
- Development of new Architectures: Designing neural network architectures tailored to the characteristics of wildfire data could improve performance. For example, models that handle intermittent time series with many zeros, such as models incorporating zero-inflated distributions or count data models, might be more appropriate.
- Evaluation on Different Fires: Expanding the datasets to include a wider variety of fires from different regions and with different characteristics could test the models' generalizability.
- Integration with Real-Time Forecasting Systems: Ultimately, the goal is to develop models that can be integrated into operational wildfire forecasting and management systems. Collaborating with fire management agencies to test models in real-time scenarios could provide valuable feedback and drive practical improvements.

CHAPTER 4

MULTIVARIATE TIME SERIES

In this chapter, we explore the analysis of multivariate time series, focusing on predicting the Burned Fire Area by incorporating exogenous features. Specifically, our objective is to forecast the Burned Fire Area based not only on its previous time steps or the differences between consecutive time steps but also with the aid of different covariates at time t , denoted as \mathbf{X}_t .

One of the primary motivations for incorporating exogenous variables is to enhance predictive performance. By including relevant covariates, we aim to capture external factors that influence wildfire behavior, thereby improving the accuracy of our forecasts. Furthermore, the inclusion of these variables aids in making the model more interpretable, as it links predictions to specific external influences, facilitating a better understanding of the underlying dynamics driving wildfire events.

4.1 BACKGROUND

A multivariate time series consists of sequential observations of multiple variables recorded at regular intervals. The main goal of multivariate time series analysis is to understand the relationships among these variables over time and to leverage this information for accurate forecasting.

Time series data in the multivariate context exhibit characteristics similar to their univariate counterparts, including trends, seasonality, cycles, and irregular fluctuations. However, the addition of multiple variables allows us to model the dynamic interactions between them, which can be crucial for capturing the complex behavior of wildfires.

There are various approaches to modeling multivariate time series data. Traditional statistical methods include models like Vector Autoregression (VAR) [104], but in this

chapter, we will focus on machine learning techniques capable of handling complex, nonlinear relationships between the Burned Fire Area and the covariates.

By integrating exogenous variables into our models, we aim to capture external influences such as weather conditions, vegetation types, and human activities that significantly impact wildfire dynamics. Understanding these relationships is crucial for developing robust models that can accurately forecast wildfire behavior.

In the following sections, we will explore various machine learning models that incorporate exogenous variables for multivariate time series forecasting. We will evaluate their performance and discuss their applicability to wildfire prediction, aiming to develop a robust model that accurately forecasts the Burned Fire Area by leveraging both historical data and additional relevant features.

4.2 METHODOLOGY

In this section, we describe the methodology employed for modeling and forecasting the Burned Fire Area using multivariate time series analysis. We outline the data preprocessing steps, the data splitting strategy for reliable evaluation, the feature selection process, and the model evaluation approach.

4.2.1 DATA PREPROCESSING

Effective use of machine learning models for time series forecasting often requires careful data preparation. One key technique is the creation of *lagged variables*, which represent the values of variables at previous time steps. This approach transforms the time series data into a supervised learning problem suitable for various machine learning algorithms.

To capture the autoregressive nature of the target variable, we create lagged features of the Burned Fire Area differences (y_t). For an autoregression of order k , we generate k lagged variables corresponding to the target feature at previous time steps: $y_{t-1}, y_{t-2}, \dots, y_{t-k}$. Similarly, we can create lagged versions of the covariates, allowing the model to consider past values of external factors that may influence the fire spread.

By constructing these lagged features, we align all variables into a consistent dataframe for subsequent modeling. However, this process reduces the number of observations in the dataset since we lose the first k observations due to the absence of preceding lagged data.

After constructing the lagged variables, we perform feature scaling. Scaling is crucial for machine learning models that are sensitive to the magnitude of input features, such as those using gradient descent optimization [105]. We apply a standard scaler

to the covariates to ensure that differences in scale do not disproportionately influence the model’s performance. Specifically, we fit the scaler on the training data and then apply the same transformation to the validation and test sets to prevent data leakage.

To predict future time steps beyond the immediate next one, we can extend this dataset using forward steps. In this approach, we aim to predict y_{t+k} , where k represents the forecasting horizon. Since future covariate values may not be available at prediction time, we only lag the target feature, assuming we have access to historical covariate information but not future covariate values.

4.2.2 DATA SPLITTING AND EVALUATION

Our data splitting strategy and evaluation metrics follow the approach described in Section 3.2.2 and Section 3.2.3. We split the data into training, validation, and test sets, ensuring that the temporal order of each wildfire event is preserved to prevent information leakage from future to past observations.

For evaluation, we use the same metrics as those used in the univariate analysis, allowing for a better comparison of model performance.

4.2.3 FEATURE SELECTION

Feature selection is crucial for improving model performance and interpretability. In the context of multivariate time series forecasting, we aim to identify the most relevant covariates and lagged variables that significantly contribute to predicting the fire growth.

While there are various feature selection methods, including filter, wrapper, and embedded methods [106], we adopt a compromise approach due to practical considerations. Specifically, we use a tree-based model (e.g., XGBoost) to compute feature importance scores based on mean decrease in impurity [107]. We perform a 3-fold cross-validation on the training set and select the top 20 features with the highest average importance scores.

This method allows us to reduce model complexity and mitigate the risk of overfitting by focusing on the most informative features. However, we acknowledge that this approach might give an unfair advantage to tree-based models like XGBoost, as the feature selection is influenced by their internal mechanisms.

4.2.4 MODEL EVALUATION

After training the models using the selected features and optimal hyperparameters, we evaluate their performance on the validation set using the specified metrics. Based on these results, we select the model that demonstrates the best predictive performance. We compare these results with the univariate models from the previous

chapter to select the best model overall. We then assess the chosen model on the test set to obtain an unbiased estimate of its generalization ability.

4.2.5 EXPLAINABILITY WITH SHAP VALUES

To interpret the predictions of our models and understand the contribution of each feature, we employ SHapley Additive exPlanations (SHAP) values [108]. SHAP provides a unified framework to compute feature importance by assigning each feature an importance value for a particular prediction.

SHAP values are based on the concept of Shapley values from cooperative game theory [109], which fairly distribute the “payout” (in this case, the model’s prediction) among the features. By analyzing SHAP values, we can gain insights into how individual features impact the model’s predictions, enhancing interpretability and trust in the model.

4.2.6 MODELS

In this section, we describe the machine learning models used for forecasting the Burned Fire Area.

Additionally, to optimize model performance, we conduct hyperparameter tuning using grid search. For each model, we define a grid of hyperparameters to perform an exhaustive search over the parameter space. The grid search is conducted using cross-validation on the training set to identify the combination of hyperparameters that yields the best performance.

BASELINE MODELS

NAIVE METHOD

The Naive Method forecasts the next time period by using the last observed value:

$$\hat{y}_{t+1} = y_t.$$

This simple approach serves as a fundamental benchmark for evaluating more complex forecasting models.

LINEAR NAIVE

The Linear Naive model enhances the Naive Method by incorporating a linear regression parameter on the previous value:

$$\hat{y}_{t+1} = \beta y_t,$$

where β is a coefficient estimated from the data.

LINEAR REGRESSION MODELS

LINEAR REGRESSION

Linear regression models the relationship between a dependent variable y and one or more independent variables \mathbf{X} , assuming a linear relationship of the form:

$$\mathbf{y} = \mathbf{X}\beta + \epsilon,$$

where β represents the coefficients to be estimated, and ϵ is the error term. The coefficients β are estimated by minimizing the sum of squared residuals.

RIDGE REGRESSION

Ridge regression introduces $L2$ regularization to prevent overfitting by penalizing large coefficients [110]. The cost function to minimize becomes:

$$\mathcal{L}(\beta) = \sum_{i=1}^n (y_i - X_i\beta)^2 + \lambda \sum_{j=1}^p \beta_j^2,$$

where λ is the regularization parameter controlling the strength of the penalty. We perform grid search over λ values to find the optimal regularization strength.

LASSO REGRESSION

Lasso regression adds $L1$ regularization, encouraging sparsity in the coefficients by penalizing their absolute values [111]:

$$\mathcal{L}(\beta) = \sum_{i=1}^n (y_i - X_i\beta)^2 + \lambda \sum_{j=1}^p |\beta_j|,$$

which can result in some coefficients being exactly zero, effectively performing feature selection. We tune λ through grid search to balance model complexity and performance.

ELASTIC NET

Elastic Net combines both $L1$ and $L2$ regularization [112]:

$$\mathcal{L}(\beta) = \sum_{i=1}^n (y_i - X_i\beta)^2 + \alpha \left(\rho \sum_{j=1}^p |\beta_j| + \frac{1-\rho}{2} \sum_{j=1}^p \beta_j^2 \right),$$

where α controls the overall strength of regularization, and ρ balances between $L1$ and $L2$ penalties. Hyperparameters α and ρ are tuned via grid search.

BAYESIAN RIDGE REGRESSION

Bayesian Ridge Regression introduces a probabilistic approach by placing a prior distribution over the coefficients β [113]. It computes a posterior distribution based on the observed data, providing estimates of uncertainty in the coefficients. Default

hyperparameters are used, as Bayesian Ridge Regression internally estimates the regularization parameters.

TREE-BASED METHODS

RANDOM FOREST

Random Forest is an ensemble method that constructs multiple decision trees using bootstrapped samples and random subsets of features [114]. The final prediction is obtained by averaging the predictions from all individual trees. Key hyperparameters include the number of estimators, maximum depth, and minimum samples required for splitting and leaf nodes, which are tuned via grid search.

GRADIENT BOOSTING

Gradient Boosting builds an ensemble of weak learners (typically decision trees) sequentially, where each new tree is trained to minimize the residual errors of the previous ensemble [107]. Hyperparameters such as learning rate, number of estimators, and maximum depth are tuned to optimize performance.

XGBOOST

XGBoost (Extreme Gradient Boosting) is an optimized implementation of gradient boosting that includes regularization and parallel processing [115]. It minimizes a regularized objective function, and hyperparameters like learning rate, number of estimators, maximum depth, subsample ratio, and column sampling are tuned via grid search.

SUPPORT VECTOR REGRESSION (SVR)

SVR extends Support Vector Machines to regression tasks, aiming to find a function $f(X)$ that deviates from the observed targets by a value no greater than ϵ [116]. We use kernel functions (e.g., linear and radial basis function), and hyperparameters such as C (regularization parameter) and γ (kernel coefficient) are tuned through grid search.

K-NEAREST NEIGHBORS (KNN)

KNN is a non-parametric method that predicts the target variable based on the average of the K nearest neighbors in the feature space [117]. Hyperparameters include the number of neighbors K and the weighting function, which are selected via grid search.

MULTI-LAYER PERCEPTRON (MLP)

An MLP is a feedforward neural network composed of input, hidden, and output layers [118]. Each neuron calculates a weighted sum of its inputs and applies a non-linear activation function. Hyperparameters—including hidden layer sizes, activation functions, learning rate, and regularization parameter α —are optimized using grid search. We also employ Recurrent Neural Networks and Transformers (TFT), as described in the univariate section but adding features to the inputs by concatenating them into channels.

HYBRID MODELS WITH STL DECOMPOSITION

Hybrid models leverage both classical time series decomposition methods and machine learning algorithms to enhance forecasting accuracy. We use Seasonal-Trend Decomposition using Loess (STL) [84], as described in Section 3.1.3, to separate the time series into trend, seasonal, and residual components:

$$Y_t = T_t + S_t + R_t,$$

We apply machine learning models to each component to capture any patterns or irregularities. The final forecast is obtained by combining the predictions of the individual components:

$$\hat{Y}_t = \hat{T}_t + \hat{S}_t + \hat{R}_t.$$

This hybrid approach allows us to exploit the strengths of both statistical decomposition and machine learning, effectively modeling both linear and nonlinear aspects of the time series data.

NEURAL ADDITIVE MODELS (NAMs)

Neural Additive Models (NAMs) are an extension of Generalized Additive Models (GAMs) that employ neural networks to learn the shape functions for each feature, enhancing both flexibility and interpretability [119]. GAMs are traditionally expressed as:

$$g(\mathbb{E}[Y]) = \beta_0 + f_1(X_1) + f_2(X_2) + \cdots + f_K(X_K),$$

In NAMs, each shape function $f_i(X_i)$ is parameterized by a neural network dedicated to that specific feature. This allows each f_i to model complex, nonlinear relationships between X_i and Y while maintaining the additive structure of the model. The NAM can be expressed as:

$$\hat{Y} = \beta_0 + f_1(X_1; \theta_1) + f_2(X_2; \theta_2) + \cdots + f_K(X_K; \theta_K),$$

where θ_i represents the parameters of the neural network modeling f_i .

Each feature X_i is passed through its own neural network f_i , which outputs a con-

tribution to the final prediction. The individual outputs are then summed together along with the intercept β_0 to produce the final prediction \hat{Y} . This architecture ensures that the effect of each feature on the prediction is distinct and additive, aiding interpretability.

4.3 RESULTS

The evaluation of various machine learning models on the FEDS and GOFER datasets reveals several key insights ([Table 4.1](#) and [Table 4.2](#)). Overall, gradient boosting methods, particularly XGBoost, demonstrate superior performance across both datasets. This aligns with the expectation that ensemble methods are effective in capturing complex patterns in tabular data.

Recall that the feature sets and temporal resolution differ between FEDS and GOFER, which may influence model performance. Therefore, caution should be exercised when interpreting the results, considering the disparity in available features. Additionally, direct comparison with the univariate models is possible because the same data pre-processing steps and data splitting were applied, including the lagging of the target feature so it corresponds to the same autoregressive lags the univariate time series had.

As expected, the hybrid model utilizing Seasonal-Trend Decomposition using Loess (STL), which combines three XGBoost models to predict trend, seasonality and residual components separately, exhibits robust performance. This is especially evident on both datasets, where it achieves strong results on the validation set, comparable to solo ensemble methods.

In contrast, recurrent neural networks and transformer (TFT) models underperform compared to other approaches. This diminished performance is likely attributable to the data-intensive nature of Transformer architectures, which require substantial amounts of data to train effectively. The FEDS dataset, in particular, may not provide sufficient data volume, hindering the performance of these models.

Table 4.1: Performance Metrics on the Validation Set of FEDS.

	MAE	RMSE	RMSLE	WAPE	WRMSPE
Naive	4.4571	18.0008	1.1636	0.8746	0.8453
Linear Naive	4.2097	18.4659	0.7474	0.8261	0.8671
KNN	3.6116	17.1417	0.6526	0.7087	0.8049
Linear	3.6920	17.3181	0.6016	0.7245	0.8132
Lasso	3.7546	16.7727	0.6023	0.7368	0.7876
Ridge	3.7768	17.4873	0.6025	0.7411	0.8212
Elastic Net	3.7452	16.9089	0.6022	0.7349	0.7940
Bayesian Ridge	3.7125	17.3355	0.6017	0.7285	0.8140
Random Forest	3.3792	16.3383	0.5763	0.6534	0.7672
Gradient Boosting	3.3447	15.7608	0.5816	0.6563	0.7451
XGBoost	3.3239	15.6670	0.5772	0.6531	0.7401
SVM	3.8059	19.1539	0.6490	0.7468	0.8994
MLP	3.7956	17.3747	0.6774	0.7448	0.8159
RNN	4.1992	17.8426	0.8160	0.7981	0.9582
TFT	5.4783	19.3160	0.9237	1.0797	1.1160
NAM	3.8601	17.7112	0.7390	0.7532	0.8411
STL	3.6698	16.7737	0.6288	0.6780	0.8910

Table 4.2: Performance Metrics on the Validation Set of GOFER.

	MAE	RMSE	RMSLE	WAPE	WRMSPE
Naive	1.1909	3.5279	0.6846	1.2177	1.0183
Linear Naive	1.0466	3.0479	0.5956	1.0702	0.8797
KNN	0.0828	0.2511	0.0411	0.3030	0.5337
Linear	0.2957	1.8432	0.1057	0.3023	0.5320
Lasso	0.2964	1.8370	0.1057	0.3030	0.5302
Ridge	0.2964	1.8490	0.1059	0.3030	0.5337
Elastic Net	0.3048	1.9039	0.1080	0.3117	0.5495
Bayesian Ridge	0.2958	1.8445	0.1058	0.3025	0.5324
Random Forest	0.0334	0.1982	0.0191	0.0341	0.0572
Gradient Boosting	0.0287	0.1597	0.0145	0.0294	0.0461
XGBoost	0.0297	0.1486	0.0144	0.0303	0.0429
SVM	0.2960	2.1776	0.0969	0.3027	0.6285
MLP	0.1020	0.2932	0.0433	0.0847	0.0846
RNN	1.0954	2.2751	0.5832	0.9181	0.9987
TFT	2.6398	4.7190	1.4745	0.9994	0.9995
NAM	0.0964	0.2804	0.0457	0.0523	0.0633
STL	0.0434	0.2037	0.0301	0.0441	0.0577

An observation across all models is the presence of some degree of overfitting—the training scores are provided in the appendix. However, this overfitting is within

expected norms and does not pose significant concerns regarding the reliability of the models.

Overall, XGBoost is the preferred model for the FEDS dataset due to its consistent performance and ability to generalize well. Although the results for GOFER are less unambiguous, XGBoost appears to be among the top two models. Thus, we will use XGBoost for GOFER as well as it will facilitate a parallel analysis with both datasets. Overall, the addition of covariates improves all models substantially when compared to the univariate case. Thus, we choose to prioritize the multivariate models presented above, as incorporating additional variables leads to a more performant and interpretable model.

4.3.1 EXPLAINABILITY

SHAP ANALYSIS

This following short section is conducted using only the FEDS dataset. Although the GOFER dataset includes many more variables due to additional lags, the overall results are similar. In GOFER, however, more weather variables at different lags, such as Vapor Pressure Deficit (VPD), appear to be important.

From the SHAP analysis ([Figure 4.1](#)), we observe that the expected value of the model output $f(X)$ is 0.785—which would be the prediction the model would make without any covariates. Most features contribute negatively to this value. For instance, the first lag of the target variable (`lag_y_1`) contributes -0.23. The only feature with a positive contribution appears to be the day/night flag (`dnFlag`), which adds +0.09 when it is daytime.

Unfortunately, the total suppression personnel feature (`totPersonnel`) does not appear to be significant overall. It is grouped with other less important features and contributes a small negative value.

We also visualize several SHAP dependence plots for key features ([Figure 4.2](#), and [Figure 4.3](#)). For the lagged fire line length (`lag_flinelen_1`), we observe that most values on the x-axis are concentrated between 0 and 2, and higher values correspond to a greater influence on the target variable. This aligns with our statistical analysis discussed earlier in Section [2.4](#).

The dependence plot for total personnel (`totPersonnel`) appears noisy, and there does not seem to be a clear effect on the target variable. This is disappointing, as total personnel was expected to be one of the more important variables. Nevertheless, even if it had a strong impact, we should be cautious in inferring causality from a predictive model.

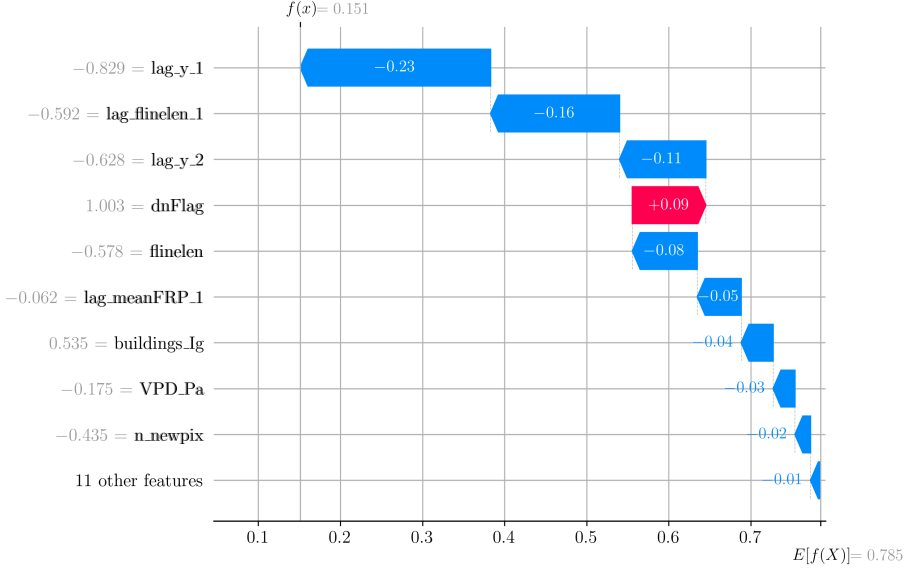


Figure 4.1: SHAP waterfall plot illustrating the contributions of individual features to the model output for a specific instance. These are also the top most important variables according to XGBoost.

For Vapor Pressure Deficit (VPD), there is a clear increasing trend in the SHAP values. The plot resembles a rotated ‘S’, indicating that low VPD values correspond to low SHAP values, and as VPD increases, the SHAP value increases as well. This suggests that higher VPD values have a greater influence on the target variable.

The lagged target variable (`lag.y.1`) shows a linear relationship in the dependence plot, where an increase in the lagged target value corresponds to an increase in the SHAP value. Overall, this indicates that larger previous values of the target variable are associated with larger contributions to the current prediction.

Despite these observations, the dependence plots provide limited actionable insights. It appears that predicting wildfires is more complex than anticipated, and no single variable produces a strong signal that correlates significantly with wildfire activity.

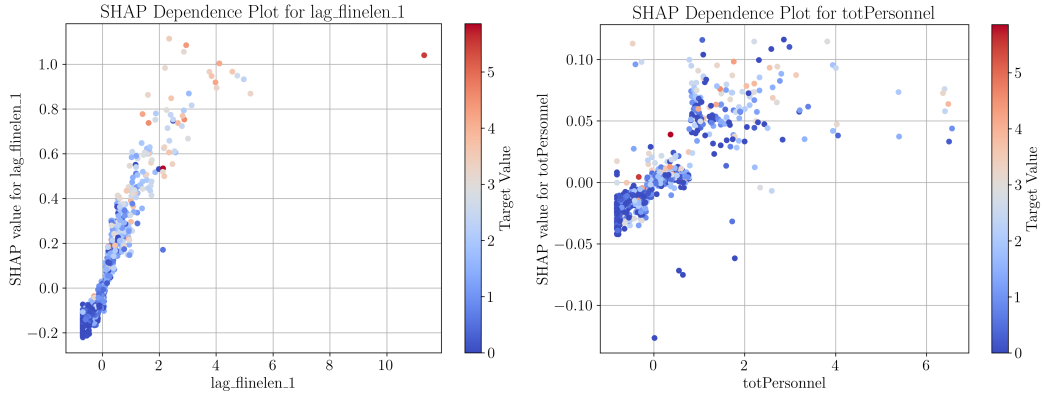


Figure 4.2: SHAP dependence plots for Previous Active Fire Line Length (left), and Total Personnel (right).

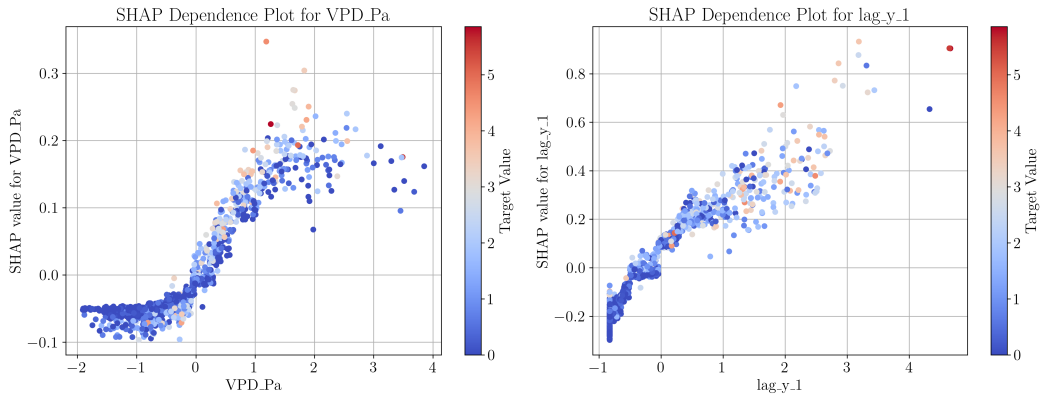


Figure 4.3: SHAP dependence plots for VPD (left), and the Previous Fire Growth (right).

QUALITATIVE EXAMPLES

To provide a qualitative example, we analyze the time series plots of the target feature and the model predictions for both datasets.

In the FEDS dataset (Figure 4.4), there is a clear daytime/nighttime effect, consistent with our findings from the statistical analysis and lag exploration¹. During nighttime, the predicted values are usually lower than during daytime. Overall, the predictions closely follow the true values, which is reflected in the accumulated burned area, indicating a reasonably accurate model.

In the GOFER dataset (Figure 4.5), we observe a fire with very large peaks in the initial hours. The model struggles to capture these peaks, resulting in discrepancies that propagate through the cumulative burned area predictions. Interestingly, the

¹This also could be seen in the SHAP dependence plots, but it is not something we can really affect nor that insightful.

daily cycle of VPD is evident in GOFER, increasing during the day and decreasing at night. While this effect is also present in FEDS, it is less pronounced but still observable as a jagged pattern.

In the FEDS data, it appears that predictions are slightly higher when the previous active fire line length and mean Fire Radiative Power (meanFRP) are larger. For VPD, the decline observed on September 22nd seems to correspond with a decline in the predictions, although it is challenging to ascertain the exact impact—or if I have been looking too much at the same data and hope to see some pattern that does not exist.

In the GOFER data, the lack of a notable effect from suppression efforts is apparent. There are instances where the fire has decreased, but there remains a significant number of personnel assigned. This makes it difficult to determine the impact of suppression efforts on the fire's progression.



Figure 4.4: Time series plot of true and predicted burned area, along with relevant features, for a selected fire in the FEDS dataset.

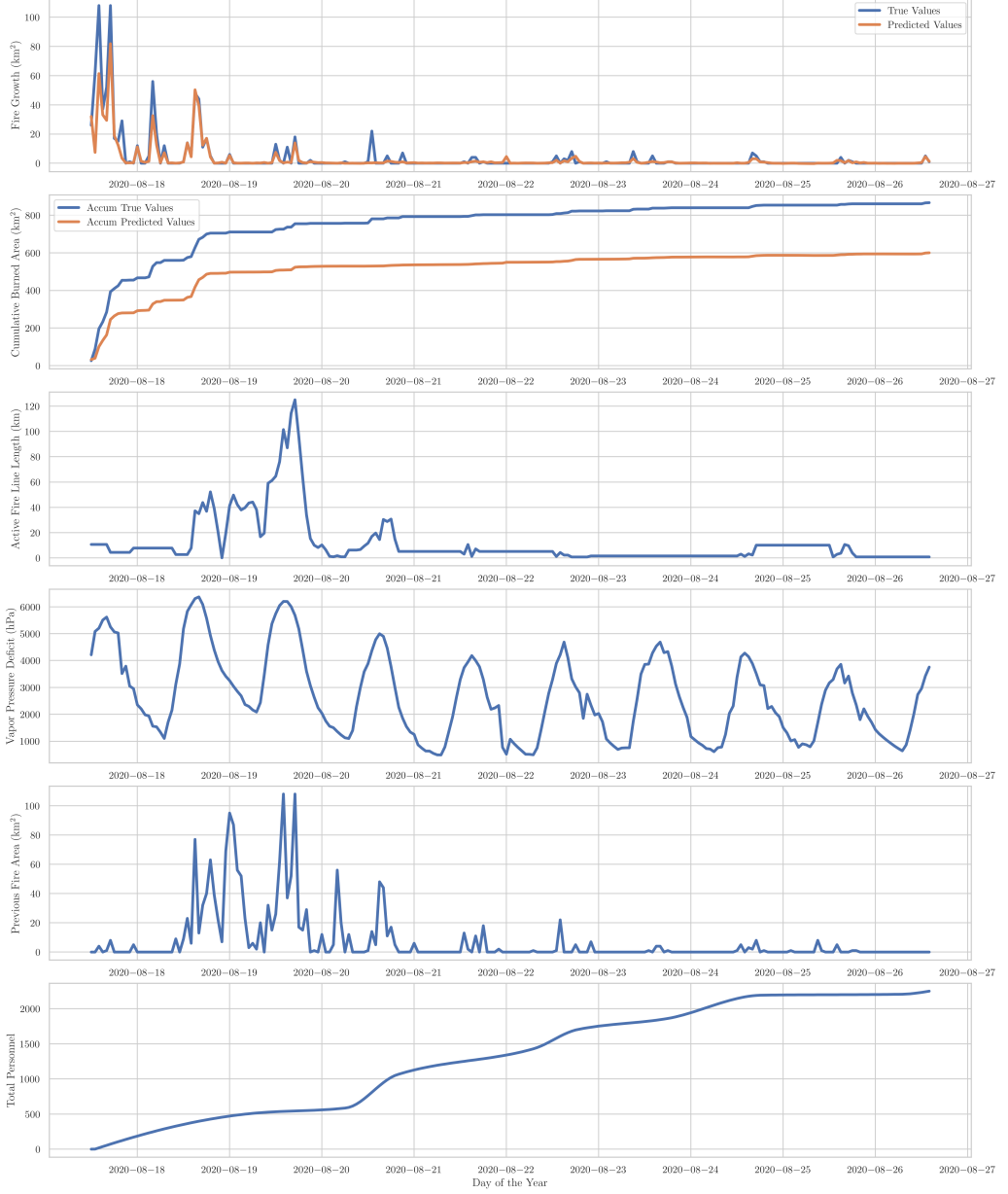


Figure 4.5: Time series plot of true and predicted burned area, along with relevant features, for a selected fire in the GOFER dataset.

4.3.2 FINAL EVALUATION METRICS

After doing feature selection and model selection, we can finally evaluate the model, where results for both can be seen in [Table 4.3](#). Overall, there is evidence of some overfitting in the models. Additionally, the FEDS dataset exhibits higher error metrics compared to GOFER, which can be attributed to the longer prediction horizon (12 hours ahead for FEDS versus 1 hour ahead for GOFER), resulting in more significant cumulative errors.

Table 4.3: Comparison of Machine Learning Models on FEDS and GOFER Datasets.

	Train	Validation	Test		Train	Validation	Test
MAE	2.8057	3.3239	4.8904	MAE	0.0050	0.0297	0.3330
RMSE	11.5780	15.6670	18.1388	RMSE	0.0187	0.1486	1.7886
RMSLE	0.5671	0.5772	0.7361	RMSLE	0.0015	0.0144	0.1110
WAPE	0.5844	0.6531	0.7186	WAPE	0.0025	0.0303	0.2740
WRMSPE	0.6350	0.7401	0.8502	WRMSPE	0.0030	0.0429	0.4032

(a) Metrics for FEDS

(b) Metrics for GOFER

4.3.3 LEAD TIME ANALYSIS

As an additional analysis, we tested the models' ability to predict further lead times beyond the original problem definition. For FEDS, which has 12-hour aggregates, we predicted y_{t+2} and y_{t+4} , representing 1-day and 2-day look-ahead forecasts, respectively. To avoid overcomplicating the report, we present the MAE on the validation set for $t + 1$ onward. The MAE values obtained were 3.3239 for $t + 1$, 3.2931 for $t + 2$, and 4.5117 for $t + 4$. Interestingly, the MAE for 24 hours ahead ($t + 2$) is slightly lower than for 12 hours ahead ($t + 1$), possibly due to the day-night cycle making it easier to predict at that interval. However, these values are not directly comparable, as they correspond to different time horizons, and each time we increase the horizon we have to delete some of the data².

For GOFER, which has 1-hour intervals, we predicted lead times of +2, +6, +12, +24, and +48 hours in advance. The MAE values obtained were 0.0297 for $t + 1$, 0.0299 for $t + 2$, 0.0312 for $t + 6$, 0.0617 for $t + 12$, 0.0619 for $t + 24$, and 0.2113 for $t + 48$. Overall, the results indicate that the models maintain reasonable performance even at extended lead times.

4.4 DISCUSSION

In this chapter, we investigated various machine learning models for forecasting the Burned Fire Area using multivariate time series analysis. Our methodology encompassed extensive data preprocessing, including the creation of lagged variables to capture temporal dependencies and scaling of covariates to ensure model stability. We evaluated a range of models—from traditional linear regression techniques to advanced ensemble methods and neural networks—using our two datasets: FEDS and GOFER.

Our results indicate that gradient boosting methods, particularly XGBoost, consis-

²These forecasts were achieved by including y_{t+k} in the dataset and adjusting the corresponding lagged features accordingly.

tently outperformed other models across both datasets. This aligns with the understanding that ensemble methods are effective at capturing complex patterns in tabular data, especially when dealing with nonlinear relationships and interactions among features [120, 121]. The hybrid model utilizing Seasonal-Trend Decomposition using Loess (STL) also demonstrated robust performance, suggesting that combining statistical decomposition with machine learning can enhance forecasting accuracy.

Conversely, recurrent neural networks and Transformer models underperformed compared to other approaches. This underperformance may be attributed to the data-intensive nature of these models, which require large amounts of data to train effectively. Given that our datasets are relatively small³, these models may not have received sufficient data to learn meaningful patterns. This, again, is no surprise if one follows the literature [120, 121].

Our SHAP analysis provided insights into feature importance and model interpretability. Disappointingly, the total suppression personnel, which we expected to be a significant factor influencing fire dynamics, did not appear to have a substantial impact on the model's predictions. The most influential features were lagged variables of the target variable and certain environmental factors like Vapor Pressure Deficit (VPD). This suggests that the immediate past behavior of the fire and specific weather conditions are more critical in predicting fire spread than some operational factors. Nevertheless, this could be an issue in the data collection, where we only have fires that have suppression. If we had a mix of fires that did not have suppression to compare, the effect firefighting has could be discerned.

The qualitative examples further demonstrated that while our models were able to capture general trends in the data, there are complexities in wildfire behavior that are difficult to model accurately. For instance, the models struggled to predict sudden spikes in fire activity, which may be influenced by unpredictable environmental changes or other factors not captured in our datasets.

Despite achieving reasonable accuracy in our predictions, there is evidence of overfitting, particularly in the FEDS dataset. This is likely due to the limited size of the dataset and the complexity of the models used. Additionally, the longer prediction horizon for FEDS (12 hours ahead) compared to GOFER (1 hour ahead) introduces more uncertainty, which may contribute to higher error metrics.

An important observation from our results is that increasing the lead time generally led to decreased model performance, as expected. However, the models maintained reasonable accuracy even at extended lead times, indicating their potential utility for short-term forecasting.

³In the context of deep learning.

4.4.1 FUTURE WORK

To enhance the applicability and effectiveness of wildfire forecasting models, future research should focus on several key areas:

- Enhanced Feature Selection: Investigate the implementation of Wrapper and Filter methods for feature selection to potentially improve model performance.
- Expanding Dataset: Incorporating data from fires that did not receive suppression efforts could provide a comparative basis to discern the true impact of firefighting activities. By analyzing a mix of suppressed and unsuppressed fires, we can move towards establishing causality rather than merely identifying correlations.
- Investigating Causal Relationships: Transitioning from purely predictive models to causal models would allow us to understand the underlying mechanisms influencing fire spread. Techniques such as causal inference and counterfactual analysis could be employed to assess the impact of suppression efforts and other interventions.
- Extended Forecasting: Exploring methods specifically designed for multi-step forecasting, such as sequence-to-sequence models or models that directly predict multiple future time steps, could improve performance for longer lead times. Additionally, assessing whether model architectures need adjustment when forecasting further into the future is an important consideration.
- Future Weather Covariates: Utilizing weather forecasts—which are pretty accurate at the resolutions we are working with—as covariates in the models could improve their ability to predict fire behavior further into the future. Incorporating anticipated changes in environmental conditions would provide the models with more relevant information for extended lead times.
- Analyzing Extended Horizons: Studying how the importance of different features changes when predicting further into the future could yield valuable insights. For instance, weather variables may become more significant at longer lead times, and understanding these dynamics can inform both modeling strategies and operational planning.
- Evaluation on Different Scenarios: Testing the models under various conditions, such as different geographic regions, fire sizes, and environmental contexts, would help assess their generalizability and robustness.

CHAPTER 5

SPATIAL-TEMPORAL MODELING

In this chapter, we delve into spatial-temporal modeling approaches for predicting the burned area of wildfires. Building upon our previous work with the Active Fire Line sampled time series conversion, which yielded moderate success, we aim to address the limitations identified in that method by incorporating spatial-temporal dynamics into our models.

The Active Fire Line sampling approach, while effective for small-scale fires where the surrounding area is relatively homogeneous, encounters significant challenges when applied to larger wildfires. One major issue is the homogenization of diverse fire dynamics within the sampled area. As fires expand, different sections of the active fire line may exhibit varying behaviors and importances, which are not adequately captured when homogenized into a single sample.

Another limitation lies in determining the appropriate sample size. In scenarios where the fire spreads over a vast area, sampling a small region fails to represent the full extent of the burnable area, potentially leading to inaccurate predictions. Additionally, the sampling process may not accurately reflect the active fire zones. The assumption that the active fire line is uniformly similar overlooks the possibility of internal zones within the fire that are still actively burning and can influence future spread. It also fails to account for variations in fire activity across different areas, making it unclear where the fire is most likely to propagate.

To overcome these challenges, we explore spatial-temporal modeling techniques that can capture the complex dynamics of wildfire spread over both space and time. By integrating detailed spatial data and temporal evolution of fires, we aim to develop more accurate predictive models that can effectively inform wildfire management and mitigation strategies.

5.1 RELATED WORK

modeling wildfire spread is a complex task due to the nonlinear, multi-scale, and stochastic nature of fire behavior. Various approaches have been developed to predict wildfire propagation, generally categorized into three main types: empirical and semi-empirical models, macroscopic-deterministic models, and stochastic grid-based models [122, 123, 124, 125, 126].

Empirical and semi-empirical models rely on statistically derived relationships to predict fire spread [127, 128]. These models are relatively straightforward to implement, computationally efficient, and can approximate fire dynamics under certain conditions. However, they are often derived from controlled experiments and may not generalize well to wildfires occurring under different environmental conditions or in diverse landscapes [123].

Macroscopic-deterministic models attempt to simulate fire spread using first-principles physics, often involving computational fluid dynamics coupled with atmospheric, heat transfer, and combustion models [129, 130, 131]. While these models aim to capture the detailed physics of fire behavior, they are computationally intensive and may not be practical for real-time forecasting or large-scale simulations. Additionally, the inherent complexity and nonlinearities in wildfire dynamics can limit the predictive accuracy of these models [122].

Stochastic grid-based models, such as Cellular Automata (CA), offer a middle ground by discretizing space and time to simulate fire spread through local interactions [132, 133, 134]. In these models, the fire propagates from one cell to its neighbors based on probabilistic rules that encapsulate the underlying physics at a desired level of resolution. CA models are versatile and can incorporate both theoretical principles and empirical relationships. They are also well-suited for integrating spatial and temporal heterogeneity, such as varying vegetation types, topography, and meteorological conditions [125].

One notable example of a stochastic grid-based model is PROPAGATOR [135]. PROPAGATOR is a stochastic cellular automaton designed for rapid fire risk assessment, utilizing high-resolution data on topography and vegetation. The model simulates multiple realizations of stochastic fire propagation, providing probabilistic maps of fire spread that can inform decision-making in civil protection and fire management. It accounts for factors such as wind speed and direction, fuel moisture content, and firebreaks, offering a practical balance between computational efficiency and modeling complexity.

Recent advancements in machine learning have also been applied to wildfire spread

modeling. Cheng et al. introduced a parameter-flexible fire prediction algorithm using machine learning and reduced-order modeling techniques to efficiently forecast burned areas [136]. In a subsequent study, they proposed a generative model using vector-quantized variational autoencoders to generate spatial-temporal sequences of wildfire burned areas, which can be used to train surrogate models for predicting wildfire dissemination [137].

Data-driven approaches utilizing deep learning have shown promise in modeling wildfire spread across large regions. A study developed a spatiotemporal graph neural network to predict the daily spread of European wildfires, indicating increased transferability across different Mediterranean countries [138]. Although the model faced challenges in achieving high accuracy due to data quality limitations, it demonstrated the potential of deep learning methods in capturing generalized patterns of wildfire spread.

Furthermore, generative algorithms have been explored for integrating physics-based wildfire spread models with satellite data. Generative adversarial networks (GANs) have been used to infer fire arrival times from satellite detections, providing necessary information to initialize coupled atmosphere-wildfire models for forecasting [139]. This approach allows for the assimilation of real-time observations to adjust model parameters, leading to more accurate future predictions.

In summary, while traditional modeling approaches have provided valuable insights into wildfire dynamics, their limitations in computational efficiency, generalizability, and predictive accuracy have prompted the exploration of hybrid and data-driven methods. By leveraging advancements in machine learning and probabilistic modeling, recent research aims to develop more accurate and efficient models for predicting wildfire spread, which is critical for effective wildfire management and mitigation strategies.

5.2 METHODOLOGY

In this section, we present our approach for modeling wildfire spread using a Cellular Automata (CA) framework and compare it with black-box neural network models. Our objective is to develop a simulator that can predict the evolution of wildfires over time and space by estimating transition probabilities based on both local interactions and external environmental factors.

5.2.1 CELLULAR AUTOMATA

We employ a Cellular Automata framework to model wildfire spread. Let s represent the state of the system, where s_i denotes the state of a specific location i , and $\mathcal{N}(i)$ represents the set of neighbors for location i . In our two-dimensional grid, we utilize

the Moore neighborhood, which includes all adjacent cells, resulting in $|\mathcal{N}(i)| = 8$.

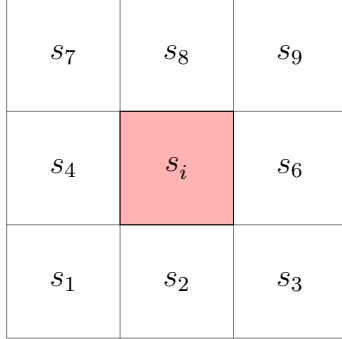


Figure 5.1: Illustration of the Moore neighborhood for a central cell s_i . Each surrounding cell represents a neighbor in the set $\mathcal{N}(i)$.

Adding a temporal dimension, the state of cell i at time t is denoted by $s_i^{(t)}$. Our goal is to define the conditional probability $p(s_i^{(t+1)}|s_{\mathcal{N}(i)}^{(t)}, s_i^{(t)})$, which determines how the state of cell i evolves based on its current state and the states of its neighbors.

We model the fire spread as a ternary state system with the following 3 states: *Unburned* (U), *Burning* (B) and *Extinguished* (E). Initially, all cells are in the *Unburned* state. A cell remains *Unburned* until a neighboring *Burning* cell ignites it, transitioning it to the *Burning* state. After burning, a cell transitions to the *Extinguished* state, indicating it has been burned. Figure 5.2 illustrates the possible state transitions between the states along with their associated probabilities.

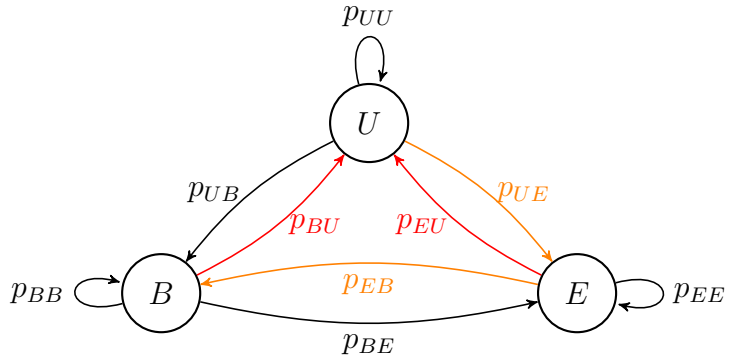


Figure 5.2: State diagram of the automata, illustrating transitions between *Unburned* (U), *Burning* (B), and *Extinguished* (E) states along with their respective probabilities. A priori, transitions marked in red have zero probability, while those in orange may have non-zero probability.

In our CA model, a cell i can transition from *Unburned* to *Burning* at time $t + 1$ if at least one neighbor $j \in \mathcal{N}(i)$ is *Burning* at time t . The probability of this transition is given by:

$$p(s_i^{(t+1)} = B \mid s_i^{(t)} = U, s_{\mathcal{N}(i)}^{(t)}, \mathbf{z}) = 1 - \prod_{j \in \mathcal{N}(i)} \left(1 - p(s_i^{(t+1)} = B \mid s_j^{(t)} = B, s_i^{(t)} = U, \mathbf{z})\right)$$

Here, $p(s_i^{(t+1)} = B \mid s_j^{(t)} = B, s_i^{(t)} = U, \mathbf{z})$ represents the conditional probability that cell i ignites due to a *Burning* neighbor j , given environmental factors \mathbf{z} . The term $1 - p(\dots)$ represents the probability that the fire does not propagate from neighbor j to cell i . The product over neighbors accounts for the combined effect of all *Burning* neighbors.

This formulation leads us to the task of defining $p_{XY}^{(t)}(i, j)$, which denotes the probability of cell i transitioning from state X to state Y at time $t + 1$, given the state of neighbor j at time t and environmental variables \mathbf{z} . [Figure 5.3](#) illustrates how the state of cell i at time $t + 1$ is influenced by the states of its neighbors at time t .

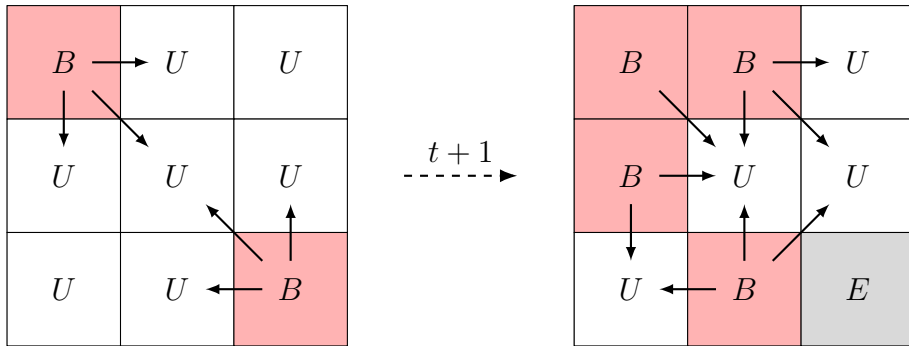


Figure 5.3: Representation of the Moore neighborhood for a cellular automata at time t and $t + 1$. The grid at t shows the initial states with potential influences on the central cell s_i indicated by arrows. The grid at $t + 1$ illustrates the state transitions where s_i and its neighbors change to $s_i^{(t+1)}$. White cells are *Unburned*, red cells are *Burning*, and gray cells are *Extinguished*.

In existing literature on CA for wildfires, typically only the transitions p_{UB} (from *Unburned* to *Burning*) and p_{BE} (from *Burning* to *Extinguished*) are considered, while all other transitions are assumed to have zero probability. The transition p_{BE} is often set to 1, implying that every *Burning* cell will become *Extinguished* in the next time step.

For example, in PROPAGATOR [126], the probability $p(s_i^{(t+1)} = B \mid s_j^{(t)} = B, s_i^{(t)} = U, \mathbf{z})$ is defined as:

$$p_{UB}^{(t)}(i, j) = \left(1 - (1 - \theta_{\text{nom}}(\text{veg}(i), \text{veg}(j)))^{\theta_{\text{wh}}^{(t)}}\right) \cdot \theta_{e_m}$$

where $\theta_{\text{nom}}(\text{veg}(i), \text{veg}(j))$ is a parameter that depends on the vegetation types at cells i and j , $\theta_{\text{wh}}^{(t)}$ combines wind and topography effects, and θ_{e_m} accounts for fuel moisture content. The exact way these parameters have been estimated is not clear

in the paper, a common occurrence in this sort of literature.

Another common definition, as proposed in [125] and extensively used in other works [134, 136, 137], is:

$$p_{UB}^{(t)}(i, j) = \theta_{\text{nom}}(i) (1 + \theta_{\text{veg}}(i)) (1 + \theta_{\text{den}}(i)) \theta_w^{(t)}(i) \theta_t(i)$$

where $\theta_{\text{nom}}(i)$ is a parameter indicating that a cell next to a burning cell will catch fire under no wind, flat terrain, and given vegetation type and density. The terms $\theta_{\text{veg}}(i)$, $\theta_{\text{den}}(i)$, $\theta_w^{(t)}(i)$, and $\theta_t(i)$ represent adjustments based on vegetation type, vegetation density, wind speed, and topography, respectively.

STATE SPACE PROBLEM DEFINITION

Given a sequence of states $\mathbf{s}^{(1)}, \mathbf{s}^{(2)}, \dots, \mathbf{s}^{(T)}$, where each $\mathbf{s}^{(t)}$ represents the state of the system at time t , we aim to estimate the parameter set θ that maximizes the likelihood of observing this sequence under our model.

Assuming that it is Markovian, the joint probability of observing the sequence is:

$$P_\theta(\mathbf{s}^{(1)}, \mathbf{s}^{(2)}, \dots, \mathbf{s}^{(T)}) = \prod_{t=1}^T P_\theta(\mathbf{s}^{(t)} \mid \mathbf{s}^{(t-1)})$$

Assuming that the state of each cell at time t depends only on its previous state and the states of its neighbors at time $t-1$, we decompose $P_\theta(\mathbf{s}^{(t)} \mid \mathbf{s}^{(t-1)})$ as:

$$P_\theta(\mathbf{s}^{(t)} \mid \mathbf{s}^{(t-1)}) = \prod_{i=1}^N P_\theta(s_i^{(t)} \mid s_i^{(t-1)}, s_{\mathcal{N}(i)}^{(t-1)})$$

Thus, the joint probability becomes:

$$P_\theta(\mathbf{s}^{(1)}, \mathbf{s}^{(2)}, \dots, \mathbf{s}^{(T)}) = \prod_{t=1}^T \prod_{i=1}^N P_\theta(s_i^{(t)} \mid s_i^{(t-1)}, s_{\mathcal{N}(i)}^{(t-1)})$$

Our objective is to maximize the log-likelihood:

$$\theta^* = \arg \max_{\theta} [\log P_\theta(\mathbf{s}^{(1)}, \mathbf{s}^{(2)}, \dots, \mathbf{s}^{(T)})] = \arg \max_{\theta} \left[\sum_{t=1}^T \sum_{i=1}^N \log P_\theta(s_i^{(t)} \mid s_i^{(t-1)}, s_{\mathcal{N}(i)}^{(t-1)}) \right]$$

Given our model's assumptions, the conditional probability $P_\theta(s_i^{(t)} = Y \mid s_i^{(t-1)} = X, s_{\mathcal{N}(i)}^{(t-1)})$ can be expressed using the transition probabilities $p_{XY}^{(t)}(i, j)$:

$$P_\theta(s_i^{(t)} = Y \mid s_i^{(t-1)} = X, s_{\mathcal{N}(i)}^{(t-1)}) = 1 - \prod_{j \in \mathcal{N}(i)} (1 - p_{XY}^{(t)}(i, j))$$

The loss function for parameter estimation, considering all possible state transitions $X \rightarrow Y$ in the set $\{U, B, E\}$, is:

$$\mathcal{L}(\theta) = - \sum_{t=1}^T \sum_{i=1}^N \sum_{X, Y \in \{U, B, E\}} \mathbb{1}_{(s_i^{(t-1)} = X, s_i^{(t)} = Y)} \log \left(1 - \prod_{j \in \mathcal{N}(i)} (1 - p_{XY}^{(t)}(i, j)) \right)$$

Here, $\mathbb{1}_{(s_i^{(t-1)} = X, s_i^{(t)} = Y)}$ is an indicator function that equals 1 when cell i transitions

from state X to state Y between times $t - 1$ and t , and 0 otherwise.

Focusing on the significant transitions p_{UB} and p_{BE} , the loss function simplifies to:

$$\begin{aligned} \mathcal{L}(\theta) = & -\sum_{t=1}^T \sum_{i=1}^N \left[\mathbb{1}_{(s_i^{(t-1)}=U, s_i^{(t)}=B)} \log \left(1 - \prod_{j \in \mathcal{N}(i)} \left(1 - p_{UB}^{(t)}(i, j) \right) \right) \right. \\ & \left. + \mathbb{1}_{(s_i^{(t-1)}=B, s_i^{(t)}=E)} \log p_{BE}^{(t)}(i) \right] \end{aligned}$$

Our goal is to find the parameter set θ that minimizes this loss function, effectively estimating the transition probabilities that best explain the observed data.

INCORPORATING LONG-DISTANCE FIRE SPREAD

In reality, wildfires can spread beyond immediate neighbors due to factors such as wind-driven embers causing spot fires at a distance, or rapid spread through highly flammable vegetation. To account for this phenomenon, we introduce a stochastic parameter that allows the fire to spread to cells beyond the immediate neighborhood.

We define an extended neighborhood $\mathcal{N}_k(i)$ for each cell i , which includes all cells within a distance k from cell i . For $k = 1$, this reduces to the standard Moore neighborhood. By increasing k , we include cells that are further away.

To model the probability of the fire spreading to cells in this extended neighborhood, we introduce a distance-dependent reachability function $p_{\text{reach}}(i, j)$, which represents the probability that the fire can reach cell i from cell j in a single time step. This function can be defined based on the distance between i and j , as well as other environmental factors.

One possible definition for $p_{\text{reach}}(i, j)$ is:

$$p_{\text{reach}}(i, j) = \exp(-\alpha \cdot d(i, j))$$

where $d(i, j)$ is the Euclidean distance between cells i and j , and α is a parameter controlling how rapidly the probability decreases with distance. A smaller α allows the fire to spread further in a single time step.

Alternatively, we can model $p_{\text{reach}}(i, j)$ as:

$$p_{\text{reach}}(i, j) = \left(\frac{1}{d(i, j)} \right)^\beta$$

where β is a parameter to be learned.

We then modify the ignition probability to account for long-distance spread:

$$p(s_i^{(t+1)} = B \mid s_i^{(t)} = U, s_{\mathcal{N}_k(i)}^{(t)}, \mathbf{z}) = 1 - \prod_{j \in \mathcal{N}_k(i)} \left(1 - p_{UB}^{(t)}(i, j) \cdot p_{\text{reach}}(i, j) \right)$$

By including $p_{\text{reach}}(i, j)$, we incorporate the reduced likelihood of fire spreading from distant cells.

The loss function is adjusted accordingly to sum over the extended neighborhood:

$$\begin{aligned} \mathcal{L}(\theta) = - \sum_{t=1}^T \sum_{i=1}^N & \left[\mathbb{1}_{(s_i^{(t-1)}=U, s_i^{(t)}=B)} \log \left(1 - \prod_{j \in \mathcal{N}_k(i)} \left(1 - p_{UB}^{(t)}(i, j) \cdot p_{\text{reach}}(i, j) \right) \right) \right. \\ & \left. + \mathbb{1}_{(s_i^{(t-1)}=B, s_i^{(t)}=E)} \log p_{BE}^{(t)}(i) \right] \end{aligned}$$

To model the variability in how far the fire can spread in a single time step, we can introduce a random variable D representing the maximum distance the fire can reach. We can model D using a probability distribution, such as a Poisson or geometric distribution, parameterized by λ :

$$P(D=d) = \frac{\lambda^d e^{-\lambda}}{d!}$$

At each time step, we sample D from this distribution to determine the extent of the neighborhood $\mathcal{N}_D(i)$ to consider for fire spread.

Alternatively, we can treat λ as a learnable parameter, optimizing it during the training process to best fit the observed data.

PARAMETERS

For the CA model, the set of parameters θ can include various factors influencing fire spread. We can, for instance, incorporate environmental variables such as wind speed (θ_{wind}), temperature (θ_{temp}), vapor pressure deficit (θ_{VPD}), etc.

These parameters are integrated into the transition probabilities through functions like logistic regression. For example, the probability of a cell transitioning from *Unburned* to *Burning* can be modeled as:

$$p_{UB}^{(t)}(i) = \sigma \left(\theta_0 + \sum_k \theta_k \cdot X_k^{(t)}(i) \right)$$

where σ is the sigmoid function, $X_k^{(t)}(i)$ represents the k -th covariate at cell i and time t , and θ_0 is the bias term, and θ_k are the logistic regression coefficients to be learned.

Moreover, we model the extinction probability $p_{BE}^{(t)}(i)$ for cell i at time t as a function of environmental factors and fuel characteristics. Similar to the ignition probability, we use logistic regression to model $p_{BE}^{(t)}(i)$:

CA ARCHITECTURE

Our model architecture is fully differentiable with respect to the parameters θ , allowing the use of gradient-based optimization methods to minimize the loss function

and effectively learn the parameters.

The overall architecture comprises the following components:

1. **Input Layer:** For each cell i , we input the covariates $\mathbf{X}^{(t)}(i)$ at time t . These covariates include environmental factors such as Vapor Pressure Deficit (VPD) and fuel characteristics, as well as the current state of the cell and its neighbors.
2. **Logistic Regression Layers:** These layers model the transition probabilities for each cell. Specifically, we compute the probability of transitioning from *Unburned* to *Burning* ($p_{UB}^{(t)}(i)$) and from *Burning* to *Extinguished* ($p_{BE}^{(t)}(i)$) using logistic regression based on the input covariates.
3. **CA Transition Layer:** Utilizing Cellular Automata dynamics, this layer aggregates ignition probabilities from all burning neighbors to determine the overall probability of a cell igniting. It also applies extinction probabilities to burning cells, updating their states accordingly.
4. **Output Layer:** The final layer outputs the predicted state $s_i^{(t+1)}$ for each cell, indicating whether it remains *Unburned*, becomes *Burning*, or transitions to *Extinguished*.

By integrating the extinction probability into our CA model, we account for both ignition and extinction processes, enhancing the model's realism and predictive capability.

5.2.2 IMAGE-TO-IMAGE PROBLEM DEFINITION

In addition to the Cellular Automata approach, we explore a data-driven, black-box methodology using neural networks for predicting wildfire spread. This method frames the problem as an image-to-image translation task, where the input is the state of the fire at time t , and the output is the predicted state at time $t + 1$.

We define the state of the system at time t as a spatial grid $\mathbf{s}^{(t)}$, where each cell $s_i^{(t)}$ represents the state at location i . The evolution of the system is modeled as:

$$\mathbf{s}^{(t+1)} = \text{NN}_\theta(\mathbf{s}^{(t)})$$

Here, NN_θ is a neural network parameterized by θ , which predicts the next state of the system given the current state. The goal is to train NN_θ to accurately forecast the spread of the wildfire based on historical data.

Our primary objective is to predict whether a location i will be burning at time $t + 1$. Therefore, we simplify the problem to a binary classification task by defining a binary

variable $b_i^{(t+1)}$, where:

$$b_i^{(t+1)} = \begin{cases} 1, & \text{if cell } i \text{ is burning at time } t + 1 \\ 0, & \text{otherwise} \end{cases}$$

To train the neural network, we use pairs of consecutive states $(\mathbf{s}^{(t)}, \mathbf{s}^{(t+1)})$. The network learns to map the input state $\mathbf{s}^{(t)}$ to the output state $\mathbf{s}^{(t+1)}$, effectively learning the dynamics of fire spread.

The loss function used for training is the binary cross-entropy loss, defined as:

$$\mathcal{L} = - \sum_{i=1}^N \left[b_i^{(t+1)} \log \hat{b}_i^{(t+1)} + (1 - b_i^{(t+1)}) \log (1 - \hat{b}_i^{(t+1)}) \right]$$

where N is the total number of cells in the grid, $b_i^{(t+1)}$ is the actual burning state of cell i at time $t + 1$, and $\hat{b}_i^{(t+1)}$ is the predicted probability that cell i is burning at time $t + 1$, output by the neural network.

Alternatively, if we consider all possible states (*Unburned*, *Burning*, *Extinguished*), we can model the problem as a multi-class classification task using the categorical cross-entropy loss:

$$\mathcal{L} = - \sum_{i=1}^N \sum_{c \in C} \mathbb{1}_{\{s_i^{(t+1)}=c\}} \log \hat{s}_{i,c}^{(t+1)}$$

where C is the set of possible states, $\mathbb{1}_{\{s_i^{(t+1)}=c\}}$ is the indicator function, which equals 1 if $s_i^{(t+1)} = c$ and 0 otherwise, and $\hat{s}_{i,c}^{(t+1)}$ is the predicted probability that cell i is in state c at time $t + 1$.

By optimizing these loss functions, the neural network learns to minimize the discrepancy between the predicted and actual states, enhancing its ability to accurately simulate the evolution of wildfire spread over time.

NEURAL NETWORK MODELS

We explore several neural network architectures for the image-to-image prediction task:

- **Fire Persistence:** As a simple baseline, similar to the approach in [140]. This model simply predicts that the burning state at time $t + 1$ will be the same as at time t . It assumes that currently burning cells will continue to burn, and no new cells will ignite. This provides a straightforward benchmark to assess the performance of the more complex neural network models.
- **Logistic Regression:** We implement a logistic regression model using a convolutional layer with a 3×3 kernel [140]. This model predicts the burning probability of each cell based on its immediate neighborhood. This approach is similar to using a single convolutional layer without activation functions beyond

the logistic sigmoid.

- **U-Net:** We utilize the U-Net architecture [141], which is designed for image segmentation tasks. The U-Net captures both local and global spatial context through its encoder-decoder structure with skip connections. For temporal data, we concatenate multiple time steps along the channel dimension to incorporate temporal information.
- **ConvLSTM:** The ConvLSTM [142] is a recurrent neural network architecture that combines convolutional operations with LSTM units. It is well-suited for spatiotemporal data, as it can capture temporal dependencies in the data while preserving spatial structure. We use a single ConvLSTM block followed by a convolutional layer to produce the output segmentation map.

5.2.3 EVALUATION METRICS

To assess the performance of our models, we utilize two primary metrics commonly used in image segmentation and classification tasks:

- **Intersection over Union (IoU):** Also known as the Jaccard Index, measures the overlap between the predicted and ground truth areas for a particular class. It is defined as:

$$\text{IoU} = \frac{|\text{Prediction} \cap \text{Ground Truth}|}{|\text{Prediction} \cup \text{Ground Truth}|} \quad (5.1)$$

This metric ranges from 0 to 1, where 1 indicates perfect overlap between the prediction and the ground truth. In the context of wildfire spread, a higher IoU indicates that the model accurately predicts the spatial extent of the burning area.

- **F1 Score:** It is the harmonic mean of precision and recall, providing a balance between these two metrics. It is defined as:

$$\text{F1 Score} = 2 \times \frac{\text{Precision} \times \text{Recall}}{\text{Precision} + \text{Recall}}$$

Where precision and recall are calculated as:

$$\text{Precision} = \frac{\text{True Positives}}{\text{True Positives} + \text{False Positives}}$$

$$\text{Recall} = \frac{\text{True Positives}}{\text{True Positives} + \text{False Negatives}}$$

In our application, the F1 score evaluates the model's ability to correctly identify burning cells while minimizing both false alarms (false positives) and missed detections (false negatives).

5.2.4 TRAINING PROCEDURE

Given the limited availability of real wildfire data—specifically, the DataCube we procured currently contains data for only one fire event—we focus on training our models using simulated data as a proof of concept. This approach allows us to validate our models’ capabilities in a controlled environment before applying them to real-world data when more becomes available.

DATA GENERATION

We generate synthetic wildfire spread data using the CA simulation framework described previously. The simulation operates on a two-dimensional grid initialized with one or more ignited cells. At each discrete time step, cells transition between states based on predefined probabilities:

- *Burning* cells may transition to the *Extinguished* state.
- *Unburned* cells may ignite and become *Burning* if they have at least one neighboring *Burning* cell.

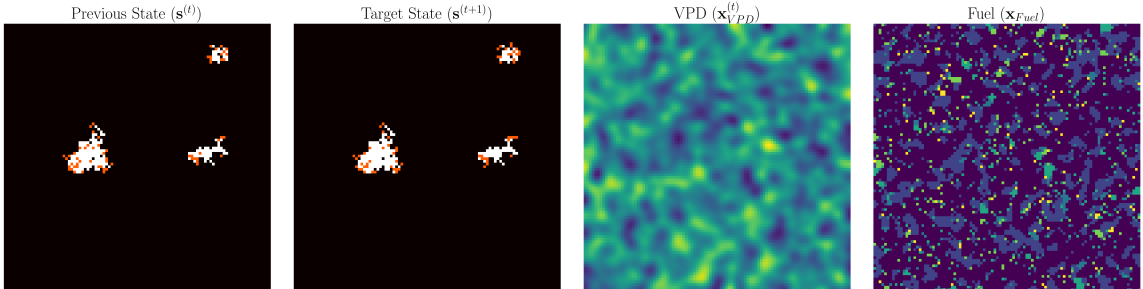


Figure 5.4: Example of a simulation at an advanced time step. From left to right: previous state, target state, VPD, and Fuel.

COVARIATES Our model incorporates two primary covariates: the fuel map and Vapor Pressure Deficit (VPD). The Fuel Map is represented as a static image that encodes different vegetation types using distinct colors. These fuel types are categorized into 6 categories, enabling differentiation of areas based on their flammability and combustion characteristics. In contrast, the VPD varies dynamically over time. To maintain spatial consistency and realism, VPD values are generated with added noise, simulating environmental fluctuations.

SIMULATION PARAMETERS Fire spread within the simulation is governed by a logistic regression model that estimates the probabilities of ignition and extinction based on environmental factors and fuel types. Using these covariates, the probability of a

cell i transitioning from *Unburned* to *Burning* at time t is computed as:

$$p_{UB}^{(t)}(i) = \sigma \left(\theta_0 + \theta_{vpd} \cdot VPD^{(t)}(i) + \theta_{fuel}(fuel(j)) - \theta_{fuel}(fuel(i)) \right)$$

where the model parameters¹ are defined as follows: the ignition coefficient for VPD is set to $\theta_{vpd} = 0.02$, and the fuel type coefficients are $\theta_{fuel} = [0.5, 0.4, 0.3, 0.2, 0.1, -1.0]$. Additionally, the intercept term is $\theta_0 = -4.5$.

For extinction, the probability that a *Burning* cell becomes *Extinguished* is directly based on its fuel type:

$$p_{BE}^{(t)}(i) = \phi_{fuel}(fuel(i))$$

where the model utilizes $\phi_{fuel} = [0.3, 0.16, 0.12, 0.10, 0.08, 1.0]$.

These probabilities are integrated into CA dynamics to update each cell's state to generate the fire states \mathbf{s} . This dual consideration of ignition and extinction processes enhances the model's realism and predictive capability by accounting for both the spread and cessation of wildfires under varying environmental conditions.

DATA PREPARATION FOR TRAINING Multiple time steps are simulated to generate sequences of grid states. These sequences are then partitioned into input-output pairs $(\mathbf{s}^{(t)}, \mathbf{s}^{(t+1)})$, where $\mathbf{s}^{(t)}$ is the grid state at time t and $\mathbf{s}^{(t+1)}$ is the subsequent state. We can lengthen the context by giving $(\mathbf{s}^{(t-k)}, \dots, \mathbf{s}^{(t)}, \mathbf{s}^{(t+1)})$. These pairs serve as the training data for both the CA model and the neural network models, enabling the models to learn the dynamics of wildfire spread.

MODEL TRAINING

CELLULAR AUTOMATA MODEL For the CA model, we optimize the parameters θ (including both ignition and extinction coefficients) by minimizing the loss function derived from the likelihood of observing the simulated data²:

$$\mathcal{L}(\theta) = - \sum_{t=1}^T \sum_{i=1}^N \log P_\theta(s_i^{(t)} \mid s_i^{(t-1)}, s_{\mathcal{N}(i)}^{(t-1)}).$$

We use gradient-based optimization methods like Adam [100] with appropriate learning rates and batch sizes. Parameters are initialized randomly between -1 and 1.

NEURAL NETWORK MODELS For neural network models, we use the same dataset of input-output pairs $(\mathbf{s}^{(t)}, \mathbf{s}^{(t+1)})$ or series. The training involves minimizing specific loss functions between the predicted and target states³:

¹These values were obtained through trial and error upon visual inspection and comparison of the VIIRS detections.

²After more trial and error, I couldn't get the sophisticated multi-step generation to work. Thus, the results are using the simplified version.

³To determine the learning rate and loss function, we ran coarse grid searches for each model separately. We combined learning rates in 10^{-i} , $1 \leq i \leq 3$ with the loss functions weighted binary

- **Logistic Regression:** Trained using the Dice loss with a learning rate of 0.1.
- **U-Net:** Utilizes a Dice loss with a learning rate of 0.001. Additionally, we use a ResNet18 [143] for its encoder.
- **ConvLSTM:** Use Jaccard loss with a learning rate of 0.01. Additionally, we use a hidden layer of size 64, and kernels of size 3×3 .

Models are trained using the AdamW optimizer [144] with default parameters ($\beta_1 = 0.9$, $\beta_2 = 0.999$, weight decay $\lambda = 0.01$). Parameters are initialized using He initialization [145].

TRAINING DETAILS

Key aspects of our training process include:

- **Image dimensions:** We use images of 128×128 pixels.
- **Learning Rate and Scheduling:** We use a base learning rate $\eta = 10^{-3}$ with cosine annealing to adjust the learning rate during training.
- **Batch Size and Iterations:** For the CA model, we use a minibatch size $b = 32$ and train for $N = 10,000$ simulations (until a fire ends). Training typically lasts up to a day, depending on model complexity. Neural network models are trained for a total of 10,000 epochs.
- **Validation and Early Stopping:** We monitor the validation loss after each epoch and retain the model with the best validation performance to prevent overfitting.
- **Data Splitting:** Ideally, data would be split into training, validation, and test sets. However, due to limited real data, we rely solely on simulated data for both training and validation in this proof of concept.

These training steps ensure effective optimization of our models, leveraging each approach's strengths to simulate wildfire spread accurately.

5.3 RESULTS

We evaluate the performance of our proposed methodology using key metrics summarized in [Table 5.1](#). This table compares four models—Cellular Automata, Logistic Regression, U-Net, and ConvLSTM—across various evaluation criteria, using different time windows. These metrics are focused on predicting whether a pixel will be *Burning*. The other two classes, *Unburned* and *Extinguished*, are excluded from the cross-entropy, focal loss, Dice loss, Jaccard loss.

analysis due to the significantly higher impact of accurately predicting burning pixels and the relative ease of correctly classifying the unburned and burned states. By concentrating on the burning class, we aim to prioritize critical predictions that are essential for timely interventions and resource allocation.

Table 5.1: Quantitative Evaluation Metrics for Wildfire Spread Models on Simulation.

Model	Window	Parameters	IoU	F1
Baseline	1	0	0.4814	0.5011
Logistic Regression	1	19	0.6171	0.7607
Cellular Automata	1	14	0.6429	0.7824
U-Net	1	14.3M	0.6690	0.8021
Cellular Automata	5	66	0.6523	0.7931
U-Net	5	14.5M	0.6622	0.7940
ConvLSTM	5	155K	0.6693	0.8102

ConvLSTM outperformed all other models, achieving the highest IoU and F1 scores. Surprisingly, increasing the time window led to improved performance, even though our simulation operates under a Markovian assumption relying solely on the previous time step. Additionally, all models exceeded the parameter-free fire persistence baseline, demonstrating the effectiveness of more advanced models.

The gains observed with an extended time window may be attributed to random variations rather than improved performance. Nevertheless, ConvLSTM remains the preferred model due to its superior performance, despite having orders of magnitude more parameters compared to other models like CA and Logistic Regression. The CA model not only achieved competitive performance with fewer parameters but also offers the advantage of having explainable parameters, which aids human comprehension. It is important to note that the CA model benefited from a predefined structural form, as we created the simulated data and knew the underlying structure; thus, this advantage might not persist in scenarios where the structural form is unknown.

PARAMETER ESTIMATION FOR THE CA MODEL

[Table 5.2](#) compares the estimated parameters (θ and ϕ) derived from the CA model against their true or simulated values. This comparison highlights the accuracy and discrepancies in the model’s parameter estimations.

Table 5.2: Parameter Estimation for Cellular Automata Model.

Parameter	True Value	Estimated Value
θ_{vpd}	0.02	-0.04
θ_{fuel}	[0.5, 0.4, 0.3, 0.2, 0.1, -1.0]	[-0.44, -0.50, 0.36, -0.11, 0.22, -2.21]
θ_0	-4.5	-3.12
ϕ_{fuel}	[0.3, 0.16, 0.12, 0.10, 0.08, 1.0]	[0.35, 0.22, 0.10, 0.16, 0.04, -0.07]

The parameter estimation results provide valuable insights into the performance of the CA model. Overall, the model demonstrates reasonable accuracy in estimating certain fuel spread rates and VPD. For example, the third and fifth fuel spread parameters ($\hat{\theta}_{\text{fuel},3} = 0.36$ and $\hat{\theta}_{\text{fuel},5} = 0.22$) are relatively close to their true values of 0.3 and 0.1, respectively. However, other parameters exhibit significant deviations. Notably, the estimation for the nonburnable-fuel spread rate ($\theta_{\text{fuel},6}$) is off, but it still aligns with the simulation's design that these fuels do not burn (e.g., water).

The spread parameters (ϕ_{fuel}) are generally acceptable, though some inconsistencies remain. For example, the extinction rate of nonburnable-fuels ($\phi_{\text{fuel},6}$) being so close to zero, which is probably the result from the parameter never being encountered during training and keeping its initial random value. This scenario that may apply to several other parameters due to their limited prevalence in the simulated environments.

Additionally, the intercept term (θ_0) is estimated to be less negative (-3.12) compared to its true value (-4.5). This discrepancy might compensate for inaccuracies in other parameters, particularly those related to fuel extinction rates and spread.

Overall, the CA model successfully identifies parameters close to the original values, facilitating straightforward interpretation of the results. While the model accurately captures certain fuel extinction rates and appropriately handles non-burning components like water, discrepancies in the spread parameters and the intercept highlight areas for potential improvement.

VISUAL COMPARISON OF FIRE SPREAD PREDICTIONS

[Figure 5.5](#) presents the CA model applied to a simulated fire scenario. While identifying the model's shortcomings is challenging even at full resolution, it appears that the model's predictions often remain confined within the existing fire boundaries and have difficulty accurately capturing the spread of the fire.

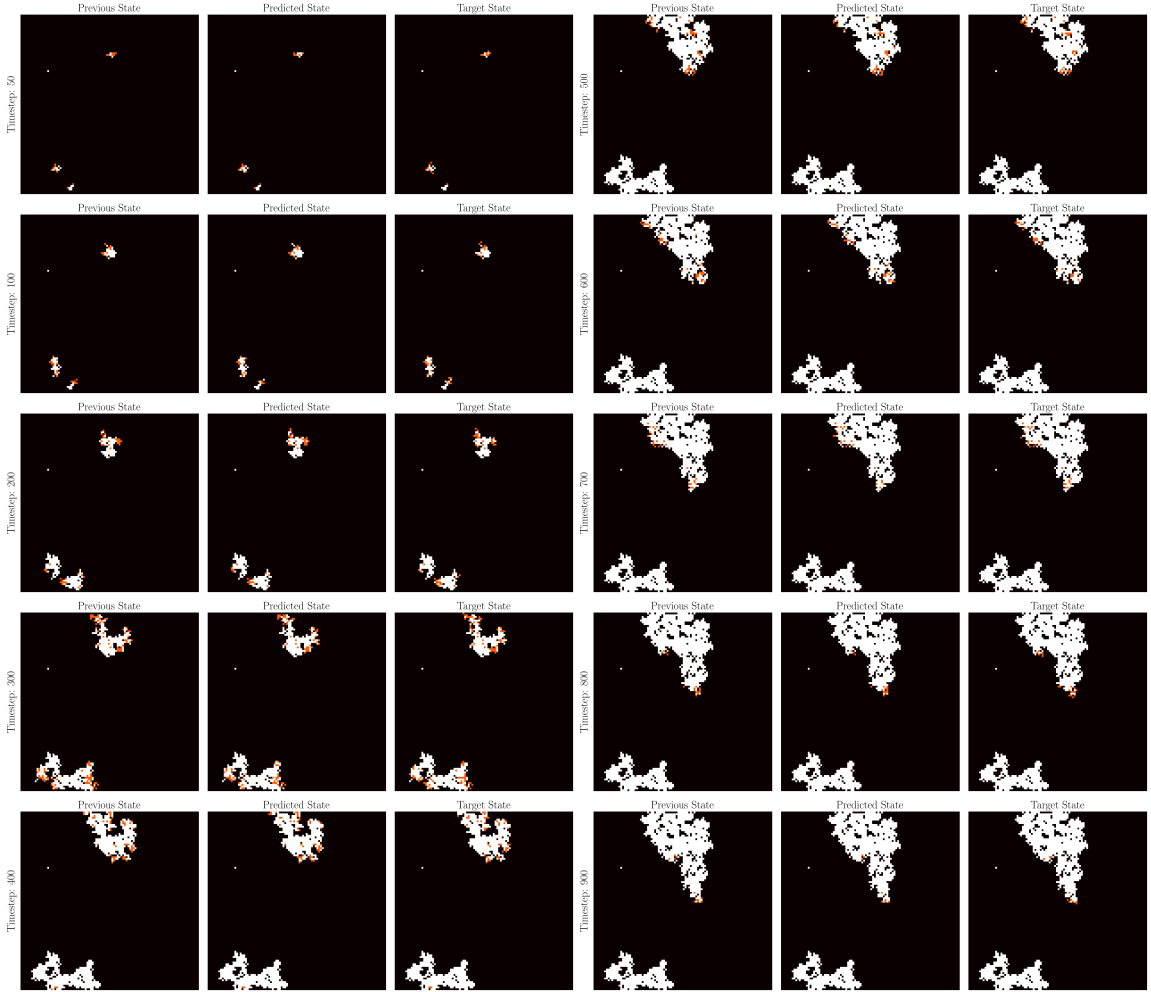


Figure 5.5: Evolution of Predicted Fire Spread. The left panel displays the predicted fire states for the first 400 time steps, while the right panel shows the corresponding target states for the subsequent 500 time steps. In the images, white indicates *Burned* areas, black represents *Unburned* regions, and red denotes *Burning* areas. For both panels we have Previous State, Prediction, and Target state. The predictions come from the CA.

5.4 DISCUSSION

In this chapter, we investigated the modeling of wildfire spread using both Cellular Automata and Neural Network approaches, focusing on their capacity to predict fire dynamics in simulated environments. While our models showed promising results on synthetic data, several challenges emerged when considering their application to real-world scenarios.

A primary research question we addressed was whether models trained on simulated data could effectively predict real wildfire events. We attempted to apply a model trained on our simulation to the Creek Fire using the DataCube dataset. However, the results were poor and are not included in this report. This outcome was antici-

pated, as our simulation was a proof of concept and lacked the complexity inherent in real-world conditions. Wildfires are influenced by numerous factors—such as heterogeneous fuel distributions, variable weather conditions, and complex terrain—that are difficult to capture accurately in simple simulations. This underscores a significant limitation: models trained exclusively on synthetic data may not generalize well to actual wildfire events.

The CA model demonstrated potential due to its interpretability and the novel formulation of its loss function. By defining the loss function based on transition probabilities between different cell states, we introduced an approach that could enhance the model’s accuracy and offer insights into the dynamics of fire spread. However, the CA model requires further refinement and validation with real datasets to confirm its effectiveness. The parameters estimated by the CA model were somewhat aligned with the true values used in the simulation, but discrepancies suggest that the model might struggle with the complexities of real-world data.

Despite the CA model’s interpretability, Neural Network models like ConvLSTM achieved slightly higher performance metrics on simulated data. However, these models are often considered “black boxes” due to their lack of transparency, making it challenging to understand the underlying processes influencing their predictions. Moreover, their performance advantage may diminish when applied to real-world data without substantial training on diverse and extensive datasets.

An important observation from our results is that increasing the temporal window of input data led to improved model performance, even though our simulation was based on a Markovian process relying solely on the previous time step. This suggests that incorporating additional temporal context can enhance model predictions, potentially capturing patterns or trends not immediately apparent in single-step transitions. However, it is challenging to ascertain the exact effect that temporal dynamics would have, especially since our simulation does not account for long-term dependencies.

It is crucial to acknowledge that predicting wildfire spread in a simulated environment is inherently less complex than in reality. In our simulation, the fire spread is limited to immediate neighbors, and often the models are predicting that burning cells will continue to burn until they extinguish. This may artificially inflate performance metrics, as it is relatively easy for models to predict such behavior. Nevertheless, the baseline persistence model, which simply assumes that the state remains the same, did not perform as well as our more advanced models. This indicates that there is still merit to our methods, as they capture aspects of the fire dynamics that the baseline does not.

5.4.1 FUTURE WORK

To enhance the applicability and effectiveness of wildfire spatio-temporal models, future research should focus on several key areas:

- Refining Simulation Models: Developing more sophisticated simulations that better mimic the complexities of real wildfires can serve as a more effective training ground for models. This includes incorporating additional environmental covariates, such as wind, humidity, and topographical features, to create a more realistic simulation environment. Nevertheless, this arises complexity in formulating the fire dynamics.
- Training on Real-World Data: This was the original intent of this chapter, nevertheless issues in timing forbade it. Training models on real-world data, such as satellite observations like those from the DataCube, can improve their ability to generalize and make accurate predictions for real-world scenarios without human bias in the model.
- Enhancing the CA Model: Further work on the CA model's loss function and parameter estimation can improve its performance. Exploring different formulations, incorporating additional environmental variables, and considering ways to increase the neighborhood or to allow for long-distance fire spread may yield better alignment with observed wildfire behavior.
- Combining Models: Investigating hybrid approaches that leverage the interpretability of CA models and the predictive power of Neural Networks could offer a balanced solution. Such models might capture complex patterns while remaining understandable to practitioners. For instance, integrating Neural Network components to estimate transition probabilities within a CA framework could enhance both performance and interpretability. This is not new and some approaches exist [146], but it would still be interesting to explore on wildfires.
- Trust: Recognizing and addressing the limitations of current models is essential. This includes improving their ability to handle the unpredictability of real-world conditions and ensuring they are robust against the variability inherent in natural systems. Techniques like uncertainty quantification and ablation studies could make models more trustworthy in real world practice.

CHAPTER 6

DISCUSSION

In this thesis, we explored various modeling approaches to predict wildfire spread in California. By utilizing both time series analytical methods and spatio-temporal modeling techniques applied to data derived from processed satellite imagery—as well as generating simulated data—we aimed to enhance predictive capabilities and provide deeper insights into the factors driving wildfire spread. Our research contributes to improved wildfire behavior modeling and supports real-time wildfire management and ecological impact assessments.

Below, we address each of the research questions posed, summarizing our findings and discussing their implications.

RESEARCH QUESTION RESPONSES

RQ1: How effectively can traditional time series models predict wildfire spread using univariate data derived from satellite imagery?

Traditional time series models are quite effective at predicting wildfire spread using satellite data. In our tests, ARIMA outperformed several neural networks. It handles noise well and works better with smaller datasets, providing reliable short-term forecasts by capturing time-based patterns.

RQ2: Can incorporating environmental covariates into multivariate time series models improve the accuracy of wildfire spread predictions compared to univariate models?

Yes, adding environmental factors to multivariate models makes wildfire predictions more accurate than using just one type of data. Including weather, fuel types, and past information helps the models better account for external influences on wildfires.

RQ3: What is the impact of suppression efforts on the predictive modeling

of wildfire spread, and how significant are these factors in the models?

The impact of suppression efforts on the predictive modeling of wildfire spread was found to be less significant than anticipated. In our analyses, features related to suppression efforts, such as the total number of firefighting personnel assigned to a fire, did not appear as significant predictors in the models. This may be due to limitations in the data, as in California all fires are fought and thus we only had data on fires that received suppression efforts, lacking a comparative baseline of fires without suppression. Hence, the models may not have been able to discern the true impact of suppression activities on fire spread.

RQ4: Can spatio-temporal models effectively predict wildfire spread in simulated environments, and what are the limitations when applying these models to real-world data?

Spatio-temporal models worked well in simulations, accurately predicting how fires spread over time and space. However, they struggled with real-world data due to the complexity of actual wildfires. This shows we need to train these models with more diverse and extensive real-world data to make them effective outside of simulations.

FUTURE WORK

In each modeling chapter, we have already described possible future work related to specific methods. Here, we summarize three key future research directions that could extend the entire project.

- Incorporating Firebreaks with Spatio-Temporal Models**

Firebreaks, which are gaps in vegetation or other combustible material, act as barriers to slow or stop the spread of wildfires. Modeling the effect of firebreaks requires incorporating spatial data on their locations and characteristics into the predictive models. The idea is to use spatio-temporal models to build a graph using the transition probabilities that can then be analyzed using graph theory to find optimal breaking points in the graph, with DomiRank for example [147].

- Tracking Suppression Efforts via Firefighters' Mobile Devices**

Another important area of future research is the incorporation of real-time data on suppression efforts, specifically by tracking the locations and movements of firefighting personnel using their mobile devices. By integrating geolocation data from firefighters' mobile phones into spatio-temporal models, we can gain insights into the deployment of resources and their direct impact on fire behavior. This would require addressing privacy and ethical considerations related

to tracking individuals, as well as developing methods to process and integrate this data in real-time.

- **Investigating Causal Relationships**

Transitioning from purely predictive models to causal models is another important direction. By employing causal inference techniques and counterfactual analysis, researchers can aim to understand the underlying mechanisms influencing fire spread and assess the effectiveness of suppression efforts and other interventions. This would help in establishing causality rather than merely identifying correlations, leading to more effective fire management strategies.

CONCLUSION

Wildfires are complex natural phenomena influenced by a multitude of factors, both environmental and human-induced. Predicting their spread remains a challenging yet vital endeavor for protecting the Earth and its inhabitants. This thesis has shed light on the capabilities and limitations of current modeling approaches, highlighting the potential of traditional statistical methods and the need for further development of advanced models.

Our research has demonstrated that traditional statistical models like ARIMA and ensemble methods like XGBoost currently offer strong performance in predicting wildfire spread using satellite-derived data. While advanced spatio-temporal neural network models hold promise, they require further development and training on extensive, high-quality datasets to handle the complexities of real-world wildfire dynamics effectively. Moreover, we found that incorporating environmental covariates enhances predictive accuracy, but operational factors like suppression efforts did not significantly impact model predictions in our study, possibly due to data limitations.

Addressing the challenges identified and pursuing the future work outlined will contribute to the advancement of wildfire behavior modeling. By integrating additional data sources, developing specialized models, and focusing on interpretability and trustworthiness, we can enhance the utility of these models for wildfire management.

CHAPTER 7

REFERENCES

- [1] William J Bond and Jon E Keeley. “Fire as a global ’herbivore’: the ecology and evolution of flammable ecosystems”. In: *Trends in Ecology & Evolution* 20.7 (2005), pp. 387–394.
- [2] Juli G Pausas and Jon E Keeley. “A burning story: the role of fire in the history of life”. In: *BioScience* 59.7 (2009), pp. 593–601.
- [3] Jon E Keeley et al. “Fire as an ecosystem process”. In: *The Encyclopedia of Biodiversity*. 2011, pp. 1–12.
- [4] Nathan L Stephenson et al. “Post-fire reference densities for giant sequoia seedlings in a new era of high-severity wildfires”. In: *Forest Ecology and Management* 562 (2024), p. 121916.
- [5] David N Soderberg et al. “Assessing giant sequoia mortality and regeneration following high-severity wildfire”. In: *Ecosphere* 15.3 (2024), e4789.
- [6] David MJS Bowman et al. “Fire in the Earth system”. In: *Science* 324.5926 (2009), pp. 481–484.
- [7] Jay D. Miller and H. Safford. “Trends in Wildfire Severity: 1984 to 2010 in the Sierra Nevada, Modoc Plateau, and Southern Cascades, California, USA”. In: *Fire Ecology* 8 (2012), pp. 41–57. DOI: [10.4996/fireecology.0803041](https://doi.org/10.4996/fireecology.0803041).
- [8] M. Goss et al. “Climate change is increasing the likelihood of extreme autumn wildfire conditions across California”. In: *Environmental Research Letters* 15 (2020). DOI: [10.1088/1748-9326/ab83a7](https://doi.org/10.1088/1748-9326/ab83a7).
- [9] Bang Nguyen Tran et al. “High-severity wildfires in temperate Australian forests have increased in extent and aggregation in recent decades”. In: *PLoS ONE* 15 (2020). DOI: [10.1371/journal.pone.0242484](https://doi.org/10.1371/journal.pone.0242484).

- [10] Matthew W. Jones et al. “Global and Regional Trends and Drivers of Fire Under Climate Change”. In: *Reviews of Geophysics* 60 (2022). DOI: [10.1029/2020rg000726](https://doi.org/10.1029/2020rg000726).
- [11] Julien Ruffault et al. “Increased likelihood of heat-induced large wildfires in the Mediterranean Basin”. In: *Scientific Reports* (2020). DOI: [10.1038/s41598-020-70069-z](https://doi.org/10.1038/s41598-020-70069-z).
- [12] K. Wei et al. “Stratosphere amplifies the global climate effect of wildfires”. In: *Science China Earth Sciences* 63 (2019), pp. 309–311. DOI: [10.1007/s11430-019-9560-3](https://doi.org/10.1007/s11430-019-9560-3).
- [13] J. Abatzoglou and A. P. Williams. “Impact of anthropogenic climate change on wildfire across western US forests”. In: *Proceedings of the National Academy of Sciences* 113 (2016), pp. 11770–11775. DOI: [10.1073/pnas.1607171113](https://doi.org/10.1073/pnas.1607171113).
- [14] Z. Holden et al. “Decreasing fire season precipitation increased recent western US forest wildfire activity”. In: *Proceedings of the National Academy of Sciences* 115 (2018), E8349–E8357. DOI: [10.1073/pnas.1802316115](https://doi.org/10.1073/pnas.1802316115).
- [15] D. Calkin, Matthew P. Thompson, and M. Finney. “Negative consequences of positive feedbacks in US wildfire management”. In: *Forest Ecosystems* 2 (2015), pp. 1–10. DOI: [10.1186/s40663-015-0033-8](https://doi.org/10.1186/s40663-015-0033-8).
- [16] Brooke et al. “Widespread severe wildfires under climate change lead to increased forest homogeneity in dry mixed-conifer forests”. In: *Ecosphere* (2019). DOI: [10.1002/ecs2.2934](https://doi.org/10.1002/ecs2.2934).
- [17] Mark A Finney et al. “On the need for a theory of wildland fire spread”. In: *International journal of wildland fire* 22.1 (2012), pp. 25–36.
- [18] Sarah McCaffrey, Robyn Wilson, and Avishek Konar. “Should I stay or should I go now? Or should I wait and see? Influences on wildfire evacuation decisions”. In: *Risk analysis* 38.7 (2018), pp. 1390–1404.
- [19] Max A Moritz et al. “Learning to coexist with wildfire”. In: *Nature* 515.7525 (2014), pp. 58–66.
- [20] W Matt Jolly et al. “Climate-induced variations in global wildfire danger from 1979 to 2013”. In: *Nature communications* 6.1 (2015), p. 7537.
- [21] Karin L Riley et al. “The relationship of large fire occurrence with drought and fire danger indices in the western USA, 1984–2008: the role of temporal scale”. In: *International Journal of Wildland Fire* 22.7 (2013), pp. 894–909.

- [22] Anthony L Westerling. “Increasing western US forest wildfire activity: sensitivity to changes in the timing of spring”. In: *Philosophical Transactions of the Royal Society B: Biological Sciences* 371.1696 (2016), p. 20150178.
- [23] California Department of Forestry and Fire Protection (CAL FIRE). *2018 Fire Siege*. 2019.
- [24] Da Wang et al. “Economic impact of California wildfires exceeds \$148.5 billion in 2018”. In: *Nature Sustainability* 4.3 (2021), pp. 252–260.
- [25] Piyush Jain et al. “A review of machine learning applications in wildfire science and management”. In: *Environmental Reviews* 28.4 (2020), pp. 478–505.
- [26] Malcolm P North et al. “Reform forest fire management”. In: *Science* 349.6254 (2015), pp. 1280–1281.
- [27] Mark A Finney et al. “A simulation of probabilistic wildfire risk components for the continental United States”. In: *Stochastic Environmental Research and Risk Assessment* 25.7 (2011), pp. 973–1000.
- [28] Scott L Stephens et al. “Temperate and boreal forest mega-fires: characteristics and challenges”. In: *Frontiers in Ecology and the Environment* 12.2 (2014), pp. 115–122.
- [29] Colleen E Reid et al. “Critical review of health impacts of wildfire smoke exposure”. In: *Environmental Health Perspectives* 124.9 (2016), pp. 1334–1343.
- [30] Lindsay M Johnston et al. “Wildfire risk management in North American boreal forests”. In: *Forestry Chronicle* 96.3 (2020), pp. 135–142.
- [31] S Veraverbeke, S Hook, and Glynn Hulley. “An alternative spectral index for rapid fire severity assessments”. In: *Remote Sensing of Environment* 123 (2012), pp. 72–80.
- [32] JT Randerson et al. “Global burned area and biomass burning emissions from small fires”. In: *Journal of Geophysical Research: Biogeosciences* 117.G4 (2012).
- [33] California Department of Forestry and Fire Protection (CAL FIRE). *2020 Fire Statistics*. 2021.
- [34] San-Miguel-Ayanz J et al. “Forest Fires in Europe, Middle East and North Africa 2017”. In: KJ-NA-29318-EN-C (print),KJ-NA-29318-EN-N (online) (2018). ISSN: 1018-5593 (print),1831-9424 (online). DOI: [10.2760/27815\(print\),10.2760/663443\(online\)](https://doi.org/10.2760/27815(print),10.2760/663443(online)).

- [35] National Institute of Standards and Technology (NIST). *Camp Fire Investigation Data Collection*. 2020.
- [36] Munich Re NatCatSERVICE. *Wildfires and Bushfires: Climate Change Increasing Wildfire Risk*. <https://www.munichre.com/en/risks/natural-disasters/wildfires.html>. Accessed: 2024-06-06. 2022.
- [37] USDA Forest Service. *Mendocino Complex BAER Assessment*. 2018.
- [38] Hannah Beausang. “Mendocino Complex wildfires cause \$56 million of insured losses”. In: *North Bay Business Journal* (Sept. 2018). URL: <https://www.northbaybusinessjournal.com>.
- [39] United States Forest Service. *August Complex Information*. National Wildfire Coordinating Group. Retrieved from the National Wildfire Coordinating Group. Jan. 2021. URL: <https://www.fs.usda.gov>.
- [40] California Legislative Analyst’s Office. *The 2023-24 Budget: Improving Legislative Oversight of CalFire’s Emergency Fire Protection Budget*. 2023.
- [41] National Institute of Standards and Technology (NIST). *The Costs and Losses of Wildfires: A Literature Review*. 2018.
- [42] Guido R Werf et al. “Global fire emissions estimates during 1997–2016”. In: *Earth System Science Data* 9.2 (2017), pp. 697–720.
- [43] AirNow. *Air Quality Index (AQI) Basics*. 2020.
- [44] National Oceanic and Atmospheric Administration (NOAA). *Smoke from US wildfires spreads to Europe*. 2020.
- [45] Copernicus Atmosphere Monitoring Service. *Monitoring the smoke from the California wildfires*. 2020.
- [46] Natural Resources Canada. *Canadian Wildland Fire Information System*. <https://cwfis.cfs.nrcan.gc.ca/>. Accessed: 2024-04-23. 2023.
- [47] Canadian Interagency Forest Fire Centre (CIFFC). *National Wildland Fire Situation Report*. <https://ciffc.net/>. Accessed: 2024-04-23. 2023.
- [48] Australian Government. “Australia’s 2019-20 Bushfire Season: A Statement by the Department of Agriculture, Water and the Environment”. In: (2020).
- [49] Luiz EO C Aragão et al. “21st Century drought-related fires counteract the decline of Amazon deforestation carbon emissions”. In: *Nature Communications* 9.1 (2018), pp. 1–12.
- [50] United Nations Environment Programme (UNEP). *Spreading like Wildfire: The Rising Threat of Extraordinary Landscape Fires*. 2021.

- [51] Daniel S Ward et al. “The changing radiative forcing of fires: global model estimates for past, present and future”. In: *Atmospheric Chemistry and Physics* 12.22 (2012), pp. 10857–10886.
- [52] Max A Moritz et al. “Learning to coexist with wildfire”. In: *Nature* 515.7525 (2014), pp. 58–66.
- [53] NASA. *MODIS Overview*. <https://modis.gsfc.nasa.gov/about/>. Accessed: 2024-03-07. 2021.
- [54] L. Giglio et al. “An enhanced contextual fire detection algorithm for MODIS”. In: *Remote Sensing of Environment* 87.2-3 (2003), pp. 273–282.
- [55] NOAA. *Visible Infrared Imaging Radiometer Suite (VIIRS)*. <https://ladsweb.modaps.eosdis.nasa.gov/missions-and-measurements/viirs/>. Accessed: 2024-04-12. 2024.
- [56] W. Schroeder et al. “The New VIIRS 375 m active fire detection data product: Algorithm description and initial assessment”. In: *Remote Sensing of Environment* 143 (2014), pp. 85–96.
- [57] NOAA. *Geostationary Operational Environmental Satellites (GOES)*. <https://www.goes-r.gov/>. Accessed: 2024-03-07. 2021.
- [58] Timothy J Schmit et al. “A closer look at the ABI on the GOES-R series”. In: *Bulletin of the American Meteorological Society* 98.4 (2017), pp. 681–698.
- [59] Joaquín Muñoz-Sabater et al. “ERA5-Land: A state-of-the-art global reanalysis dataset for land applications”. In: *Earth system science data* 13.9 (2021), pp. 4349–4383.
- [60] U.S. Department of the Interior, U.S. Department of Agriculture. *LANDFIRE Program*. <https://www.landfire.gov/>. Accessed: 2024-03-07. 2021.
- [61] M. A. Finney. *FARSITE: Fire Area Simulator—model development and evaluation*. Research Paper RMRS-RP-4. USDA Forest Service, Rocky Mountain Research Station, 2004.
- [62] R. D. Stratton. *Guidance on spatial wildfire analysis: models, tools, and techniques*. General Technical Report RMRS-GTR-183. USDA Forest Service, Rocky Mountain Research Station, 2006.
- [63] J. Dewitz. *National Land Cover Database (NLCD) 2016 Products*. <https://www.mrlc.gov/data>. U.S. Geological Survey data release. Accessed: 2024-10-07. 2019.

- [64] Microsoft. *U.S. Building Footprints*. <https://github.com/microsoft/USBuildingFootprints>. Accessed: 2024-10-07. 2018.
- [65] National Wildfire Coordinating Group (NWCG). *ICS-209 Incident Status Summary*. <https://www.nwcg.gov/publications/ics-209>. Accessed: 2024-10-07. 2012.
- [66] C. Christodoulou et al. “Multimodal Dataset for Wildfire Risk Prediction in Cyprus”. In: *Proceedings of the 12th ACM Multimedia Systems Conference*. 2021, pp. 256–261.
- [67] Ioannis Prapas, Spyros Kondylatos, and Ioannis Papoutsis. *FireCube: A Daily Datacube for the Modeling and Analysis of Wildfires in Greece*. Zenodo. Cite all versions by using this DOI, which will resolve to the latest version. 2021. DOI: [10.5281/zenodo.4943353](https://doi.org/10.5281/zenodo.4943353).
- [68] J. Wu et al. “SMLFire1.0: a stochastic machine learning (SML) model for wildfire activity in the western United States”. In: *Geoscientific Model Development* 14.9 (2021), pp. 5749–5764.
- [69] W. Jiao et al. “Next Day Wildfire Spread: A Machine Learning Dataset to Predict Wildfire Spreading From Remote-Sensing Data”. In: *IEEE Access* 10 (2022), pp. 40436–40447.
- [70] Spyridon Kondylatos et al. “Mesogeos: A multi-purpose dataset for data-driven wildfire modeling in the Mediterranean”. In: *Advances in Neural Information Processing Systems* 36 (2024).
- [71] Sebastian Gerard, Yu Zhao, and Josephine Sullivan. “WildfireSpreadTS: A dataset of multi-modal time series for wildfire spread prediction”. In: *Advances in Neural Information Processing Systems* 36 (2023), pp. 74515–74529.
- [72] Mark Finco et al. “Monitoring trends and burn severity (MTBS): Monitoring wildfire activity for the past quarter century using Landsat data”. In: *Moving from status to trends: Forest Inventory and Analysis (FIA) symposium*. Vol. 2012. 2012, pp. 4–6.
- [73] Yang Chen et al. “California wildfire spread derived using VIIRS satellite observations and an object-based tracking system”. In: *Scientific data* 9.1 (2022), p. 249.
- [74] Tianjia Liu et al. “Systematically tracking the hourly progression of large wildfires using GOES satellite observations”. In: *Earth System Science Data Discussions* 2023 (2023), pp. 1–40.

- [75] Louis Giglio, Wilfrid Schroeder, and Christopher O Justice. “The collection 6 MODIS active fire detection algorithm and fire products”. In: *Remote sensing of environment* 178 (2016), pp. 31–41.
- [76] Martin J Wooster et al. “Retrieval of biomass combustion rates and totals from fire radiative power observations: FRP derivation and calibration relationships between biomass consumption and fire radiative energy release”. In: *Journal of Geophysical Research: Atmospheres* 110.D24 (2005).
- [77] F Sedano and JT https Randerson. “Multi-scale influence of vapor pressure deficit on fire ignition and spread in boreal forest ecosystems”. In: *Biogeosciences* 11.14 (2014), pp. 3739–3755.
- [78] Richard Seager et al. “Climatology, variability, and trends in the US vapor pressure deficit, an important fire-related meteorological quantity”. In: *Journal of Applied Meteorology and Climatology* 54.6 (2015), pp. 1121–1141.
- [79] Roger D Ottmar et al. “Fuel characteristic classification system”. In: *Presentation at the 2nd International Wildland Fire Ecology and Fire Management Congress* http://ams.confex.com/ams/FIRE2003/techprogram/paper_67236.htm. 2003.
- [80] Joe H Scott. *Standard fire behavior fuel models: a comprehensive set for use with Rothermel's surface fire spread model*. US Department of Agriculture, Forest Service, Rocky Mountain Research Station, 2005.
- [81] James Richard Anderson. *A land use and land cover classification system for use with remote sensor data*. Vol. 964. US Government Printing Office, 1976.
- [82] Denis Kwiatkowski et al. “Testing the null hypothesis of stationarity against the alternative of a unit root: How sure are we that economic time series have a unit root?” In: *Journal of econometrics* 54.1-3 (1992), pp. 159–178.
- [83] David A Dickey and Wayne A Fuller. “Distribution of the estimators for autoregressive time series with a unit root”. In: *Journal of the American statistical association* 74.366a (1979), pp. 427–431.
- [84] Robert B Cleveland et al. “STL: A seasonal-trend decomposition”. In: *J. off. Stat* 6.1 (1990), pp. 3–73.
- [85] Rob J Hyndman and George Athanasopoulos. *Forecasting: principles and practice*. OTexts, 2018.
- [86] George E. P. Box and Gwilym M. Jenkins. *Time Series Analysis: Forecasting and Control*. Holden-Day, 1970.

- [87] Hirotugu Akaike. “A New Look at the Statistical Model Identification”. In: *IEEE Transactions on Automatic Control* 19.6 (1974), pp. 716–723. DOI: [10.1109/TAC.1974.1100705](https://doi.org/10.1109/TAC.1974.1100705).
- [88] Rob J. Hyndman et al. “A state space framework for automatic forecasting using exponential smoothing methods”. In: *International Journal of Forecasting* 18.3 (2002), pp. 439–454.
- [89] Ivan Svetunkov and Nikolaos Kourentzes. *Complex Exponential Smoothing: Modelling Seasonality and Multiple Seasonalities*. 2015. arXiv: [1503.02819 \[stat.AP\]](https://arxiv.org/abs/1503.02819). URL: <https://arxiv.org/abs/1503.02819>.
- [90] Vassilis F. Assimakopoulos and Konstantinos K. Nikolopoulos. “The Theta Model: A Decomposition Approach to Forecasting”. In: *International Journal of Forecasting* 16.4 (2000), pp. 521–530. DOI: [10.1016/S0169-2070\(99\)00037-9](https://doi.org/10.1016/S0169-2070(99)00037-9).
- [91] Yoshua Bengio, Patrice Simard, and Paolo Frasconi. “Learning Long-Term Dependencies with Gradient Descent is Difficult”. In: *IEEE Transactions on Neural Networks* 5.2 (1994), pp. 157–166. DOI: [10.1109/72.296918](https://doi.org/10.1109/72.296918).
- [92] Sepp Hochreiter and Jürgen Schmidhuber. “Long Short-Term Memory”. In: *Neural Computation* 9.8 (1997), pp. 1735–1780. DOI: [10.1162/neco.1997.9.8.1735](https://doi.org/10.1162/neco.1997.9.8.1735).
- [93] David Salinas et al. “DeepAR: Probabilistic forecasting with autoregressive recurrent networks”. In: *International journal of forecasting* 36.3 (2020), pp. 1181–1191.
- [94] Boris N Oreshkin et al. “N-BEATS: Neural basis expansion analysis for interpretable time series forecasting”. In: *arXiv preprint arXiv:1905.10437* (2019).
- [95] Byungseok Kim, Ayan De, and Kaushik Roy. *Time-mixer: An All-MLP Architecture for Time Series Forecasting*. 2022. arXiv: [2206.07272 \[cs.LG\]](https://arxiv.org/abs/2206.07272). URL: <https://arxiv.org/abs/2206.07272>.
- [96] Bryan Lim et al. “Temporal Fusion Transformers for Interpretable Multi-horizon Time Series Forecasting”. In: *International Journal of Forecasting* 37.4 (2021), pp. 1748–1764. DOI: [10.1016/j.ijforecast.2021.01.005](https://doi.org/10.1016/j.ijforecast.2021.01.005).
- [97] Haoyi Zhou et al. “Informer: Beyond efficient transformer for long sequence time-series forecasting”. In: *Proceedings of the AAAI conference on artificial intelligence*. Vol. 35. 12. 2021, pp. 11106–11115.
- [98] Haixu Wu et al. “Timesnet: Temporal 2d-variation modeling for general time series analysis”. In: *arXiv preprint arXiv:2210.02186* (2022).

- [99] Sean J. Taylor and Benjamin Letham. “Forecasting at Scale”. In: *The American Statistician* 72.1 (2018), pp. 37–45. DOI: [10.1080/00031305.2017.1380080](https://doi.org/10.1080/00031305.2017.1380080).
- [100] Diederik P Kingma. “Adam: A method for stochastic optimization”. In: *arXiv preprint arXiv:1412.6980* (2014).
- [101] J Scott Armstrong and Michael C Grohman. “A comparative study of methods for long-range market forecasting”. In: *Management Science* 19.2 (1972), pp. 211–221.
- [102] Leonard J Tashman. “Out-of-sample tests of forecasting accuracy: an analysis and review”. In: *International journal of forecasting* 16.4 (2000), pp. 437–450.
- [103] Chris Tofallis. “A better measure of relative prediction accuracy for model selection and model estimation”. In: *Journal of the Operational Research Society* 66.8 (2015), pp. 1352–1362.
- [104] Christopher A Sims. “Macroeconomics and reality”. In: *Econometrica: journal of the Econometric Society* (1980), pp. 1–48.
- [105] Anil K Jain and Ricardo C Dubes. “Score normalization in multimodal biometric systems”. In: *Pattern recognition* 38.12 (2005), pp. 2270–2285.
- [106] Isabelle Guyon and André Elisseeff. “An introduction to variable and feature selection”. In: *Journal of machine learning research* 3 (2003), pp. 1157–1182.
- [107] Jerome H Friedman. “Greedy function approximation: a gradient boosting machine”. In: *Annals of statistics* (2001), pp. 1189–1232.
- [108] Scott M Lundberg and Su-In Lee. “A unified approach to interpreting model predictions”. In: *Advances in neural information processing systems*. 2017, pp. 4765–4774.
- [109] Lloyd S Shapley. “A value for n-person games”. In: *Contributions to the Theory of Games*. Vol. 2. Princeton University Press, 1953, pp. 307–317.
- [110] Arthur E Hoerl and Robert W Kennard. “Ridge regression: Biased estimation for nonorthogonal problems”. In: *Technometrics* 12.1 (1970), pp. 55–67.
- [111] Robert Tibshirani. “Regression shrinkage and selection via the lasso”. In: *Journal of the Royal Statistical Society: Series B (Methodological)* 58.1 (1996), pp. 267–288.

- [112] Hui Zou and Trevor Hastie. “Regularization and variable selection via the elastic net”. In: *Journal of the Royal Statistical Society: Series B (Statistical Methodology)* 67.2 (2005), pp. 301–320.
- [113] David JC MacKay. “Bayesian interpolation”. In: *Neural computation* 4.3 (1992), pp. 415–447.
- [114] Leo Breiman. “Random forests”. In: *Machine learning* 45.1 (2001), pp. 5–32.
- [115] Tianqi Chen and Carlos Guestrin. “Xgboost: A scalable tree boosting system”. In: *Proceedings of the 22nd ACM SIGKDD international conference on knowledge discovery and data mining*. 2016, pp. 785–794.
- [116] Harris Drucker et al. “Support vector regression machines”. In: *Advances in neural information processing systems* 9 (1996).
- [117] Naomi S Altman. “An introduction to kernel and nearest-neighbor non-parametric regression”. In: *The American Statistician* 46.3 (1992), pp. 175–185.
- [118] David E Rumelhart, Geoffrey E Hinton, and Ronald J Williams. “Learning representations by back-propagating errors”. In: *Nature* 323.6088 (1986), pp. 533–536.
- [119] Rishabh Agarwal et al. “Neural additive models: Interpretable machine learning with neural nets”. In: *Advances in neural information processing systems* 34 (2021), pp. 4699–4711.
- [120] Yury Gorishniy et al. “Revisiting deep learning models for tabular data”. In: *Advances in Neural Information Processing Systems* 34 (2021), pp. 18932–18943.
- [121] Léo Grinsztajn, Edouard Oyallon, and Gaël Varoquaux. “Why do tree-based models still outperform deep learning on typical tabular data?” In: *Advances in neural information processing systems* 35 (2022), pp. 507–520.
- [122] A. L. Sullivan. “Wildland surface fire spread modeling, 1990–2007. 1: Physical and quasi-physical models”. In: *International Journal of Wildland Fire* 18.4 (2009), pp. 349–368.
- [123] A. L. Sullivan. “Wildland surface fire spread modeling, 1990–2007. 2: Empirical and quasi-empirical models”. In: *International Journal of Wildland Fire* 18.4 (2009), pp. 369–386.
- [124] A. L. Sullivan. “Wildland surface fire spread modeling, 1990–2007. 3: Simulation and mathematical analogue models”. In: *International Journal of Wildland Fire* 18.4 (2009), pp. 387–403.

- [125] Alex Alexandridis et al. “A cellular automata model for forest fire spread prediction: The case of the wildfire that swept through Spetses Island in 1990”. In: *Applied Mathematics and Computation* 204.1 (2008), pp. 191–201.
- [126] Andrea Trucchia et al. “PROPAGATOR: An operational cellular-automata based wildfire simulator”. In: *Fire* 3.3 (2020), p. 26.
- [127] P. Fernandes. “Fire spread prediction in shrub fuels in Portugal”. In: *Forest Ecology and Management* 144.1-3 (2001), pp. 67–74.
- [128] R. C. Rothermel. *A Mathematical Model for Predicting Fire Spread in Wildland Fuels*. Tech. rep. INT-115. USDA Forest Service, Intermountain Forest and Range Experiment Station, 1972.
- [129] F. A. Albini. “A model for fire spread in wildland fuels by radiation”. In: *Combustion Science and Technology* 42.5-6 (1985), pp. 229–258.
- [130] M. I. Asensio and L. Ferragut. “On a wildland fire model with radiation”. In: *International Journal for Numerical Methods in Engineering* 54.1 (2002), pp. 137–157.
- [131] W. Mell et al. “A physics-based approach to modelling grassland fires”. In: *International Journal of Wildland Fire* 16.1 (2007), pp. 1–22.
- [132] S. G. Berjak and J. W. Hearne. “An improved cellular automaton model for simulating fire in a spatially heterogeneous Savanna system”. In: *Ecological Modelling* 148.2 (2002), pp. 133–151.
- [133] T. Ghisu et al. “An optimal Cellular Automata algorithm for simulating wildfire spread”. In: *Environmental Modelling & Software* 71 (2015), pp. 1–14.
- [134] Joana Gouveia Freire and Carlos Castro DaCamara. “Using cellular automata to simulate wildfire propagation and to assist in fire management”. In: *Natural hazards and earth system sciences* 19.1 (2019), pp. 169–179.
- [135] A. Trucchia, G. Pagnini, and M. Ditaranto. “PROPAGATOR: A stochastic cellular automaton model for wildland fire spread able to simulate the effect of different vegetation and wind conditions”. In: *Mathematical and Computational Forestry & Natural-Resource Sciences* 12.2 (2020), pp. 1–17.
- [136] Sibo Cheng et al. “Parameter flexible wildfire prediction using machine learning techniques: Forward and inverse modelling”. In: *Remote Sensing* 14.13 (2022), p. 3228.

- [137] Sibo Cheng, Yike Guo, and Rossella Arcucci. “A Generative Model for Surrogates of Spatial-Temporal Wildfire Nowcasting”. In: *IEEE Transactions on Emerging Topics in Computational Intelligence* 7.5 (2023), pp. 1420–1430. DOI: [10.1109/TETCI.2023.3298535](https://doi.org/10.1109/TETCI.2023.3298535).
- [138] D. Krapohl et al. “Data-Driven Wildfire Spread Modeling of European Wildfires Using a Spatiotemporal Graph Neural Network”. In: *ISPRS Annals of the Photogrammetry, Remote Sensing and Spatial Information Sciences* V-3-2022 (2022), pp. 289–296.
- [139] J. A. Malen et al. “Generative algorithms for fusion of physics-based wildfire spread models with satellite data for initializing wildfire forecasts”. In: *Natural Hazards and Earth System Sciences* 23.1 (2023), pp. 135–155.
- [140] Fantine Huot et al. “Next day wildfire spread: A machine learning dataset to predict wildfire spreading from remote-sensing data”. In: *IEEE Transactions on Geoscience and Remote Sensing* 60 (2022), pp. 1–13.
- [141] Olaf Ronneberger, Philipp Fischer, and Thomas Brox. “U-net: Convolutional networks for biomedical image segmentation”. In: *Medical image computing and computer-assisted intervention–MICCAI 2015: 18th international conference, Munich, Germany, October 5–9, 2015, proceedings, part III* 18. Springer. 2015, pp. 234–241.
- [142] Xingjian Shi et al. “Convolutional LSTM network: A machine learning approach for precipitation nowcasting”. In: *Advances in neural information processing systems* 28 (2015).
- [143] Kaiming He et al. “Deep residual learning for image recognition”. In: *Proceedings of the IEEE conference on computer vision and pattern recognition*. 2016, pp. 770–778.
- [144] I Loshchilov. “Decoupled weight decay regularization”. In: *arXiv preprint arXiv:1711.05101* (2017).
- [145] Kaiming He et al. “Delving deep into rectifiers: Surpassing human-level performance on imagenet classification”. In: *Proceedings of the IEEE international conference on computer vision*. 2015, pp. 1026–1034.
- [146] Mattie Tesfaldet, Derek Nowrouzezahrai, and Chris Pal. “Attention-based neural cellular automata”. In: *Advances in Neural Information Processing Systems* 35 (2022), pp. 8174–8186.
- [147] Marcus Engsig et al. “DomiRank Centrality reveals structural fragility of complex networks via node dominance”. In: *Nature communications* 15.1 (2024), p. 56.